Innovative Approaches to Study CNS-Leukemia in Childhood BCP-ALL: Insights from iPSC-Derived Organoids

Inaugural Dissertation

for the attainment of the title of
Doctor in the Faculty of Mathematics and Natural Sciences
at Heinrich Heine University Düsseldorf

presented by

Philip Gebing, M.Sc.
from Düsseldorf, Germany

November 15, 2024
Düsseldorf, Germany

from the institute for Pediatric Oncology, Hematology, and Clinical Immunology
at the University Clinic Düsseldorf

Published by permission of the
Faculty of Mathematics and Natural Sciences at
Heinrich Heine University Düsseldorf

Supervisor: Prof. Dr. Arndt Borkhardt
Co-supervisor: Prof. Dr. Holger Gohlke

Declaration

From the Clinic for Pediatric Oncology, Hematology, and Clinical Immunology and the university clinic Düsseldorf (UKD) Published by permission of the Faculty of Mathematics and Natural Sciences at Heinrich-Heine-University Düsseldorf Supervisor: Prof. Dr. Arndt Borkhardt Co-supervisor: Prof. Dr. Holger Gohlke

The work presented in this thesis was performed and documented between October 2019 and June 2024 at the Clinic for Pediatric Oncology, Hematology, and Clinical Immunology and the university clinic Düsseldorf (UKD) under the supervision of Dr.rer.nat. Sanil Bhatia and Dr.rer.nat. Ute Fischer, as part of AG Bhatia.

Declaration of Authorship
I declare that the thesis submitted is my work without using impermissible aids, considering the "Rules on the Principles for Safeguarding Good Scientific Practice at Heinrich Heine University Düsseldorf". All direct or indirect sources are acknowledged in the bibliography as references. I further declare that I have neither submitted this nor a similar thesis to any other examination board to obtain a degree.

Signature: .....
Date: .....

Acknowledgements

The successful completion of this work is a testament to the support and contributions of many, for which I am profoundly grateful.

Firstly, I want to express my sincere appreciation to Dr. Sanil Bhatia for the opportunity to write this thesis within his research group. Your exceptional scientific supervision and encouragement for independent work have been invaluable. Your mentorship and our collaborative efforts on this project have consistently maintained my enthusiasm and motivation.

I also want to extend my thanks to Dr. Ute Fischer for joining this project and providing her extensive experience and knowledge.

Furthermore, I want to thank Prof. Dr. Arndt Borkhardt for providing me the opportunity to conduct my dissertation within the Department of Pediatric Oncology, Hematology, and Clinical Immunology. I am particularly grateful for his comprehensive reviews of my progress and his willingness to be my primary supervisor.

Additionally, I am thankful to Prof. Holger Gohlke for assuming the role of secondary supervisor, offering insightful discussions.

I am very grateful for the support from our collaborators at the Center for Advanced Imaging at the HHU, Dr. Sebastian Hänsch and apl. Prof. Dr. Stefanie Weidtkamp-Peters. The extensive training and access they had provided were crucial to the success of my work.

I want to acknowledge the entire AG Bhatia team for their steadfast support and camaraderie throughout my project. Special thanks go to Julian Schliehe-Diecks for the analysis and visualization of the bioinformatic data. I also want to thank Melina Vogt for her work on our cell culture models. I am very grateful for Silke's support; her exceptional oversight of lab operations made even the trickiest days in the lab run smoothly. Additionally, I would like to extend my thanks to the rest of the KMT team. I appreciate Pawel, not only for our technical discussions and debates, but also for providing essential flow cytometry data and contributing extensively during complex experiments. I also thank Vera for providing stem cell cultures, which were instrumental for the success of our organoids.

I also wish to thank everyone at the Christiane + Claudia Hempel-Stiftung for their financial and professional support.

Lastly, I extend my heartfelt thanks to my family and friends for their continuous encouragement and support over the years.

Contents

Glossary of Terms

Glossary of Terms

Term	Description
ALL	Acute Lymphoblastic Leukemia
AP-1	Activating Transcription Factor 1
BMP	Bone Morphogenic Protein
BM	Bone Marrow
BCP	B-Cell Precursor
BTK	Bruton's Tyrosine Kinase
CB	Cord Blood
CD	Cluster of Differentiation
CFDA-SE	Carboxyfluorescein Diacetate Succinimidyl Ester
CFSE	Carboxyfluorescein Succinimidyl Ester
CLP	Common Lymphoid Progenitors
CR	Complete Remission
CXCR/CCR	Chemokine Receptor
DAPI	4',6-diamidino-2-phenylindole
DOA	Days-of-age
ERK	Extracellular signal-regulated kinase
ES	Embryonic Stem (Cell)
FACS	Fluorescence-activated Cell Sorting
FA	Formaldehyde
FGF2	Fetal Growth Factor 2
Fgf	Fibroblast Growth Factors

Table 1 – continued from previous page

Term	Description
IP	Intermediate Progenitor
LMMP	Lymphoid-primed Multi-Potent Progenitors
MAP2	Microtubule-Associated Protein 2
MIP	Maximum Intensity Projection
MMP	Multi-Potent Progenitors
ORG	Organoid
OSVZ	Outer Subventricular Zone
OWB	Organoid Washing Buffer
PAX6	Paired-Box Protein
PDX	Patient-derived Xenograft
SAE	Serious Adverse Events
SFEBq	Serum-free floating culture
SOX2	SRY-box 2
SVZ	Subventricular Zone
TBR1	T-Box Brain Transcription Factor 1
TRE	Transcriptional Response Elements
TUJ1	Beta-Three Tubulin 1
VZ	Ventricular Zone
Wnt	Wingless-related integration site
2D/3D	Two-/Three-dimensional
aSC	Organ-restricted Adult Stem Cells
iPS	Induced Pluripotent Stem (Cell)

List of Figures

List of Tables

List of Publications

List of Publications Included in This Thesis

- **In Press**, Blood Advances
  Gebing, P., Loizou, S., Hänsch, S., Schliehe-Diecks, J., Spory, L., Stachura, P., Pandyra, A. A., Wang, H., Zhuang, Z., Schrappe, M., Cario, G., Alsadeq, A., Schewe, D. M., Borkhardt, A., Lenk, L., Fischer, U., Bhatia, S., Jepsen, V. H., Vogt, M. A brain organoid/ALL co-culture model reveals the AP-1 pathway as critically associated with CNS involvement of BCP-ALL. Blood Advances (2024)
  Author Contribution: This publication is based on my PhD project. I was responsible for the organoid cultivation and establishing a novel organoid co-culture assay, including their execution, imaging, and analysis. I also established microscopy protocols and created a novel computer analysis pipeline as a new application for spatial analysis of organoids. Further, I produced all figures with the exception of figures 5A-D and figure 6.
  Contributions by the other authors included in this thesis: RNA sequencing data analysis (Schliehe-Diecks, J.) as well as FACS data (Stachura, P.), AP-1 reporter model (Vogt, M.), iPS cell cultures (Jepsen, M), CD79a knockdowns (Lenk, L.).

List of Publications Not Included in This Thesis

- Vogt, M., Dienstbier, N., Schliehe-Diecks, J. et al. Co-targeting HSP90 alpha and CDK7 overcomes resistance against HSP90 inhibitors in BCR::ABL1^{+} leukemia cells. Cell Death Dis 14, 799 (2023). `https://doi.org/10.1038/s41419-023-06337-3`
  Author Contribution: I helped in staining 2D monolayers of cell culture models used in this manuscript, performed confocal imaging on said cell models for the

main author, and produced figure 6E.

- Sinatra L, Yang J, Schliehe-Diecks J, Dienstbier N, Vogt M, Gebing P, Bachmann LM, Sönnichsen M, Lenz T, Stühler K, Schöler A, Borkhardt A, Bhatia S, Hansen FK. Solid-Phase Synthesis of Cereblon-Recruiting Selective Histone Deacetylase 6 Degraders (HDAC6 PROTACs) with Antileukemic Activity. J Med Chem. 2022 Dec 22;65(24):16860-16878. doi: 10.1021/acs.jmedchem.2c01659. Epub 2022 Dec 6. PMID: 36473103.
  Author Contribution: I helped in staining 2D monolayers of cell culture models used in this manuscript, performed confocal imaging on said cell models for the main author, and produced figure 4.

Abstracts

- Gebing, P.; Hänsch, S.; Lenk, L.; Schewe, D.; Borkhardt, A.; Fischer, U.; Bhatia, S.. P320: *TCF3::PBX1*leukemia INVADES IPSC-DERIVED CEREBRAL ORGANOIDS. HemaSphere 6():p 220-221, June 2022. | DOI: 10.1097/01.HS9.0000844168.40177.79
  Author Contribution: I am the first author, responsible for establishing the cerebral organoids and expanding their culture for a wide array of experiments. These were then used by me to conduct novel brain organoid-leukemia co-culture experiments. I also established 3D confocal imaging, tissue clearing techniques, and designed analysis methods to study leukemic cell engraftment. I also generated the figure shown in this publication.

- Philip Gebing, Stefanos Loizou, Sebastian Hänsch, Julian Schliehe-Diecks, Lea Spory, Pawel Stachura, Aleksandra Pandyra, Martin Schrappe, Gunnar Cario, Ameera Alsadeq, Denis Martin Schewe, Arndt Borkhardt, Lennart Lenk, Ute Fischer, Sanil Bhatia; CNS Invasion of *TCF3::PBX1*$^{+}$ leukemia Cells Requires Upregulation of AP-1 Signaling As Revealed By Brain Organoid Model. Blood 2023; 142 (Supplement 1): 1407. doi: https://doi.org/10.1182/blood-2023-178613
  Author Contribution: I am the first author, responsible for broadening the cocultivation assays to isolate infiltrated and non-infiltrated leukemia cells from organoids for downstream analysis. I also established a novel computer analysis

pipeline for reliable analysis of large image data batches. I also generated the figure shown in this publication.

Zusammenfassung

Die Involvierung des zentralen Nervensystems (ZNS) bei der Behandlung von B-Zell-Vorläufer-Akuter-Lymphoblastenleukämie (engl. BCP-ALL) im Kindesalter bleibt eine klinische Herausforderung. Toxizitäten als Nebenwirkung der Therapie haben tiefgreifende Auswirkungen auf die Lebensqualität der Patienten. Krankheitsrückfälle (Rezidiv) im ZNS können bei einer großen Anzahl von Hochrisikopatienten häufig auftreten[1,2]. Die bei der Befallung des ZNS involvierten biologischen Mechanismen, sind noch nicht vollständig erforscht und werden weitesgehend im Rahmen von 2D-Zellkultur- und *in vivo*-Mausmodellen untersucht. Es bestehen wesentliche Unterschiede im zellulären Aufbau zwischen menschlichem und murinem ZNS, welches die Verwendbarkeit von *in vivo* Erkenntnissen beeinträchtigt. Die aus humanen Stammzellen gezüchteten Hirnorganoide gehen auf einige dieser Nachteile ein und stellen daher einen ergänzenden Ansatz zur Untersuchung der ZNS-Leukämie dar. Die Grundlage des Projekts ist die Untersuchung von BCP-ALL Zellkulturen welche in der ZNS-Leukämie erkrankung bekannt sind. Hier wurden Organoide und leukämische Zellen für einen längeren Zeitraum kokultiviert und deren Interaktion unter Fluoreszensmikroskopie gemessen. Tatsächlich wächst die Hochrisikogruppe der *TCF3::PBX1*-positiven Subtypen nach 14 Tagen unter die Oberfläche der Organoide. Die für das Experiment isolierten pluripotenten Stammzellen oder menschlichen B-Lymphozyten zeigten deutlich weniger Interaktion. Darüber hinaus wuchsen andere Hochrisikoleukämie-Untergruppen, darunter *BCR::ABL1* und *TCF3::HLF* in Hirnorganoide hinein. *Live-Cell* Analysen wurden verwendet um die Zellmigration von BCP-ALL
zu Organoiden zu bestätigen. Dabei wurden von Zellen der Hochrisikogruppe deutlich längere Distanzen gegenüber der Kontrollzellen zurückgelegt. Ein wichtiger Meilenstein innerhalb des Projekts war die Entwicklung einer neuartigen Computer-Analyse *Pipeline* zur präzisen Messung der leukämischen Zellen relativ zum Volumen der Organoide.

Solche Pipelines verfügen über eine enorme Durchsatzrate, welches bei der hohen Anzahl von Leukämiezellen in den Organoiden vorteilhaft ist. Darüber hinaus können hier präzise Angaben zur Eindringtiefe ermessen werden. Hier lieferte das Verhalten von BCP-ALL ein klareres Bild, auf welcher Ebene sich die Zellpopulationen im Organoid verteilen. Interessant ist das Verhalten von leukämischen Entitäten mit bekanntlich-geringerer ZNS-Erkrankungen, welche sich viel näher zu gesunden pluripotenten Stammzellen oder B-Lymphozyten verhalten. Dies unterstreicht die Anwendbarkeit solcher Analysen bei Organoiden und fügt weitere tools zur Forschung hinzu. Die Inhibierung spezifischer B-Zell- und Chemokin-Rezeptorsignal-Komponenten ist in der Literatur zur ZNS-Leukämie bereits erforscht worden. Entsprechend den Daten eines kürzlich publizierten Mäusemodells, führte ein Knockdown der CD79a/Igα (Prä-BCR-Komponente) sowie die Inhibierung durch den Chemokin-Rezeptor-CXCR4-Antagonisten Plerixafor, zu einem verringerten Einwachsen von *TCF3::PBX1*-positiven Zellen in Organoiden. Die Mechanismen welche die leukämische Ausbreitung im ZNS antreiben sind ein aktiver Forschungsbereich. Die Entnahme infiltrierter und nicht infiltrierter BCP-ALL-Zellen aus Organoiden lieferte erste Einblicke in transkriptionelle Veränderungen nach der Einwachsung in Organoiden. Eine RNA-Sequenzierung dieser Proben zeigte eine Erhöhung des *activating transcription factor* (AP-1)-pathways, insbesondere seiner Komponenten FOSB, FOS und JUN. Diese Mitglieder haben bereits eine Ähnlichkeit zur ZNS-Leukämie bei T-ALL Patienten gezeigt. Hier offenbaren infiltrierte Zellen eine Verschiebung im Energiestoffwechsel, wie sie von Krebszellen in Reaktion auf hypoxische Umgebungen mittlerweile bekannt ist. Die Beteiligung von AP-1 wurde schließlich auch durch Durchflusszytometrie und Immunfluoreszenzanalyse von infiltrierten und nicht infiltrierten Zellen geprüft. Um den Zeitpunkt der Aktivierung von AP-1 genauer festzustellen, wurde eine mit einem AP-1-GFP-Reporter transduzierte BCP-ALL Zellinie mit Organoiden kokultiviert. *Live-Cell* Messungen konnten schlieslich die Aktivität von AP-1, anhand der erhöhten Fluoreszenz des GFP-Reporter, in der Migrationsphase der ALL-Zellen feststellen. Zusammenfassend präsentierte dieses Projekt die Kokultur Assay zwischen Hirnorganoiden und BCP-ALL-Leukämie als neuartiges Modell im Rahmen der Untersuchung der ZNS-Leukämie. Die Überlappung klinischer Daten sowie die Ergebnisse der bereits etablierten *in vitro* und *in vivo* Modelle sprechen für die Spezifizität des Hirnorganoids als komplementäres Modell.

Summary

The involvement of the central nervous system (CNS) remains a clinical challenge in the treatment of childhood B-cell precursor acute lymphoblastic leukemia (BCP-ALL). Treatment-related toxicities significantly impact patients' quality of life, and CNS relapse is frequent, particularly among high-risk patients. Despite extensive investigation, the underlying biological mechanisms driving CNS invasion in BCP-ALL remain incompletely understood. Current research predominantly relies on 2D cell culture and *in vivo* mouse models, which may not faithfully replicate human CNS architecture and cellular identity. To address these limitations, human brain organoids offer a complementary approach for studying CNS invasion in BCP-ALL. In this project, a novel co-culture assay between leukemia and cerebral organoids was established. Notably, the high-risk group *TCF3::PBX1*$^{+}$ leukemia exhibited robust engraftment, commensurate with their time exposed to organoids. This stood in contrast to human haematopoietic stem and progenitor cells (HSPCs). Further, other high-risk leukemia subgroups (e.g. *BCR::ABL1*, *TCF3::HLF*) also identified prominent engraftment in cerebral organoids during co-culture assay. This stood in contrast to HSPCs. Live-cell analysis revealed the directed migration of BCP-ALL towards organoids, while moving significantly longer distances than HSPCs under the same conditions. Further, Chronic myelocytic leukemia (CML) which are not typically associated with the CNS disease was adopted as another control for the co-culture assay. The project also introduced a novel spatial analysis pipeline for the precise measurement of leukemic engraftment into organoids. Interestingly, the analysis of engraftment behavior highlighted fractions of BCP-ALL populations disseminating into deeper organoid regions, while CML cells and healthy HSPCs used as controls did not exhibit such deep migration into the organoids. In line with murine model data, blocking specific pre-B-cell and chemokine receptor signaling components, such as CD79a/Igα (preBCR component) or pre-treatment with

the CXCR4 antagonist Plerixafor, significantly reduced invasion of *TCF3::PBX1*$^{+}$ BCP-ALL cells into the organoids. Furthermore, RNA sequencing of infiltrated and non-infiltrated BCP-ALL cells isolated from organoids unveiled transcriptional upregulation of the activating transcription factor (AP-1) pathway, particularly involving FOSB, FOS, and JUN components. Flow cytometry, immunofluorescence analyses and AP-1 reporter assay data confirmed AP-1 involvement during the migration of BCP-ALL cells into the cerebral organoid. In summary, a co-culture invasion assay utilizing cerebral organoids and BCP-ALL leukemia presents a novel platform for investigating and targeting signaling pathways implicated in CNS invasion.

Chapter 1

Introduction

1.1 Hematopoiesis

The diverse pool of human blood cell types shares a common origin. By the process of haematopoiesis, multipotent, self-renewing stem cells differentiate into all cell lineages of the blood. Hematopoietic stem cells (HSCs) are located within the bone marrow's endosteum and sinusoidal blood vessels where their localization, self-renewal, and differentiation are controlled[3,4]. These immature blood cells residing in the bone marrow (BM) differentiate in a complex, hierarchical process, followed by their emigration to the periphery to undergo further maturation and carry out their effector function(s)[3]. Multipotent progenitors (MPPs) give rise to "lineage-committed" lymphoid or myeloid progenitors, which deliver highly specialised blood cell types (fig. 1). Under healthy conditions, transcriptional regulators (including cytokines and hormones) control the proliferation and quiescence of HSPCs by limiting their cell cycle transit, such as the T helper 1 (Th1)-derived cytokine oncostatin M (OSM). It has been long known that chronic stimulation of CD4+ T cells maintains normal haematopoiesis[5]. Critically, dysregulating the balance between proliferation and differentiation may be an accepted driver of leukemogenesis[6].

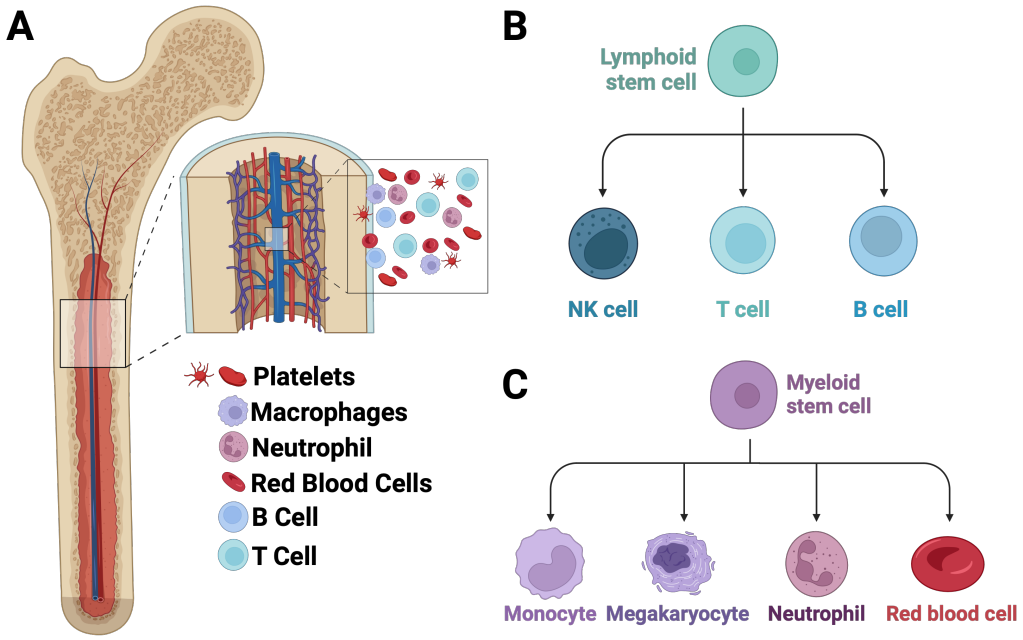

Figure 1: Hematopoiesis - A Graphical Illustration of Lymphoid and Myeloid Lineages: The bone marrow niche generates many differentiated cell types via lymphoid and myeloid stem cell differentiation. (A) The bone marrow (BM) contains various multi-potent progenitor cells created during hematopoiesis. Their differentiated lymphoid and myeloid cell types emanate into the bloodstream. (B) The lymphoid lineage gives rise to natural killer (NK) cells, T-cell, and B-cells. (C) The Myeloid lineage leads to the production of monocytes, megacaryocytes, neutrophils, and red blood cells.

1.2 Leukemia: A Brief Overview

1.2.1 Hematological Malignancies and their Global Prevalence

Leukemia (from *Greek* 'leukos' meaning white, 'haima' meaning blood) is a term used to describe various types of blood cancer classified according to their characteristics, such as morphology, immunophenotype, cytogenetic and molecular abnormalities, and clinical features. The diseases are classified into four main categories based on their clinical features, which are myeloid or lymphoid lineage and acute or chronic. This classification helps relate to the appropriate treatment approach. Acute myeloid leukemia (AML), acute lymphocytic leukemia/lymphoma (ALL), chronic lymphocytic leukemia/ small

lymphocytic lymphoma (CLL/SLL) and chronic myeloid leukemia (CML) form the most commonly studied leukemias. Broadly, hematological malignancies are widely accepted to result from aberrant hematopoietic processes by leukemic stem cells (LSCs), capable of self-renewal and differentiation. In the case of B-lymphoid malignancies, multi-potent progenitors (MPPs) give rise to lymphoid-primed multi-potent progenitors (LMPP), multi-lymphoid progenitors (MLP), common lymphoid progenitors (CLP), ProB-progenitors, PreB-cells, and finally mature B-cells[7]. Subtypes in childhood ALL can be of the T- or B-cell lineage, and their localization to developmental compartments had been revealed through immunophenotype screens in the 1970s and 1980s. ALL can result from the deregulated proliferation process of the lymphoblastic population, leading to their arrest at an immature stage. This group may be subdivided into infant ALL (iALL) or childhood-ALL at below or above 12 months of age respectively[7]. Since the period in which ALL during childhood was considered fatal, novel treatment protocols have boasted 5-year overall survival rates of 85-90% and above[8,9]. This thesis is centered around BCP-ALL to which an extended introduction is depicted below.

The B-lymphoid lineage or B-cell precursor acute lymphoblastic leukemia (BCP-ALL) is reported to make up 80% of childhood ALL. Childhood BCP-ALL is responsible for a third of pediatric cancers in the developed world, adding around 10-45 cases per million children annually, with around 1 in 2000 likely to be at risk of developing ALL before 15 years of age[10]. Even more, BCP-ALL is a complex disease with varied incidence rates across the globe. These rates are influenced by factors such as geography, environment, and genetics. While it can be challenging to consolidate specific incidence rates due to these variations, high-quality studies and surveillance reports provide valuable insights into the trends and challenges associated with BCP-ALL. BCP-ALL is the most common type of leukemia in children, with varying incidence rates in different regions. In developed countries, the incidence of ALL in children is around 30-40 cases per million. The age-standardized incidence rate has shown a modest annual increase of 0.6%, indicating a relatively stable incidence rate in recent years. For example, a study from the Netherlands reported a stable incidence rate with a slight increase over a 26-year period, with the age-standardized incidence rate being 37 cases per million children aged 0–17 years[11]. A population-level analysis into relative survival across Germany and the United States in adult ALL showed a 5-year relative survival of 43.4% and 35.5% respectively[12].

1.2.2 Molecular Subtypes

1.2.2.1 TCF3::PBX1

Modifications to the genome, most prominently chromosomal translocations, give rise to fusion proteins responsible for driving abnormal cellular change. In BCP-ALL several translocations are linked to inferior clinical outcomes compared to patients lacking them. The underlying fusion gene *TCF3::PBX1* (formerly referred to as *E2A::PBX1*) is formed by the chromosomal translocation t(1;19)(q23;p13). It arises in around 5-10% of BCP-ALL patients, 5% of pediatric ALL patients, and has been shown to 'readily emerge' *in utero* during fetal hematopoiesis while remaining clinically inconspicuous. It was previously shown that although the contemporary treatment regiments are providing an overall favorable outcome for patients, it is overcome by an overall high incidence of CNS relapse[13]. CNS involvement at diagnosis is seen in 4-7% of adult patients[14], and in 2-5% of pediatric ALL[15]. A third of pediatric ALL patients experiencing relapse involve the CNS compartment[15,16,17].

1.2.2.2 BCR::ABL1

The BCR::ABL1 oncoprotein is encoded by the *BCR::ABL1* fusion gene. The gene is the result of a reciprocal translocation between the Abelson leukemia virus (ABL or ABL1) gene on the long arm of chromosome 9 at position q34.1, and the breakpoint cluster region (BCR) gene on the long arm of chromosome 22 at position q11.2. This translocation t(9;22)(q34;q11) yields a highly truncated chromosome 22, also commonly referred to as the Philadelphia (Ph) chromosome. While it is associated with chronic myeloid leukemia (CML), another manifestation is found in a small, high-risk group in BCP-ALL. *BCR::ABL1*$^+$ BCP-ALL cases carry an unfavorably higher incidence of CNS-leukemia, in fact, it is represented in approximately 15% of BCP-ALL cases. In the case of adult ALL, this figure varies significantly, ranging from 15 to 50%, increasing with age. Statistical data concerning relapse during clinical trials of *BCR::ABL1*$^+$ patients revealed 23% relapse of which 10% experienced isolated CNS-, or combined CNS and BM relapses[18]. Of note, the introduction of Ph-status documentation of all patients before initiating therapy as a common practice has significantly boosted survival rates[19].

1.2.2.3 TCF3::HLF

The TCF3::HLF oncoprotein (formerly referred to as *E2A-HLF*) forms from the chromosomal translocation t(17;19)(q22;p13) and was first identified and reported in 1991[20,21,22,23]. It is a rare genetic subtype of ALL seen in less than 0.5% of pediatric ALL, and is accompanied with poor prognosis and considered universally fatal within 2 years of initial diagnosis[22]. CNS involvement at diagnosis[24].

1.2.2.4 MLL-r/KMT2A-r

The rearrangement of the *KMT2A* (*Lysine [K]-specific MethylTransferase 2A* gene, formerly *mixed lineage leukemia 1* (MLL1) occurs in 4-5% of *de novo* adult, up to 22% of pediatric patients and 75% of infant leukemias[25,26]. The majority of *KMT2A* rearrangements (KMT2A-r) are associated with poor prognosis, as well as therapy-related side effects[26]. In fact, KMT2A-r can manifest as therapy-related leukemias, whereby their formation is attributable to prior treatment with certain chemotherapeutic agents[27]. Furthermore, KMT2A-r ALL have been shown to relapse early in addition to high incidence of CNS involvement. KMT2A-r rearrangement in adults with ALL is seen as a high-risk genetic abnormality, typically benefiting from allogeneic hematopoietic stem cell transplantation[28].

1.3 Central Nervous System Involvement in BCP-ALL

1.3.1 The Limitations of Conventional Classification Tools for CNS-Leukemia

CNS involvement at diagnosis of BCP-ALL is a critical factor for prognosis and therapy planning. CNS relapse, occurring either at diagnosis or later during therapy, poses a significant challenge in the treatment of BCP-ALL. Although it is less common at initial diagnosis, the risk persists throughout treatment and into remission. The global incidence of CNS relapse in BCP-ALL is difficult to quantify due to varying diagnostic criteria, treatment protocols, and follow-up practices across different studies and regions. The conventional classification of the stage of CNS disease determines the total count of white blood cells in the cerebrospinal fluid (CSF), along with the microscopic analysis of a cytocentrifuged CSF sample to identify leukemic blasts. In the 1970s, the diagnosis of CNS involvement in BCP-ALL relied on this specific tool. A cell count of $10/mm^3$ represented a major indicator of CNS disease[29]. The presence of lymphoblasts and the

number of leukocytes is a classification criterium for CNS infiltration into three risk groups (CNS 1-3)[1]. Given the major technological developments over the half-century, more advanced and sensitive diagnostic criteria and techniques for CNS involvement have emerged. Flow cytometry (FC) and polymerase chain reaction (PCR) are advanced diagnostic techniques which now reveal minimal residual disease (MRD) in the CNS at the submicroscopic level, significantly bolstering current diagnosis capabilities. FC can perform physical and chemical analyses of cell populations within the CSF, identifying and characterizing abnormal cells in the process. PCR takes a different approach by amplifying the snippets of genetic material within leukemic cells, vastly improving the detection of MRD. While this diagnostic method has been around for a while, there is ongoing debate regarding whether cytology can accurately indicate the level of leukemic infiltration and the likelihood of experiencing a relapse in the CNS. Evidence points to methodological issues, e.g. in the preservation of samples and discrimination between malignant and benign T-lymphocytes. Furthermore, doubt has been cast on the representability of these assays when considering the clinical picture. Although an initial diagnosis classifies around 2-5% of patients as CNS3 in ALL, as much as three-quarters of this group relapse before CNS-directed therapy is usually adopted[1,2].

1.3.2 Current Practices of Detection and Classification of Risk Factors

CNS disease relapse in BCP-ALL remains a major challenge today. The lack of highly sensitive biomarkers available is a major barrier to accurate prediction of relapse in pediatric ALL patients. Crucially, a balance between the best possible treatment and the risk of toxicity and long-term damage to patients requires careful balancing. Current diagnostic tools (FC and/or PCR) play a role in predicting multi-year cumulative survival. It has been recently discovered that patients who test positive for either CNSflow+ (using flow cytometry) or CNScomb+ (using a combination of cytospin and flow cytometry) at the time of diagnosis, have a higher likelihood of experiencing relapse within 4 years, as compared to those who test negative using these methods[30]. Specifically, CNSflow+ and CNScomb+ are significant predictors of relapse, underscoring the importance of advanced diagnostic tools in identifying patients at higher risk for targeted interventions. It was shown recently how PCR and cytospin, a method of concentrating cells from the CSF onto a microscopy slide by centrifugation, diverge when compared head-to-head. For instance, analysis of cell-free DNA from CSF of pediatric ALL patients detected CNS dissemination in 20–47% of cases compared to

5–17% by cytospin, indicating a significant occurrence of CNS involvement at diagnosis. A recent study showed that 28% of patients had CNS involvement at diagnosis according to flow cytometry, while only 3% were detected by cytospin. The flow positive (CNSflow+) group had a 10.7% 3-year cumulative incidence of relapse, compared to 6.9% for the flow negative group. A different study investigating FC detection indicated a 5-year cumulative incidence of relapse of 29% for the flow positive group versus 7% for the flow negative group, highlighting the importance of detecting CNS involvement as it can affect the prognosis[1]. It also suggests the necessity for more sensitive techniques like flow cytometry or next-generation sequencing to assess treatment response in the CNS. Critically, the contrast in CNS involvement rates between detection methods is highly relevant regarding relapse rates. In summary, evolving detection methods have helped clinicians improve diagnosis, particularly in the evaluation of MRD and the risk of relapse. Yet it must be stressed that room for better predictors of CNS disease, particularly with the emergence of new biomarkers, is needed in the future.

1.3.3 Leukemia Pathways to the CNS

To provide a clearer breakdown of leukemia dissemination into the CNS, a detailed cross-sectional cartoon is depicted below. The CNS comprises the brain and spinal cord. The meninges protecting the brain are a layered structure with embedded vessels serving the brain (fig. 2). These include the outer dura mater, separated from the inner meninges by the subdural space. The inner meninges include the arachnoid and pia mater (fig. 2B), collectively known as the leptomeninges (fig. 2C), which coat the brain parenchyma (functional brain tissue). The subarachnoid space sits between the arachnoid and pia mater, harboring cerebral vessels and the cerebrospinal fluid/ liquor cerebrospinalis (CSF) (fig. 2I). The CSF is produced in the choroid plexus, an epithelial layer in the walls of the lateral ventricles. To add to the different components of the meningeal layers, CSF is also resorbed from the subarachnoid space into the blood via the pacchionian granulations (arachnoid granulations) (fig. 2F). Blood is carried to the CNS via the vertebral and internal carotid arteries. Even though blood flow to the brain and meninges are distinct, both systems drain into the cranial sinuses. Most recently, reports show that a third of relapse cases in pediatric ALL experience intermittent, leptomeningeal metastasis of the leukemic cells circulating in the vessels[31].

Several loci are considered for invasion of leukemia cells, including via the Virchow-

Robin spaces through the blood-brain barrier, through the meningeal microvessel or via the blood-CSF barrier at the choroid plexus[32] (fig. 2). Interestingly, leukemic cells had been observed to pass directly into the leptomeninges from the bone marrow by passing through vertebral and calvarial bone fenestrations[33]. Recently, CNS involvement was thought to mainly affect the meninges, which consist of the pia, dura, and arachnoid mater, through which leukemia cells may expand or remain as focal lesions. However their entry may be facilitated by a selection of entries[32]. Lymphocytes may cross microvessels blood-brain-barrier (BBB) into the parenchyma (fig. 2, ①), the blood-leptomeningeal barrier (BLMB) of the pia mater (fig. 2, ②), as well as the blood-cerebrospinal fluid barrier (BCSFB) (fig. 2, ③). Additionally, it is believed that leukemia cells may utilize bridging veins within the skull and meninges to reach the CNS, bypassing other potential entry routes. Finally, leukemia could use the dural lymphatics to transport leukocytes to and from the parenchyma and subarachnoid space (fig. 2, ⑤. To summarize, BCP-ALL dissemination into the CNS may follow multiple routes.

1.3.4 Molecular Underpinnings Driving Infiltration and Cell Quiescence

1.3.4.1 Cell Migration and Dissemination

Metastasis is a crucial stage in the development of tumors. It happens when cells from the original tumor acquire the ability to migrate, enter the bloodstream or lymph vessels, move to a different location, and leave the vessel system. Metastasized cancer is responsible for around 90% of cancer-related deaths[34,35,36,37]. Some of the cellular components required for tumor invasion are represented in leukemic cells. B-cell invasion into the CNS can begin with the rolling and tethering processes through venues of blood vessels along the BBB, including microvascular endothelial cells. Selectins, a family of cell surface glycoproteins (E-, P-, and L-selectins), are involved in leukocyte cell trafficking (L-selectin). L-selectin can be expressed on leukemia cells, and the extent of their expression has been linked to highly metastatic disease. The leukemia cells are thought to tether through P/E-selectin initially. Others present interaction of the intercellular adhesion molecule 'ICAM1' with the B-cell receptor and finally with the chemokine ligand-receptor, allowing the B-cells to escape through tight junctions via the process of trans-endothelial/paracellular/trans-cellular migration. Another family of surface proteins, Integrins, are known to be involved in multiple aspects of metastasis, including invasion and pro-survival pathway activation. During hematogenous metastasis, they

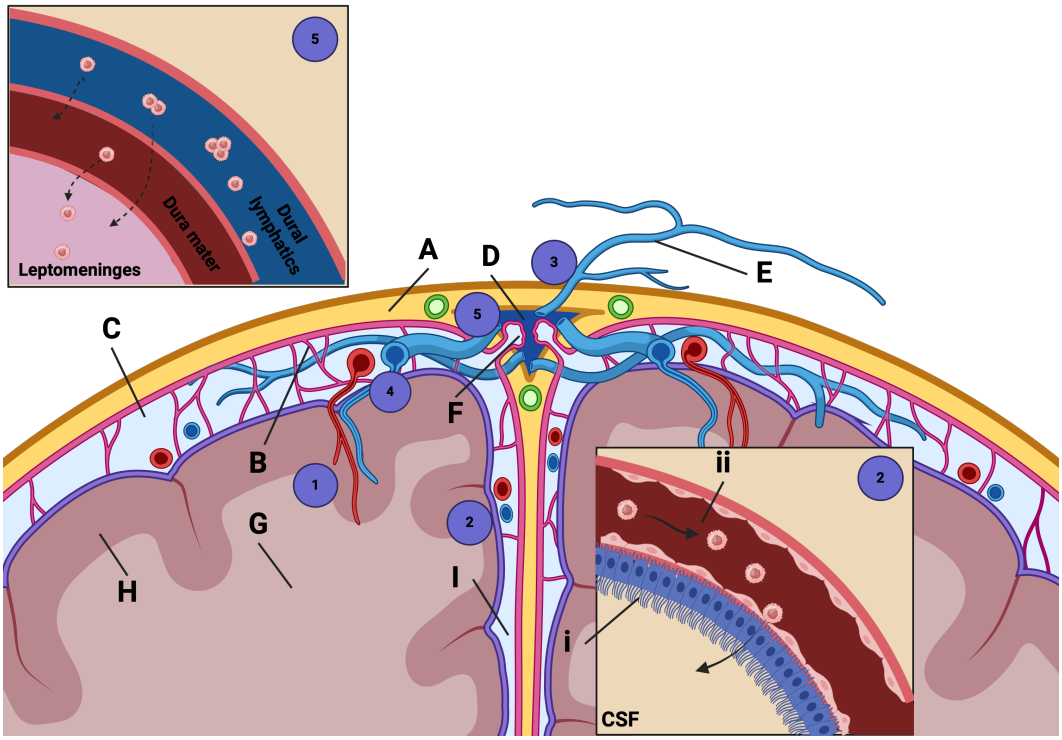

Figure 2: BCP-ALL Paths to Entry to the CNS Niche- Cartoon depicting a coronal section of the human brain labeled A-I and 1-4. (A) Skull, (B) Pia Arachnoida, (C) Leptomeninges, (D) Superior Sagittal Sinus, (E) Emissary Vein, (F) Arachnoid Granulations, (G) White Matter, (H) Cerebral Cortex, (I) Cerebrospinal Fluid. Numbers ① through ⑤: ① Blood Brain Barrier (BBB), ② Blood-cerebrospinal Fluid Barrier (BCSFB), ③ Veins traversing the skull and meninges, ④ Blood Leptomeningeal Barrier (BLMB), ⑤ Dural lymphatics may drive lymphocyte movement across the pyrenchyme and subarachnoid space

direct leukemia cell attachment to vessel walls and entry into the metastatic niche. Several molecular pathways and their components have been linked to CNS infiltration in the past[38,39]. Pre-B-lymphocytes express the antigen receptor pre-B-cell receptor (pre-BCR). The pre-BCR is a receptor tyrosine kinase mediating the proliferation and differentiation of B cells through antigen stimulation. Recently the pre-B cell receptor and its signaling units CD79a and CD79b were shown to regulate CNS involvement[31,40]. In fact, targeting of the CD79b component by antibodies showed robust anti-leukemia efficacy and reduced CNS-ALL burden in ALL models[40]. The ZAP70 (*Zeta-chain-associated protein kinase 70*)-kinase is a downstream signaling component of the BCR. In chronic lymphoid leukemia (CLL), it has been shown to

enhance B-cell migration towards chemokines[41,42]. ZAP-70 expression has also been reported in 56-59% of BCP-ALL cases. In T-ALL, ZAP-70 interconnected with the pre-BCR signaling, has been previously shown to promote CNS infiltration[43,44]. This was dependent on ERK1/2-mediated induction of the chemokine receptors CCR7 and CXCR4. The Ras/Raf/MEK/extracellular signal-regulated kinase (ERK) pathway represents one of the critical pathways for pre-BCR signaling in healthy and malignant B cells, and CXCR4 is also being directly controlled by pre-BCR-signaling via Bruton's tyrosine kinase (BTK)[45,46,47]. A variety of chemokine receptors, such as CXCR3, CXCR4, and CCR7, present on normal lymphocytes encourage migration to the CNS which expresses the corresponding ligands in the endothelium of the brain and the epithelium of the choroid plexus. The expression of the chemokine receptor CXCR4, highly prevalent in most hematological malignancies, on the surface of ALL B-cells is increased compared to healthy cells. Its cooperative ligand CXCL20 is enriched in the human brain. Meanwhile the key driver of migration and entry of self-reactive T-and B-lymphocytes into the CNS has been linked to inflammatory conditions. Moreover, the CXCR4 ligand stromal-derived factor 1 (SDF-1), also referred to as CXCL12, has been linked to transendothelial migration in ALL[48]. In a preclinical model of BCP-ALL, the targeted inhibition of CXCR4 and its ligand stromal-derived factor 1 (SDF-1) signaling via the small-molecule inhibitor plerixafor in mice prevented dissemination of BCP-ALL blasts into the skull, vertebral bone marrow and subarachnoid space[49]. Furthermore, cellular pathways controlling cell motility are induced due to integrin activation. Chemokines, cytokines, and growth factors are soluble factors known to drive metastatic disease by guiding the chemotaxis, invasion, and colonization of liquid and solid tumors. The BM, CNS and skin are vital compartments affected by leukemia, in which SDF-1 is synthesized and secreted, luring in leukemia cells via chemoattraction. More specifically, its expression initiates early during cortical development, thereafter exhibiting high levels in both the developing cortex and meninges. Postnatally, SDF-1 maintains consistent expression in various brain regions, including the hippocampus, persisting throughout the organism's lifespan[50].

VEGF reportedly regulates neovascularisation/angiogenesis and endothelial cell growth in normal and abnormal situations. It also plays a critical role in controlling vascular permeability, transendothelial migration, and cellular survival[51,52,53,54]. Lymphocytes and leukemia cells are known to use transendothelial migration to traverse the endothe-

lial layer. This depends on the presence of integrins and other adhesion molecules on their surface to bring about the morphological changes needed[55,56,57,58]. Leukemia cells secrete VEGF and express functional VEGF receptor (VEGFR) which contributes to tumor growth and dissemination. More to the point, VEGF can promote transendothelial migration of ALL cells, whereby VEGF/VEGFR2 signaling interference of endothelial cell kinases disrupts their barrier function, enabling cancer cell extravasation[38]. VEGF was found to drive leukemia proliferation, migration, matrix metallopeptidase-9 production, and breaking down the BBB by disrupting tight junctions. Treatments on mice primary xenografts could reduce leukemia burden in the CNS, but no other compartments. Interestingly, data from Akers et al. show that ALL leukemia blasts do not induce an inflammatory phenotype in the brain microvasculature endothelial cells associated with extravasation[59].

1.3.4.2 Fusion Protein-Interleukin Interactions

Patients with the TCF3::PBX1 fusion protein show a higher number of cases of CNS involvement at initial diagnosis and relapse[13]. The Tyrosine-kinase MER was initially identified as a molecular target for CNS involvement; MER is unregulated in many BCP-ALL patient samples; however, there currently is no evidence to point out that TCF3::PBX1 directly regulated MER. PBX1 has been shown to alter IL7 receptor signaling and high expression of IL7R. Other sources claim PBX1 may positively mediate ALL survival within the CNS[60,45]. A blood brain barrier (BBB) co-culture model with BCP-ALL cells revealed resistance to the CNS-directed therapeutic drugs cytarabine and methotrexate, driven by PBX1[45]. Others reported decreased sensitivity to these drugs in apoptosis and proliferation assays in cells expressing PBX1[61]. Furthermore, protection of leukemia blasts within a choroid plexus niche was reduced via shRNA (but not control shRNA) knockdown of PBX1 in a co-culture of blasts and CPs[60].

1.3.4.3 Cell Survival in the CNS and Response to Hypoxia

New insights into signaling pathways regulating/affecting CNS homing and survival in BCP-ALL have emerged in recent years. Understanding the mechanism of action regulating CNS relapse could provide avenues for directed therapy to minimise toxicity. Leukemia cell survival and resistance to chemotherapy pose a significant challenge to overcome with newer therapeutics. In pediatric AML, CXCR4 expression has been previously introduced as an adaptation to chemotherapy[62]. BCR signaling via the

ERK pathway represents one of the pathways mediating cell survival[1,44,63,64,65]. Higher VEGF expression has been associated with cell adaptation to hypoxia[1,66]. These findings were further explored in the same study. Human VEGF in xenograft mice was targeted by administering Bevacizumab, a monoclonal VEGF antibody that blocks the binding of VEGF to either VEGFR-1 or VEGFR-2. CNS-leukemia, but not BM or Spleen leukemia, was reduced, in addition to a reduction of meningeal infiltrates, which remained unchanged in control mice. High levels of VEGF expression remained in both CNS and BM, indicating that human VEGF governs the ablation of the leukemia burden in the CNS[38]. Adaptation in BCP-ALL associated with treatment failures are especially relevant after dissemination into the CNS niche.

Hypoxic conditions occur in spaces with below-optimal oxygen concentrations. Meanwhile, cancer cells are known to require large amounts of energy to sustain growth. One of the hallmarks of cancer describes the adaptation in energy metabolism; however, this shift would introduce nutrition deficiency and accumulating waste affecting nearby non-tumor cells. Glycolysis in normal cells generates energy, but tumor cells produce lactate through high glycolysis activity, known as the Warburg effect observed by Otto H. Warburg in the early 20th century[67]. The hypoxic conditions that can occur in the bone marrow have long been favored to promote the survival of leukemic cells within this niche. In fact, the hypoxia-gene expression has been documented in leukemia cells under low physiological oxygen levels experienced in the CNS[66]. The state of hypoxia is significant for various bodily functions such as cell metabolism, survival, proliferation, and angiogenesis, as well as for disease processes like cancer development and metastasis[68,69,70]. Novel treatment strategies have been sought to prevent adaptations of leukemia cells to the low oxygen and nutrient levels in the CSF environment of the meninges. Hypoxia also contributes to leukemia resistance to chemotherapy and radiotherapy and promotes its progression[71,72,73]. Methotrexate (MTX), a folate analogue used in childhood BCP-ALL and auto-immune disease treatment, inhibits deoxyribonucleic acid (DNA) synthesis by depleting thymidylate and purine nucleotides. This induces cell death through DNA strand breakages and cell death. Prednisolone (PRD), a glucocorticoid that binds the glucocorticoid receptor (GR), is used in ALL treatment. Cell cultivation under normoxic (21% O2) or hypoxic (5% O2) conditions, followed by treatment with MTX and PRD, revealed a protective effect of the hypoxic condition on the viability of tested BCP-ALL cell lines. Further

analysis of these cells revealed that hypoxia may modulate the expression of pro- and anti-apoptotic proteins, thereby promoting chemotherapy resistance in BCP-ALL[71]. A study comparing ALL cells from the CNS and bone marrow revealed that adaptations to hypoxia were present in CNS-leukemia. The study used whole human-genome expression analysis to screen sample pairs from meningeal infiltrates. BCP-ALL xenograft mice showed VEGF expression after transplantation. VEGF expression is significantly increased in ALL cells derived from the CNS2[71]. Moreover, the role of VEGF in mediating transendothelial migration and cancer dissemination was detailed above. Leukemia cells in the CNS are thought to acquire a state of quiescence. Here, the microenvironment plays a supporting role in generating survival signals in leukemic cells. Such has been considered to be supported by members of the AP-1 pathway[74]. The transcription factor activator protein 1, or AP-1, are a family of dimers consisting of the JUN, FOS, FOSB and other activating transcription factor protein families. The component JUN is elevated in AML and supports cell growth and survival in AML. AP-1 has also been associated with hematological cancers, including ALL[74,75]. Specifically, FOSB is associated with CNS-leukemia[76]. Recent evidence has shown success in targeted inhibition of AP-1 in cancers, such as MLL-r leukemia[75].

1.3.5 Conventional Treatment Strategies and CNS Prophylaxis

Studies conducted in the 1970s suggest that before routine CNS prophylaxis, 50% to 75% of children experienced CNS relapse, usually within months of the original diagnosis. This high rate of early CNS relapse suggests that occult CNS leukemia was present from the outset, emphasising the limitations of past detection methods in identifying subclinical CNS disease[1,29]. A central nervous system (CNS)-directed therapy can be taken up early in clinical treatment; however, it should be specific to the treatment subject in question[77]. CNS relapse was reported in more than 30% of patients without a prophylactic regimen[78]. The goal of their inception was to prevent CNS infiltration; however, it has since been reported that the CNS is likely affected at the onset of the disease. Current CNS-directed treatment involves intrathecal/systemic administration of glucocorticoids (dexamethasone), intrathecal/intravenous (high-dose) delivery of methotrexate and cytarabine, and asparaginase[14]. The success of such a treatment regimen had already been revealed in long-term follow-ups during the late 90s, adopting dose-intensive therapy courses of Hyper-CVAD (hyperfractionated cyclophosphamide, vincristine, doxorubicin, and dexamethasone)[79]. Intrathecal (IT)

therapy, involving the direct injection of chemotherapy into the CSF, is crucial for CNS-directed therapy due to the poor CSF penetration of many systemic anticancer agents. The COG AALL1131 trial explored the efficacy of prophylactic triple intrathecal therapy (TIT) (methotrexate, cytarabine, and hydrocortisone) versus single intrathecal therapy (methotrexate alone) post-induction in high-risk BCP-ALL patients aged 1–31 years, excluding CNS3 patients. The trial was halted due to a since TIT could not be deemed superior to IT MTX. While a non-significant trend towards reduced CNS relapse rates was observed in the TIT group, it was met by an increase in isolated bone marrow relapses. Lastly, neurological toxicity rates did not differ between the IT MTX and TIT treatment groups. Taking the current leaps in the successful treatment of ALL patients aside, we still face room for improvement in diagnosis and the potential prospect of life for patients after therapy[80,81]. Early prophylactic radiation therapy has since been replaced by intensive systemic, intrathecal applications of chemotherapeutic agents such as methotrexate and cytarabine (Ara-C)[16]. An example study in adult patients for Ph-positive ALL included a combinational treatment of imatinib or dasatinib with prednisone and CNS prophylaxis, leading to a complete remission rate (CR) of 96% to 100%[82,83]. However, this is usually accompanied by severe side-effects affecting patients quality of life.

1.3.6 Current Limitations in BCP-ALL Treatment Efficacy due to Toxicity

Detrimental short-/long-term burden to the CNS (including haemorrhages, leukoencephalopathies, chemical meningitis, and neuropsychological and spinal dysfunctions) still lingers[84]. Treatments are often accompanied by but are not limited to, high neurotoxicity of irradiation, increased risk for secondary neoplasia, endocrinopathy, and neurocognitive dysfunction. "Serious Adverse Events" (SAE) have been observed in 4-12% of children[85]. From a broader perspective, the current use of therapy control has significantly improved the healing and survival rate of children diagnosed with ALL. This, however, should not undermine the need for therapies with low long-term toxic side effects and, if necessary, better use of CNS treatments while trying to limit their use. Regarding CNS-BCP-ALL, cells are mainly found in the meninges that cover the brain and spinal cord and only spread to the brain tissue during the advanced stages of the disease[86]. It has been suggested that since CNS involvement in children with ALL appears at diagnosis, drugs targeting leukemia cell migration to the CNS may merit limited clinical success. Additionally, further research is required to verify if the

migration from blood and bone marrow persists after the first seeding. This can be explored through pre-clinical or clinical models, where treatment is initiated once CNS involvement is detected. Treatment is also limited by the need for more efficacious drugs that pass the CSF to the site of residing leukemia cells. Various chemotherapies, including vincristine and methotrexate, are currently used for ALL treatments. These chemotherapies work by blocking the cell cycle and inducing cell death. Novel drugs have been used to target the dissemination of leukemia into leptomeninges. CXCR4 antagonists Plerixafor and BL/8040, block the CXCR4/mediated migration across meningeal blood vessels[1]. However, cell survival mechanisms resulting from critical molecular adaptations in leukemia cells challenge new treatment strategies.

1.3.7 Promising Targeted Therapies Tackling Molecular Adaptations in CNS-BCP-ALL

Recent research has focused on understanding the biology of CNS involvement in BCP-ALL to develop targeted therapies. Studies have explored metabolic adaptations of leukemic cells to the CNS environment and identified potential therapeutic targets such as VEGF and mRNA translation, which could offer new avenues for treatment[1]. One promising approach involves the use of combined inhibition targeting the anti-apoptotic regulators BCL-2 and MCL-1. When used in combination in preclinical models like patient-derived xenografts, this has shown significant reductions in leukemia loads. This suggests a powerful strategy against high-risk BCP-ALL by co-inhibiting BCL-2 and MCL-1 and enhancing therapeutic outcomes through targeting the mitochondrial apoptosis pathway, which plays a critical role in the survival and treatment resistance of cancer cells, particularly in BCP-ALL[87]. Another important pharmacological option is Blinatumomab, a bispecific T-cell engaging (BiTE) antibody construct that recruits T cells to target CD19 on BCP-ALL cells. While Blinatumomab is more effective than standard cytostatic agents, not all patients respond to the treatment. A study focusing on predictors of efficacy for Blinatumomab in BCP-ALL patients revealed that non-responders showed impaired CD19-BiTE-mediated cytotoxicity *in vitro*. This research suggests that the functionality of patient-derived T cells, particularly their ability to proliferate and exert cytotoxic effects in the presence of Blinatumomab, could serve as biomarkers for identifying potential non-responders before or early during treatment[88]. These studies provide insight into current pharmacological strategies

against BCP-ALL, underscoring the importance of targeted therapies and the need for personalized treatment approaches based on specific patient and disease characteristics. As research advances, integrating these novel therapies into clinical practice could improve outcomes for patients with BCP-ALL, providing more effective and potentially less toxic treatment alternatives.

1.4 A Brief Overview of Preclinical Model Sytems in BCP-ALL

1.4.1 2D *in vitro* Cell Culture Models Can Not Represent Three-Dimensional Tissue Microenvironments

Researchers have long relied on two-dimensional (2D) cell cultures and animal models to study tissue and organs' formation, function, and pathology. However, critical areas for improvement in their ability to accurately reflect the complex three-dimensional environment limit their use case. In this regard, it has been shown how cell-cell/cell-matrix interactions and morphology differ between 2D and 3D cultured cells. Although two-dimensional (2D) cell cultures are a well-established and versatile model system, conventional monolayer cultures do not fully recapitulate the physiology of biological tissues[89,90,91,92,93]. Furthermore, the complex cortical layers of the brain cannot be modeled under 2D conditions.

1.4.2 Rodent Model Systems: Benefits and Shortcomings

Murine models have long been used as a means to recapitulate human ALL. These can be categorized into spontaneous, induced, transgenic, and transplant murine models. The first three centre around the animal tumor, while transplantable models include allogeneic and xenogeneic transplantation, most commonly involving human tumor xenografts in immunodeficient mice. With the onset of the (NSG) mouse model, a total absence of NK cells was achieved, negating the need for irradiation before the injection of leukemia cells. At its core, the NSG model combines a knockout of the IL-2 receptor gamma common-gamma-chain with the "nonobese diabetic/severe combined immunodeficiency" (NOD-SCID)[94]. These have become invaluable for establishing PDX models for drug screening pipelines and preclinical trials. Transgenic models intend to introduce the known genetic alterations associated with leukemia into mice. The latter is an approach to immunocompromise mice to enable consistent and stable leukemia

engraftment. Progress in developing syngeneic models has led to the onset of inducible models that control transgene expression. Introducing these genetic aberrations into mice allows a better understanding of pathways underlying leukemogenesis, thus contributing to potential therapeutic targets. However, drawbacks to the model's efficacy remain. Recreating the human disease in mice can, for instance, be significantly affected by the choice of promoter used in gene expression. Furthermore, protein-protein interactions between human and mouse models may differ. Syngeneic models, however, benefit in modeling leukemogenesis by conserving key microenvironment factors that may otherwise have to be introduced at physiological levels in xenograft mice. Early models of an immunodeficient murine model involved pre-irradiation of mice before transplantation[94,95]. The inherent advantage to these models comes partly from the species' relatively low cost and short life cycles. What is more, 99% of human genes have been found to exist in mice, while gene homology may be up to 78.5%. Tumor growth in the spontaneous tumor models conveniently anneals to that of human tumors, which may reveal the effect of genetic factors on tumorigenesis. Inducible models, introducing genetic perturbations via exogenous carcinogens, greatly benefit from less complexity, a shorter experimental timeline, and higher reproducibility. Disadvantages of the murine model include their association with high expenses, significant time investment, and ethical considerations[96,97]. Given their long experimental cycle and high cost, these attributes have been associated with the spontaneous animal tumor model. Moreover, inducible models may yield higher mortality and variability of lesions. Many transplantable tumor models' immunodeficiency needs to be handled in an aseptic environment. Furthermore, not all human tumors, such as in leukemia, successfully engraft in rodent models. Harvested human cancer cells from the animal likely require separation from the murine material, adding to the complexity[94,95].

1.4.3 Brain Architecture and Development in Rodents and Humans

The early development of the central nervous system (CNS) differs significantly between rodents and humans. The ventricular zone is where stem and progenitor cells reside, undergoing different types of division. Symmetric division occurs early in the division, leading to the initial amplification of the progenitor pool. Later, asymmetrical division occurs whereby a secondary division leads to another progenitor, which migrates outward to become a neuron. In another case, it may also form intermediate progenitor

cells (IPs), which divide into two terminally differentiating neurons once more. These are examples of direct and indirect neurogenesis, respectively. During the developmental phase of the CNS in rodents and humans, the posterior brain is similar, while the cortex is vastly expanded. In addition to the ventricular zone (VZ) and the cortical plate (CP), the human brain contains the outer subventricular zone (SVZ). The SVZ includes a specialised cell type known as "outer radial glial" (oRG) cells, seldom found in rodents. During neurogenesis, oRG cells behave as a transit-amplifying population. oRGs are neuronal progenitor cells (NPCs) that asymmetrically divide into IPs. As a result, the continuous asymmetrical cell division in the developing human cortex can yield vastly greater populations of neurons compared to rodents. This contributes to the prospect that certain aspects of brain development cannot accurately be modeled using rodent systems[98].

1.5 The Organoid as an Emerging 3D *In Vitro* Model

1.5.1 Emergence of The Organoid Term and Current Definition

Between 1965 and 1985, the term "organoid" referred chiefly to experiments in developmental biology involving dissociation and reaggregation. In the last decade, this term experienced a revival. The near-endless capacity to self-renew and differentiate into a large swathe of cell lineages made ES and hiPS cell technology invaluable in developmental biology. A great pioneer arrived in Yoshiki Sasai and his colleagues sought to exploit a new use case. They proposed that 3D cultivation of pluripotent stem cells would unlock an inherent capability to self-rearrange and organize in layered structures driven by their genetic program. In this way, they sought to investigate spatial patterning and morphogenesis in early organogenesis *in vitro*[99,100,101]. An organoid can be defined as an *in vitro* multi-cellular unit that can recapitulate the structure and functional characteristics of a particular organ or tissue within the body. These can take many forms, annealing to the organs in our body that it is trying to mimic. While the point at which something becomes an organoid is open to discussion, it should carry complexity, multi-cellularity, and three-dimensionality distinct from traditional monolayer cell cultures. Organoids can be generated using stem cells. As the stem cells differentiate and self-organize, the desired structure of the organoids is formed. This is one of the numerous methods of generating organoids[102,103]. The advantage of using stem cells lies in their self-organization

and formation of intricate structures (such as kidney nephrons). Hence in the field, researchers are using this approach to understand the formation process of, e.g. brain tissue, kidney tissue, etc., as well as using it as a basis to understand the disease states (e.g. microcephaly in the brain organoid model/kidney disease phenotype).

1.5.2 Brain Organoids: Stem Cell Differentiation and Patterning Factors

The advancements in stem cell research made in recent decades have led to revolutionary approaches in stem cell research. Tools enabling the re-programming of human somatic cells to produce hiPS cells which can be precisely pushed along a specific cell lineage have introduced methods of human embryonic, as well as organ development and disease[104]. In the last decade, pioneering work on the three-dimensional stem cell culture by Yoshiki Sasai laid the foundation of what organoid research would become. It is known that spontaneous neural differentiation occurs in embryonic stem (ES) cells without intervening with inhibitors (e.g. BMP, Nodal, Wnt). This was termed a "neural-default state" for ES cells years ago[99]. Using a serum-free floating culture (SFEBq), Sasai and colleagues achieved neuroectoderm formation and identified stratified cortical development in organoids. Organoids can be cultivated from two categories of stem cells: (i) pluripotent embryonic stem (ES) cells and induced pluripotent stem (iPS) cells, and (ii) organ-restricted adult stem cells (aSCs). Omitting any patterning factors (Fgf, Wnt, BMP) led to the formation of rostral hypothalamic tissue. Applications of said patterning factors allow for control of alternate regional identities. Significant overlap to human tissues exists in the types of patterning or extrinsic signaling molecules adopted, indicating that inhibitions of critical pathways such as BMP, GSK3β or Wnt are vital to generating well-differentiated neuronal populations[105]. Lancaster and Knoblich have been credited for generating matrix-embedded organoids bearing multiple brain regions[103]. Recent publications involving cerebral organoids have, in one way or another, built on their organoid publications. The composition of culturing media has emerged as a critical factor to guarantee high-quality organoids. Lancaster et al. adopted retinoic acid early since it is reported to support neuronal differentiation *in vivo*[102]. Gabriel and colleagues introduced modifications with an ALK5 inhibitor (SB431542) and an AMPK pathway inhibitor (Dorsomorphin) (table 10). In this example, spheroids generated from hiPS cells are treated with inhibitors to activate key pathways promoting neuronal differentiation of the neurosphere while suppressing the bone morphogenic protein

(BMP) and the TGFβ/activin/nodal signaling pathway[106,107,108,109]. Combining these factors may enhance neural differentiation more effectively than using retinoic acid alone.

1.5.3 Cerebral Organoids: Structure and Characterization

Cerebral organoids are named as such, as they were designed to recapitulate structural features found in the developing neocortex. It should be pointed out that organoids develop for an extensive time but are limited by the culturing technologies available today. The formation of neural rosette-like structures shows this maturation that forms the distinct layers of the pseudo-neuroepithelium[105] (fig. 3). They are typically layered in several layers of development, beginning from the lumen (centermost part of rosettes), where early progenitors reside. Like the human neocortex, the further the structure expands, the more differentiated cell types one would find. To summarize, the ventricular or rosette-like structures bear a defined radial outgrowth from their centre, starting with outer radial glia towards more differentiated neurons at the apical site of these rosettes. If one imagines a single slice of these structures, progenitor cells (Nestin/SOX2), outer radial glial cells (oRG) (PAX6), and ventricular radial glial cells (vRG) (PAX6, HOPX, FAM107A) make up the ventricular and sub-ventricular zones within the basal layers. Deep-layer and upper-layer neurons in the apical layers can include astrocytes (GFAP) and neurons positive for a range of markers (e.g. MAP2, TUJ1, TBR1, Reelin). Many abundant proteins have been identified for neuronal cell types in organoids.

1.5.4 Applications of Organoids in CNS Cancer Research

1.5.4.1 Tumor-modeling Organoid Systems

In their early development, "organotypic tumor spheroids" were one example of patient tissue-derived organoids[110]. Here, " organoids " are aimed to closely mimic human tumor tissue for *in vitro* studies. Today, their terminology resembles their purpose closer; "tumoroids" or "tumor organoids". While early cultures involved serum-supplemented media, modern protocols closer anneal that of healthy tissue organoids, being serum-free; however, patterning factors are omitted to mainly produce tumor cells. Difficulties exist in the success rate of generating these organoids *in vitro*. To their advantage, mimicking patient tumors is superior to conventional *in vitro* models since they carry the key *in vivo* features and survivability *ex vivo*. Clonal

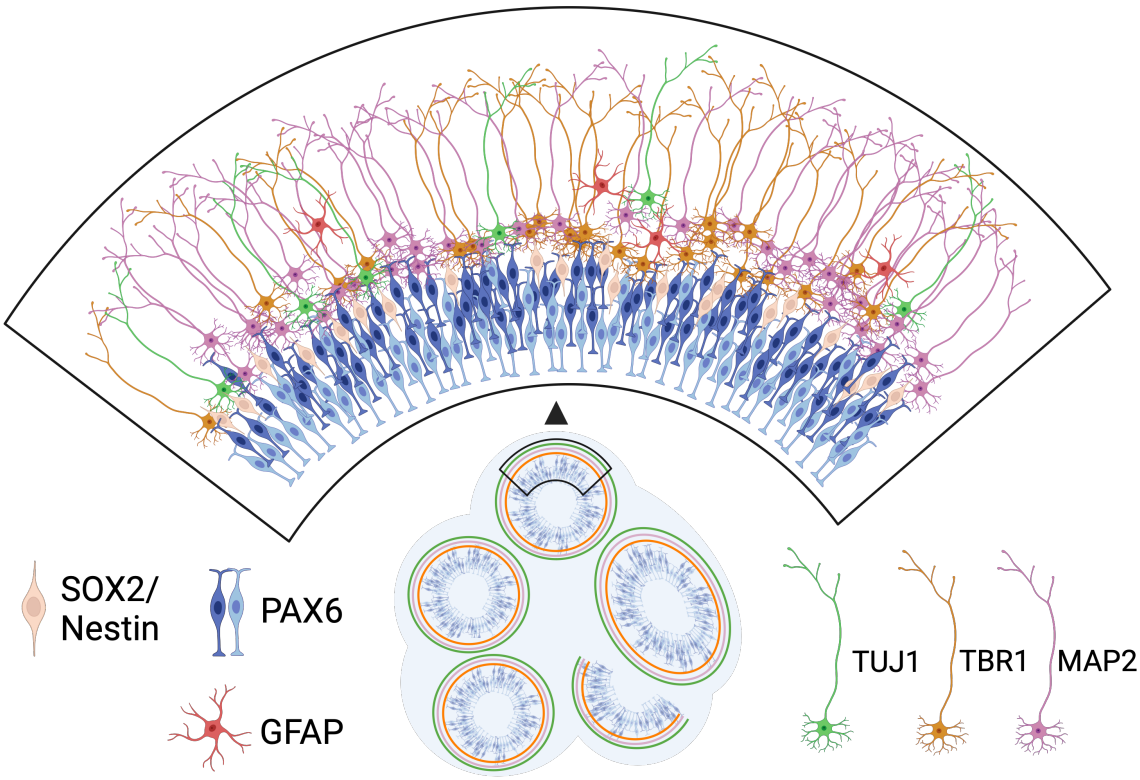

Figure 3: Structural Organization and Cellular Identity in Matured Cerebral Organoids- The schematic illustration shows the structure and cellular identity typical for cerebral organoids (bottom-centre). The neuroectoderm (top-centre), which becomes prominent during the early stages of organoid maturation, can best be characterized by the immunochemical staining of slices. Rosette-like structures emerge from immature organoids and experience a radian outgrowth into multiple zones. Ventricular radial glial (vRG) cells, commonly positive for PAX6, form the ventricular zone (VZ). During maturation, multiple progenitor layers emerge, adding subventricular (SVZ) and outer subventricular zones (OSVZ) bearing outer radial glial (oRG) cells; these cell types are critical in the asymmetrical cell division of the developing human cortex. Cells of the OSVZ give rise to intermediate progenitors (IPs) and neurons which surround the ventricular zone. hiPSare detectable with anti-SOX2/Nestin markers. Neurons express markers such as beta-three tubulin (TUJ1), T-box brain protein 1 (TBR1), and even microtubule-associated protein 2 (MAP2)[99,100].

evolution, i.e. the degree of genetic heterogeneity resulting from extended *ex vivo* culture, is not limiting their application. Thus, expanded tumor organoids can be matched with healthy organoids. Glioblastoma (GBM) multiforme is a rapidly growing and aggressive brain tumor. Tumor organoids derived from GBM patient biopsies

were already created in the 1980s. Even then, it was shown that the genomic profile and cellular and molecular phenotypes of the original patient tumor were conserved, whereas primary cell cultures were deviating away. Also, the inter- and intra-tumoral heterogeneity of the tumor were represented[110,111,112,113]. Drawbacks in this model exist, which will become relevant for healthy tissue organoids (stem-cell-derived organoids) in subsequent chapters. In short, vascularisation of the tumor tissue is a crucial component lost *ex vivo*, accompanied by losing an immune component. Brain, breast, kidney, and liver tumor organoids are only a tiny subset published today.

1.5.4.2 Tissue-modeling Organoid Systems

Recent shifts to interrogate human cancer in 3D cultures show a more progressive research field. Molecular mechanisms of patient tumors can be studied by newer 3D *in vitro* models. Furthermore, increasing the adoption of 3D models can improve protocols and drive modern tissue engineering. Such developments have occurred with the onset of stem cell-derived organoids. Brain organoids are a stem cell-based 3D *in vitro* model, which partially resemble the brain of their donor host in the regional organization and cell identity[102]. Organoid technologies have already become a valuable tool in biomedical research, as a model of organ function and a potential screening method for pharmacological studies[113,114,115]. The versatility of organoid technology provides a range of applications in the field, primarily by forming human structures that can be grown in the lab. It has traditionally been challenging to interrogate human tissue/organs in the lab since these must be developed from patient-derived material. Such an approach would interfere with the prime directive in patient care; to improve the health and maintenance of the patient. Luckily, the organoid model may provide a way around this issue, allowing researchers to study human diseases that could not have been studied before. Research around the cultivation and characterization of human brain organoids has been evolving rapidly over the last few years, such that they can be tailored to model specific regions of the brain (i.e. cerebrum, midbrain, frontal lobe etc.)[113,114,115]. However, stem cell-based 3D culture models are gaining traction in cancer research[116,117]. Recent research on co-culture assays of cerebral organoids with glioblastoma stem cells (GSCs) yielded positive results to consider their application in CNS invasion studies[115,118]. Moreover, a newly published organoid protocol has tackled hematological disease by creating organoids bearing a bone marrow-specific

environment[119]. Studying cancers *in vitro* has also seen a different approach to stem cell-based organoid models through *biomimetic*. This term refers to a branch in bioengineering aiming to raise the cell and matrix complexity of 3D models[120]. This approach shows more relevance in creatig *solid* tumors. That said, cerebral organoid models had never been employed in ALL research.

1.5.4.3 Pre-Clinical Applications of iPS-derived Organoids

A significant proportion of leukemia patients will face the likelihood of CNS disease. The mechanisms of invasion and adaptation of cells to a hostile environment are core targets for novel treatments. Murine and 2D monolayer cell models form part of the pre-clinical model group, providing new mechanistic insights. Unfortunately, both systems feature inherent disadvantages. Furthermore, an increasingly stronger push towards alternative pre-clinical models has been seen with the adoption of the organoid model. However, this model has been chiefly adopted for brain cancer research, such as glioblastoma stem cells (GSCs). GSCs are adherent cells shown to interact and invade organoids by forming invading protrusions. Patient-derived samples have also been used to test the specificity of the model. By comparison, BCP-ALL leukemia cell *in vitro* cultures are primarily in suspension. Until now, the capability of leukemia cells to engraft into brain organoids has been unknown. The field of CNS leukemia has yet to approach organoids as a model of invasion. Drug compound testing using preclinical models is highly relevant and is an avenue that has been studied with GSC-organoid experiments. Investigating the effect of drug compounds on cell engraftment in the context of leukemia will be another first. The analysis of brain organoids has seen rapid development in recent years. Organoids are most often imaged using laser scanning confocal microscopes or, most recently, using advanced light-sheet microscopes. Image analysis can be performed to reveal events and structural features of organoids. However, such applications can be prohibitively expensive and require maintenance. Novel computer pipelines offering automation in analysing large batches of organoid images exist but have yet to become mainstream. An example of this approach, combined with the precision of light-sheet microscopy, has delivered stunning insights into the organization and development of brain organoids[121,122]. A new type of pipeline to fully characterize the engraftment of cells into organoids is urgently needed.

This PhD thesis focuses on the suitability of the *in vitro* brain organoid model to

determine the migration of BCP-ALL cells into the CNS tissue. To achieve this goal, ALL cells with the translocation *TCF3::PBX1* (a risk factor for brain metastases) will be cultivated together with brain organoids. In parallel, other clinically relevant subtypes, CNS low-positive samples, and CD34+ HSPC cells will be tested as negative controls. The evaluation is performed by confocal microscopy, as the ALL cells are coupled with a fluorescent molecule and thus can be detected in the brain organoids.

Aims and Objectives

The human organoid is emerging as a competitive alternative to the well-established pre-clinical models of the last decades. A growing body of literature is beginning to address initial barriers, incorporating it as a pre-clinical model. BCP-ALL leukemia is frequently associated with a detrimental CNS-component, while treatment requires new biomarkers and therapeutics to improve the prognosis for patients. Established *in vitro* and *in vivo* models continue to test potential therapeutic targets for CNS disease; however, several shortcomings of both limit a faithful recapitulation of human biology. Pluripotent stem cell research has already let to the generation of diverse cell types, driving the progression of increasingly complex organoid models. Brain organoids are a diverse group of organoids, mimicking different regions of the human CNS. Cerebral organoids (specific to the human cerebrum) have already found a footing in cancer research as models of cell invasion. No models of BCP-ALL CNS disease exist; furthermore, new analysis pipelines for cell invasion are required. This thesis details how cerebral organoids may pose a promising model for CNS leukemia research and aims to implement the missing developments listed below.

① Establishment of a first-of-its-kind invasion assay between leukemias and cerebral organoids. The aim is to set standardized experimental conditions and test the specificity of the system by comparing high-risk CNS-leukemias and controls with low to no CNS-implications.

② Establishment of a novel computational pipeline to study leukemia engraftment characteristics. This can provide a qualitative assessment of proportion and depth of leukemia infiltration.

③ Targeting CNS leukemia relevant pathways like CD79a/Igα or CXCR4-SDF-1 in leukemia cells to validate translatability between organoid co-culture and *in vivo* murine models

④ CNS-infiltrating leukemias can utilize cellular adaptations for their survival. The aim is to test whether organoid-leukemia undergo transcriptional modifications as a direct consequence of, engraftment which may be consistent in the literature.

Chapter 2

Materials and Methods

The following methods were conducted as previously described in Gebing et al. *in press*, Blood Advances.

2.1 Cerebral Organoid Cultivation: A Step-by-Step Workflow

2.1.1 Considerations and Disclosures to the Protocol

This project expanded upon existing protocols for cultivating cerebral organoids while introducing alterations to the workflow[102,115,123]. In this way, cerebral organoids were cultured without particular patterning factors while supplementing factors previously documented to improve neuroepithelial outgrowth[123].

2.1.2 Human hiPS cells Cultivation

2.1.2.1 Equipment Required for Human ES and hiPS cell Culture

To effectively carry out the protocols described in this manual, specific equipment is essential, including: an incubator that can maintain a stable environment at 37°C with 95% humidity in a 5% CO2 atmosphere, crucial for consistent biological sample cultivation; a low-speed centrifuge with a swinging bucket rotor, operated with the brake activated to ensure sample integrity; Pipette-Aid and serological pipettes for precise liquid handling; a pipettor with disposable tips for efficient sample transfer; an inverted microscope capable of 20X to 100X magnification for detailed examination of samples; an isopropanol freezing container, recommended for controlled freezing

procedures to preserve biological integrity; freezers for long-term storage, including a unit capable of reaching -150°C or a liquid nitrogen vapor tank for ultra-low temperature storage, a -80°C freezer for long-term preservation, and a -20°C freezer for standard freezing requirements; and a refrigerator that maintains temperatures between 2°C and 8°C for cooling samples, ensuring stability and preventing degradation.

2.1.2.2 Cultivation of Human-Induced Pluripotent Stem Cell Cultures

GelTrexTM (table 8) matrix solution was used t coat culture well for iPS cell culture (fig. 4A). For every 1ml of matrix solution, 10 μl of GelTrex was diluted in 1000 μl of DMEM-F12 (table 8) media in a 15ml Falcon tube, and thoroughly mixed. Sufficient matrix solution was added to coat culture ware to cover the surface of cell culture dishes (table 9). The dishes/plates were placed in the incubator for 1hr if intended for immediate use. For medium to long-term storage, dishes/plates were sealed with parafilm and stored at 4°C or -20°C for short- to long-term storage. The coated dishes/plates were placed in the incubator for 30-60min before use for iPSCs. For recommended passaging methods, refer to the StemCell Technologies iPSC cultivation guide. In brief, human iPSC cultures were held under feeder-free conditions on culture dishes (table 8) pre-coated with GelTrex. mTeSRTM Plus media was prepared for cell culture by adding 100ml of mTeSRTM Plus Supplement to 400ml of mTeSRTM Plus Basal Medium in a filtering tower with 0.22 μm filter (table 8). mTeSRTM Plus medium is only stable for two weeks after preparation. Alternatively, the medium was aliquoted, stored at -20°C for up to 6 months (even at -80°C), and thawed whenever required. Daily media changes were made whenever required to prevent unwanted cell differentiation.

2.1.2.3 Human hiPS cell Lines

HW8 iPSCs (table 3) were generated from normal PBMCs using the CytoTune-iPS 2.0 Sendai Reprogramming kit (A16517, Thermo Fisher Scientific, Waltham, MA, USA) following written informed consent. Study approval was obtained by the internal review board at the National Institutes of Health (NIH, protocol number: 16CN 069). Note: Different iPSC lines were used to exclude any donor-specific impact (table 3).

2.1.3 Neurospheres to Organoids

2.1.3.1 Generating Neurospheres from iPSCs

High-quality, low-passage iPSCs were grown on a Geltrex coating (table 8) in mTeSR Plus to 70-80% confluency and checked for differentiation (fig. 4B-C). Cells are washed in PBS for 5 minutes. Accutase, an enzyme-based cell-detachment reagent (table 8), is added for 5 minutes incubating at 37°C (fig. 4D). After adding an equal amount of DMEM-F12, cells are centrifuged at 400g for 5 minutes. The cell pellet is then re-suspended in 1 ml of STEMdiff™ Neural Induction Medium (table 8) and counted using an automated cell counter (Beckmann-Coulter) (for a U-bottom 96-well plate 35,000 cells are seeded per well) (fig. 4E). The required amount of suspension volume is taken (making sure to resuspend the cells, as they will sink to the bottom of the tube in which they are contained), and sufficient neural induction media is added to it, depending on the number of plates required (10ml per plate)(fig. 5A). Plates are seeded using a multichannel pipette by pipetting the cell suspension from a sterile, plastic reservoir (make sure only to use the same pipette tip 3 or 4 times) (fig. 5B). The plate(s) is(are) then centrifuged at 500g for 3 minutes (fig. 5C), after which the plates are checked to see whether the cells have formed a quasi-circular pattern in the centre of the well (fig. 5D).

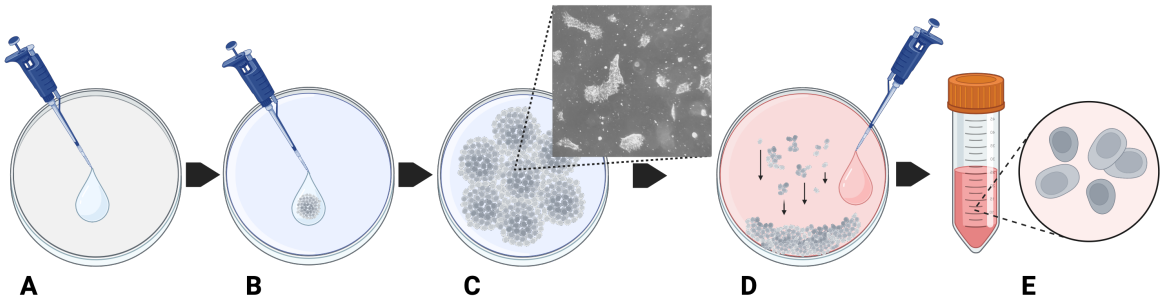

Figure 4: Workflow: Generation of iPSCs: Matrigel coating of cultureware (A) is required for hiPS cell attachment to its surface (B, C). At moderate to high confluency, cells are detached by enzymatic removal (D) to create a single-cell suspension (E).

Day 0; plates were cultured for five days, with media change on days 2 and 4. Neurosphere medium is prepared from a multitude of components: 1:1 (v/v) DMEM/F12 and Neurobasal Medium. Supplements: 1:200 (v/v) N2 supplement, 1:100 (v/v) B27 supplement (w/o) vitamin A, 1:100 L-glutamine, 0.05 mM nonessential amino acids (MEM-NEAA), 100 U/mL penicillin, 100 μg/mL streptomycin, 1.6 g/L insulin, and

0.05 mM β-mercaptoethanol (see table 8. Neurospheres are removed from each 96-well plate using a wide-bore P200 pipette tip, adding at most two neurospheres to a single well of a 24-well plate. Excess media was removed, and 500 μl of neurosphere medium was added. The day 0 neurospheres are then incubated for four days by adding 500 μl of the medium on day 2.

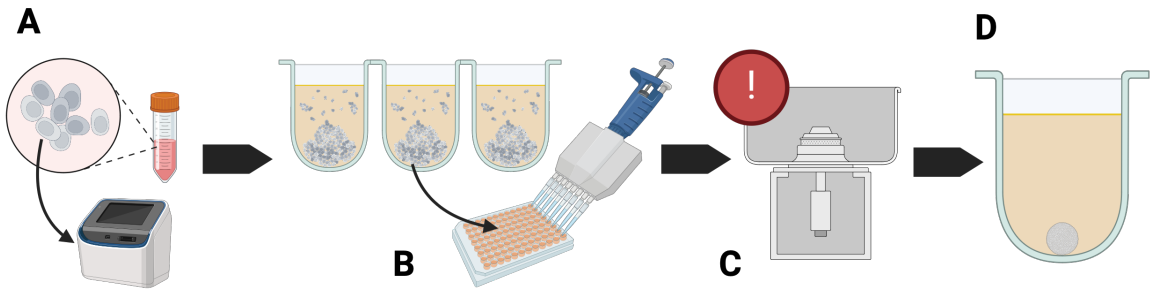

Figure 5: Workflow: Prepping and Plating of hiPSC Suspensions for Neurosphere Formation: (A) An automatic cell counter determines the cell concentration in the hiPS cell suspension. (B) 35,000 cells are seeded per well of a 96-well plate. (C) Centrifugation of the plates forces the single-cell suspension to the bottom of each well. (D) Within a few hours, hiPS cells will form spherical aggregates.

2.1.4 Long-term Culture and Expansion of Cerebral Organoids

Neurospheres are removed on day 4 (see section 2.1.3) using a wide bore pipette (fig. 6A) and added to a spinner flask (CELLSPIN/PFEIFFER, (table 4) with 100ml of organoid media (fig. 6B). The CELLSPIN platform is set to a rotational speed of 15rpm for organoid expansion (fig. 6C). Organoid medium constitutes a similar recipe as neurosphere medium but with the addition of the ALK5 inhibitor (5 μM) SB431542 (table 10) and the AMPK pathway inhibitor (0.5 μM) Dorsomorphin (table 10). Organoid media are also supplemented with factors promoting cell differentiation and survival. N2 Supplement (table 8): This supplement is composed of Insulin, human Transferrin (glycoprotein found in blood plasma is crucial for regulating iron levels and facilitating the delivery of ferric ions.), Putrescine (critical in regulating cell division, differentiation, and maturation, as well as apoptosis), Selenite, and Progesterone. B27 Supplement (table 8): This supplement comprises Vitamins, Proteins, and other components (e.g. monosaccharides). Finally, half of the organoid medium was replaced with fresh media weekly.

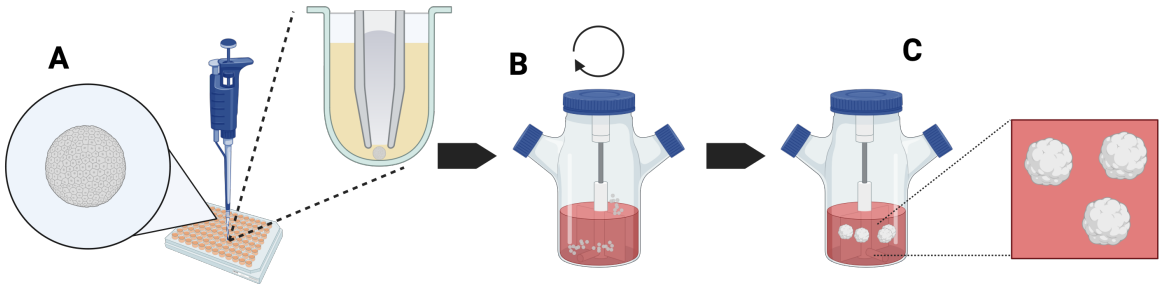

Figure 6: Workflow: Recovery of Early Organoids for Long-Term Culture to Maturation: (A) Spheroids found in the center of each well are carefully removed with a cut-tip pipette. (B) These neurosphere are transferred to a swirling flask set to 25RPM. (C) Organoids mature over time and significantly gain in size within the first month of culture.

2.2 Leukemia and Hematopoietic Stem Cell Culture

2.2.1 BCP-ALL Suspension Culture

All leukemic cell lines listed in table 1 were cultured in RPMI1640 GlutaMAX table 8 supplemented with 10-15% FCS (table 8) and penicillin/streptomycin (table 8). The cell line authentication was regularly performed by short tandem repeat profiling. Primary *TCF3::PBX1*$^{+}$ patient sample (PDX) was obtained from diagnosed or relapsed patients after informed consent approval of the local ethics committee. PDX cells were transplanted in 5- to 9-week-old NSG mice, and at bulk disease detection, the recipient mice were sacrificed upon developing clinical disease signatures. The transplanted leukemia cells were purified (>90% human cells) and adapted to *ex vivo* culture.

2.2.2 Cell Isolation Protocols

2.2.2.1 Isolation of HSPCs (CD34+) from Human Placental Cord Blood

Placental cord blood was received from the José Carreras Stem Cell Bank (University Clinic Düsseldorf). The blood is diluted 1:1 in 1XPBS before separation with Ficoll-PaqueTM Plus (Cytiva). Red blood cell lysis is performed with lysis buffer pH7.4 (Zentralapotheke Uniklinik Düsseldorf) for 5 minutes at RT. The cell suspension is then counted using an automated cell counter (Beckmann-Coulter) to determine the total cell count. CD34+ cells (here termed Human Pluripotent Stem Cells, HSPCs) were enriched using the EasySepTM isolation kit from StemCell Technologies (table 6). Two kits by STEMCELL (EasySepTM Human Cord Blood CD34 Positive Selection Kit II and

Table 1: List of Leukemic Entities Cultured as part of this Project

Cell Name	Fusion Gene	Subtype
697	*TCF3::PBX1*	BCP-ALL
Kasumi2	*TCF3::PBX1*	BCP-ALL
PDX1*	*TCF3::PBX1*	BCP-ALL
HAL01	*TCF3::HLF*	BCP-ALL
SUPB15	*BCR::ABL1*	BCP-ALL
PDX3*	*BCR::ABL1*	BCP-ALL
KCL	*BCR::ABL1*	CML
K562	*BCR::ABL1*	CML
PDX2*(ini**)	*KMT2A*	ALL
PDX2*(rel***)	*KMT2A*	ALL

* = patient-derived xenograft
** = *initial* cell sample
*** = *relapse* cell sample

EasySepTM Magnet, table 5) were used as per the manufacturer's protocol. The isolated cell suspension is then analyzed using flow cytometry to check for CD34+ expression levels and viability. The viability of CD34+ cells was also monitored 14 days post-co-culture by FACS. Over 85% CD34+ and viable cells were used in co-culture experiments.

2.2.2.2 Isolation of CD19+ B-lymphocytes from Human Buffy Coats

Buffy coats donated to the Blutspendezentrale (Universitätsklinikum Düsseldorf, Moorenstr. 5, Düsseldorf) and received on the day of isolation were used for B-lymphocyte-positive isolation. Buffy coats from healthy donors were used to harvest CD19+ B-lymphocytes using the EasySep™ Direct Human B Cell Isolation kit from StemCell Technologies. This kit allows for direct isolation from whoel blood without needing Ficoll. Flow cytometry was used to stain isolated cells with CD19+, resulting in a purity of 98% and viability of 99%.

2.2.3 Stable Live-Cell Fluorescence Staining via CFDA-SE

Carboxyfluorescein Diacetate Succinimidyl Ester (CFDA-SE) (table 6) is a fluorescent labelling dye primarily used for cell tracking and proliferation assays. The molecule is highlighted for its stable cell binding, minimal toxicity with less than 5% cell death, and

suitability as a fluorochrome for cell labeling. Cytoplasmic endonuclease enzymes can cleave the diacetate group from the molecule to form Carboxyfluorescein Succinimidyl Ester (CFSE), which in turn becomes excitable at 488nm wavelength light (498nm peak) and emission at 517nm[124]. To confirm that the CFSE signal is still present after 14 days, all cells were recovered from wells in which organoids and leukemia cells had been co-cultured. Whole organoids were also mashed to include cells enfrafted in them. The resulting cell suspension was stained with CD19+ to compare the signal with CFSE to see if all CD19+ cells are double-positive with CFSE compared to controls.

2.2.4 Lentiviral Transduction of Cells

This protocol and the lentiviral transduction of cells was provided by Melina Vogt.

Generation of 697 AP-1 models using LentiX™ Single Shots and Lipofectamine 3000

Lenti-X HEK293T cells (1 million (M) cells) were plated into a 6-well plate in Lentivirus Packaging medium (50 ml Opti-MEM + 2.5 ml FBS + 0.5 ml sodium pyruvate (table 8)) and grown until they reached around 80% confluence. The lentiviral vector plasmid (7 μg, table 2 containing the target sequence was diluted in Opti-MEM, supplemented with 6 μL P300 Reagent (table 8) to a final volume of 250 μL. Additionally, Lipofectamine 3000 (7 μL, table 8) was diluted in Opti-MEM to a final volume of 250 μL. Afterwards, both mixtures were combined (1:1) to reach a total volume of 500 μL, which was subsequently added to Lenti-X Packaging Single shots (table 8). The mixture was vortexed and incubated for 10 min at RT. After short centrifugation of the tube, the entire nanoparticle complex solution was added dropwise to the cell culture medium, and the plates were incubated at 37°C for 48 h. After incubating the cells for 48 h with the viral solution, cells were centrifuged and washed to remove any residual viral particles. The lentiviral supernatant was harvested, filtered through a 0.45 μm filter to remove cellular debris, and added to LentiX Concentrator (one volume of concentrator was diluted with three volumes of supernatant; (table 8)). The mixture was incubated at 4°C for 30 min and centrifuged (1500 x g for 45 min at 4°C). Afterwards, the supernatant was removed, and the pellets were resuspended in media. 100,000 cells of the 697 cell line were centrifuged and resuspended in previously prepared virus solution and added to a 12- well plate. AP-1 and NEG cells were selected by treatment with Puromycin, and cells were 90+% pure for 697.

Table 2: List of Plasmids Used for Lentiviral Transduction

Function	Vector	Selection	Cat. No.
AP-1 Reporter	pGreenFire 2.0 AP-1 Reporter	Puromycin	TR452PA-P
Control	pGreenFire 2.0 mCMV	Puromycin	TR411PA-P

2.2.5 Knockdown Experiments

Cell knockdown models were generated and provided by publication co-author (*in press*, Blood Advances) as previously described[65]. Short hairpin (sh) RNA-mediated knockdown in ALL cell lines were performed as described previously[125]. The shCD79a target sequence (TTCATAAAGGTTTTCATCTTCA) was designed with SplashRNA[126].

2.2.6 Mitomycin-C Treatment

The BCP-ALL cell line 697 was cultivated to 70-80% confluency in 12-well plate and treated with Mitomycin-C at a final concentration of 30nM in RPMI-Glutamax + 1% P/S + 20% FBS (Table 5). All cells were collected and stained with CFDA-SE at a final concentration of 20 μM before introduction into co-culture with mature cerebral organoids. The co-culture was performed according to the standardised protocol (section 2.3.1).

2.3 Co-culture Assays

2.3.1 Standardised Protocol for 14-Day Co-culture Assays

Mature cerebral organoids were grown from iPSC lines (table 3) according to section 2.1.3. Organoids were observed for quality and condition, and the required amount for each experiment was transferred to a 12-well plate (one organoid/well). All wells were washed with PBS to clean organoids from any debris. Each well containing an organoid received 1.5ml of the organoid medium. Cells stained with CFDA-SE at a final concentration of (20 μM) were added at 10,000 cells per well (unless otherwise specific in the particular experiment). Media changes were performed every third day by replacing half of the media from the wells. All experiment plates were left on a shaker platform (table 4) in

the incubator for 14 days, unless otherwise specified (fig. 7).

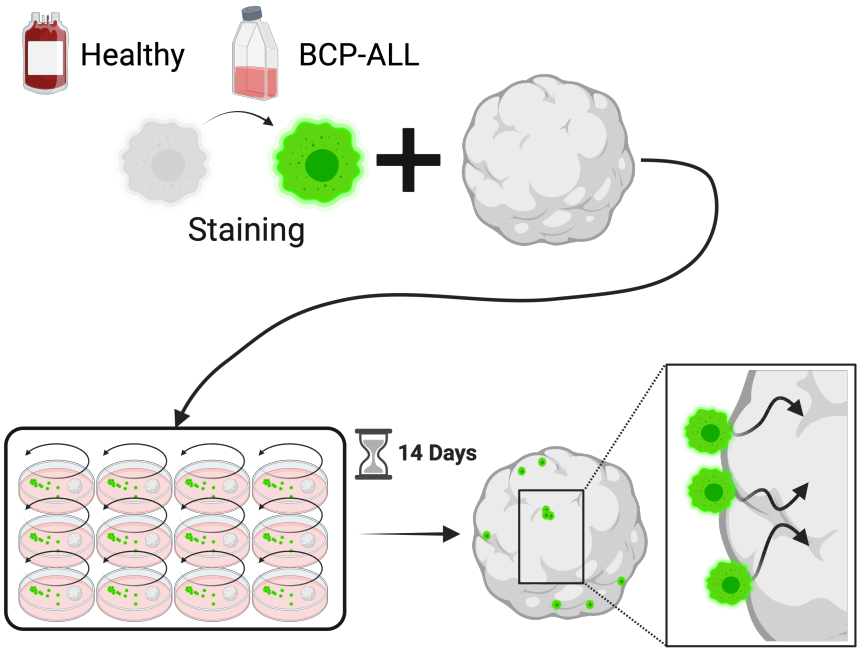

Figure 7: Workflow: Co-culture Assay between of Stable-Stained BCP-ALL Cells and Cerebral Organoids: *Top* - Healthy cells (buffy coat-isolated B-lymphocytes or cord blood-derived HSPCs) and leukemic entities require stable staining via dye to be visible long into co-culture and within organoids. *Bottom* - For investigating cell engraftment between leukemia and controls, co-cultures are running for up to 14 days. Any transmigration of leukemic cells underneath the organoid surface and further in will be visible under microscopy.

2.4 Limited Dilution Experiment

Cells were stained with a final concentration of 20 μM CFSE, per the established protocol (section 2.2.3). Instead of seeding 10,000 cells per organoid, it was decided to dilute the positive control to add 10, 50, 100, 1000, and 5000 cells per organoid (limited dilution series).

2.5 Toxicity Screening

2.5.1 AMD3100 "Plerixafor" (CXCR4 Inhibitor)

An initial drug screening was performed for AMD3100 "Plerixafor"[62] (5mg) by preparing single dilutions of 0.1mM stock to make 1.0 μM, 0.8 μM, 0.4 μM, 0.2 μM, 0.1 μM, 0.05 μM, each as seven repeats per concentration. The com-

pound was dissolved in 100% EtOH (table 7). As a control, the BCP-ALL cells 697 were treated with EtOH at the maximum concentration used (from stock concentration).

2.5.2 T-5224 (c-Fos/AP-1 Inhibitor)

T-5224 ihibits the transcription factor cFos/activator protein AP-1 by specifically inhibiting the DNA-binding ability of c-Fos/c-Jun[127,128]. The 697 and Kasumi2 cell lines were seeded at 0.5M cells per ml in 12-well plates to test multiple concentrations of T-5224 in solution. T-5224 is dissolved in DMSO. T-5224 was added at final concentrations of 10 μM and 1 μM while DMSO treated cells were added as a control to the BCP-ALL cell line 697. Cell viability was measured using an automated cell counter (Beckmann Coulter). Cell remained viable at 10 μM, with 93.1% viability in the 1 μM condition (*data not shown*)

2.6 Cerebral Organoid: Post-Assay Procedures

2.6.1 Organoid Handling: Pipetting Techniques

Adding or removing liquids from vessels can risk damaging or destroying organoids. It was found that the pipette tips should be held near the surface of liquids when aspirating while slowly moving down with the lowering waterline. Furthermore, organoids will move most when the most fluid has been removed. Adding liquid away from the organoid is recommended to prevent any damage (fig. 8A). Washing organoids inside flat well plates requires careful handling. For aspiration, tilting the container will help to remove all liquids without touching the organoid (fig. 8B). Rapid aspiration (red arrows) may lift organoids towards the pipette tip, risking aspiration of the organoid (green arrow). Some liquid may, however, remain, which can be prevented by using round-bottom tubes.

2.6.2 Organoid Washing Buffer

A washing buffer composed of 1XPBS w. 2% Triton-X100, 5% BSA (Sigma-Aldrich), 0.05% NaN (Sodium Azide) was adapted from previous organoid research field[129]. After all Triton and BSA completely dissolve, the solution is filtered through a pump-driven 0.22 μm strainer. A quencher solution of 1XTBS was added for 5-10 minutes at RT after removing FA waste. 1ml of an organoid washing buffer was added to each organoid for overnight blocking at 4°C (some protocols mention up to 3 days of incubation). A DAPI nuclear stain (table 6) labeled all nuclei as a reference for the CFSE-stained cells.

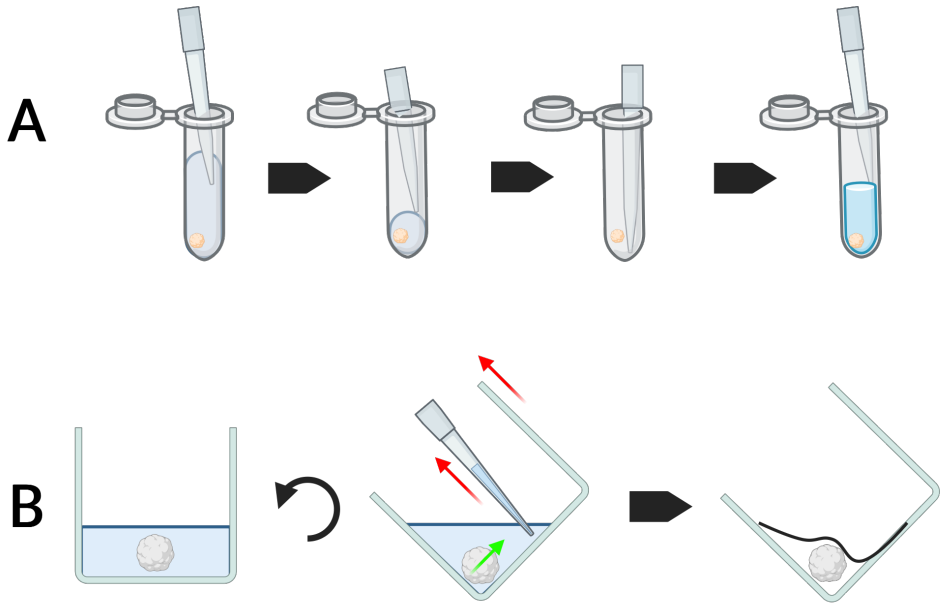

Figure 8: Workflow: Techniques Required for Gentle Removal and Treatment of Organoids: Careful pipetting of organoids is recommended to prevent damage or accidental removal during the fixation/staining periods. (A) Round-bottom Eppendorf tubes provide enough room for organoids and adequate volumes of washing buffer and are sealable to protect organoids from dust and debris. (B) It is recommended to tilt culture plates and not entirely remove all liquid when removing organoids from cell culture.

An example protocol by Sigma-Aldrich using a recommended dilution of 1:600 dilution of an 8 μM DAPI stock solution was used. All samples were incubated for 30 minutes at RT with occasional rocking/shaking by hand.

2.6.3 3D Culture Fixation and Immunofluorescence Staining

Organoids were fixed overnight in 4% formaldehyde (FA) at 4°C and quenched in 1x TBS solution. Blocking was achieved with a washing buffer composed of 1x PBS w. 2% Triton-X100, 5% BSA (Sigma-Aldrich), 0.05% NaN (Sodium Azide) adapted from previous organoid research field[129]. Primary and secondary antibodies (table 6) were prepared in an organoid-washing buffer. Organoids that do not carry a fluorophore were stained with either mitogen-associated protein 2 (MAP2) or beta-three-tubulin III (TUJ1) to stain for protein markers highly abundant in mature neurons, thus marking the surface of the organoids. Cerebral organoids cultured from fluorescent

iPSC cells (table 3) express their own TagRFP-T; no additional staining was required to mark the surface of the organoids. Organoids are washed in 1XTBS solution (10X TBS is made from 100ml 1M Tris (pH 7.5) and 1400mM NaCl in H2O) in-between immunofluorescence staining. Tris is an excellent buffer for various biochemical purposes due to its high buffer capacity, water solubility, and enzyme reaction resistance. It is commonly used to stabilise reaction systems, given that its pH has a stable buffer capacity within the range of 7.5-9.0.

Note: Organoids based on the mtag-RFPt hiPS cell line were utilized in the initial stages of the experiments prior to transitioning to non-fluorescent organoids, which were subsequently stained with anti-MAP2 antibodies in all subsequent experiments. It is noteworthy that these early organoids were not employed for spatial analysis in our computational pipeline outlined in section 2.8.2.

2.6.4 Dehydration via a Dilution Range of 1-Propanol

Following incubating the final fluorescent dye (e.g. DAPI), all washing buffer from the Eppendorf containing the organoid was removed. During the dehydration stage (before clearing), organoids are incubated in a step-wise increasing concentration of 1-Propanol (table 7). A stock solution of 99.9% anhydrous 1-Propanol is diluted in 1X D-PBS, preparing 30, 50, and 70% 1-Propanol-PBS solutions (almost pure 99.9% 1-Propanol is added before clearing). The pH of the dilution is kept between pH9.0 and pH9.2 by placing the solution on a stirrer plate and adding a stock solution of tri-ethanolamine (table 7) (for a 50-100ml solution, a few drops of triethanolamine would suffice). Each organoid is incubated in 30% 1-Propanol for at least 4hrs at 4°C. Afterwards, the diluted 1-Propanol was carefully replaced by 50% 1-Propanol, and the process was repeated for 70% and 99.9% 1-Propanol. The organoid was washed again (1-2 times) in 99.9% 1-Propanol until the supernatant was clear).

2.6.5 Organoid Sample Clearing and Mounting for Confocal Imaging

Fluorescence microscopy visualizes specific antigens by means of primary antibodies targeting antigens, and secondary antibody conjugated with fluorophores. Confocal

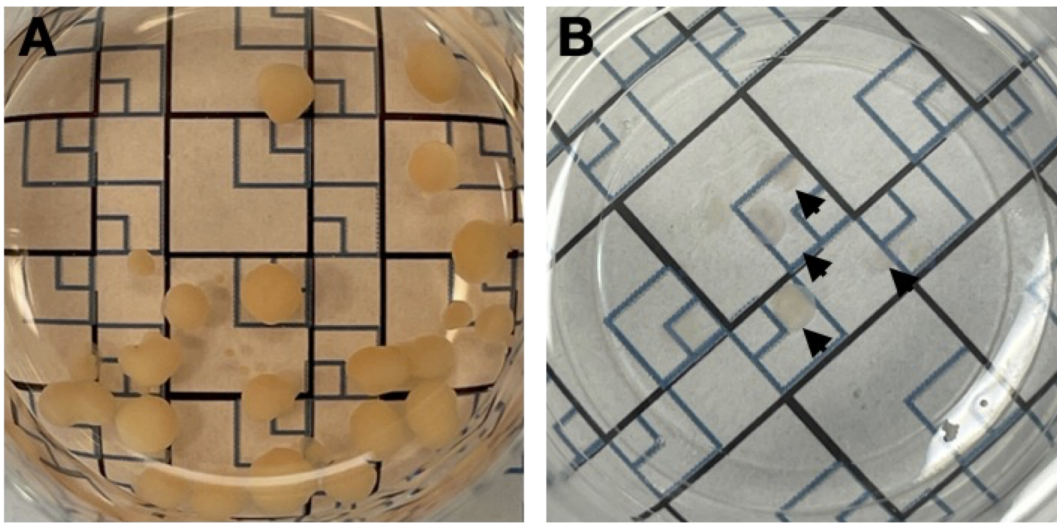

Figure 9: Organoid Clearing for Tissue Transparency - Cerebral organoid samples previously incubated in 99.9% 1-Propanol can be cleared in ethyl cinnamate solution. (A) Mature cerebral organoids in culture media. (B) Cleared organoids (black arrows) are almost translucent after incubation in ethyl cinnamate. Scale paper: Large black box (1.0mm), Middle blue box (5mm), Smallest blue box (2.5mm).

microscopy is a pivotal tool for biological analysis as it enables higher resolution and greater contrast by reducing out-of-focus or background fluorescence, offering a more detailed view of cellular structures and dynamics. To this day, a wide range of protocols have been developed that are usually non-toxic, preserve the endogenous fluorescence of the tissue, and are compatible with a wide range of tissue types. However, disadvantages to their use case remain. Some protocols require up to a week, omitting the duration needed for antibody labelling and imaging. This may be prohibitive for larger screens and higher numbers of samples. It was decided to avoid the 3D reconstruction of many paraffin-embedded slices for leukemia-organoid co-culture assays. Not only does the size of the tissue expend the complexity and time required for imaging, but the risk of distortion ins may impact the model's accuracy when working on the scale of a few leukemia cells in a larger tissue. In essence, it was preferred to identify the spaces within the organoid in which invading cells target. More importantly, and as was described earlier, scalability and accelerated throughput of organoid-leukemia co-cultures are a target of this project. This necessitated 3D whole organoid imaging as a highly non-trivial process as an alternative to traditional 2D slices.

The protocol used for sample mounting and clearing anneals to previously described techniques[129]. After sample dehydration in 99.9% 1-Propanol (pH not adjusted) for at least 4 hours at 4°C (light-protected), all samples were ready for clearing. All alcohol is slowly removed with a P1000 pipette to be filtered and reused. 99% Ethyl Cinnamate (ECi) solution (table 7) is gradually added to saturate the organoid. It was found that 2ml round-bottom Eppendorf tubes reliably prevented samples from sticking to the bottom. All Eppendorfs are incubated at RT for around 1hr on a gyratory rocker or similar apparatus to allow movement of organoids within the Eppendorf. Organoids may be checked on occasion to check for their gradual gain in transparency by holding the Eppendorf against a light source. When fully cleared, organoids are identified by their prism-like scattering of the light source (section 2.6.4). Keeping organoids of experimental conditions separate from another, caused some initial challenged faced challenges in storing all samples effectively.

Note: Ethyl cinnamate can corrupt polystyrene plastic, making finding a suitable imaging platform difficult. Plastics recommended by Masselink et al.[129] were eventually chosen, with which full z-stacks of all organoids are recorded.

2.6.6 H&E and IF Stain Procedure for Paraffin-embedded Sections

All samples were paraffin-embedded and sliced at a thickness of 4 μM and underwent the following treatment for paraffin removal: (I) 5 min incubation in Xylene (II) Wash with 20-times back-and-forth rocking in Xylene (III) 5 min wash in 100% EtOH (IV) 100%EtOH wash (V) 95%/70%/50% EtOH wash (VI) 50:50 (wt/vol.) 1XPBS:dH20. Organoid sections were permeabilised by adding 0.1% Triton X-100 solution for 15 min. 200-300 μl of either 10% goat serum (table 8) or 10% donkey serum (table 8) in 1XTBS blocking solution was added for either i) 1hr at RT or ii) overnight at 4°C in a humidity cassette. Both primary and secondary antibodies were diluted in blocking solutions. A few drops (approx. 50 μl) of primary antibody were added and left to incubate overnight at 4°C in a humidity cassette. All sections were washed three times with an appropriate volume of 1XTBS for a total of 15 min between stainings. A few drops (approx. 50 μl) of secondary antibody (table 6) were added

for 1-1.5 hours at RT, protected from light. All sections were given a final wash in 1XTBS for 3x15 minutes. Finally, a 300 nM solution of DAPI (table 6) was prepared from an 8 μM stock and added for 5 minutes, followed by a single 1XTBS wash. All slides containing sections were then mounted using 1-2 drops of ProLong Gold Antifade reagent (table 6), and a rectangular coverslip (table 8) was carefully placed on top.

2.7 Imaging

2.7.1 Confocal Imaging

Whole cerebral organoids (unused or used in co-cultures) and 2D cell monolayers were measured on an Olympus FV3000 confocal laser scanning microscope. The image acquisition settings are shown below and remain unchanged unless changes are specified in the figure legends.

2.7.1.1 Image Data Storage and Figure Creation Tool

An Omero image server was used to process and develop figures from all confocal images. Cartoon illustrations in this thesis created with `BioRender.com`. Maximum intensity projections of co-culture data were generated using Fiji (open-source) or directly within the Omero-figure plugin. A representative image is shown below depicting the orthogonal viewer tool used adopted for select figures (section 2.7.1.1). This tool was used to help determine whether single or multiple fluorescence signals originate from below the surface of organoids.

2.7.1.2 Confocal Microscope Datasheet

2D and 3D confocal immunofluorescence was performed using a Fluoview3000 confocal laser scanning microscope (Olympus) running FV31S-SW software at Version 2.6.1.243. *Bright-Z* function was utilized where necessary to compensate for significant signal loss. The system had a UPLSAPO 60X NA1.35 oil immersion objective for slides or a UPLSAPO 10X2 NA0.4 dry objective for imaging whole organoids using internal HSD GaAsP detectors. To measure multiple markers, the following settings for excitation and emission were used: DAPI (excitation (ex.): 405 nm, emission (em.): 430 nm-470 nm), AlexaFluor488 (ex.: 488 nm, em.: 500 nm-540 nm), AlexaFluor594 (ex.: 594 nm, em.: 610 nm-710 nm), AlexaFluor647 (ex.: 647 nm, em.: 650 nm-750 nm), tagRFP-t

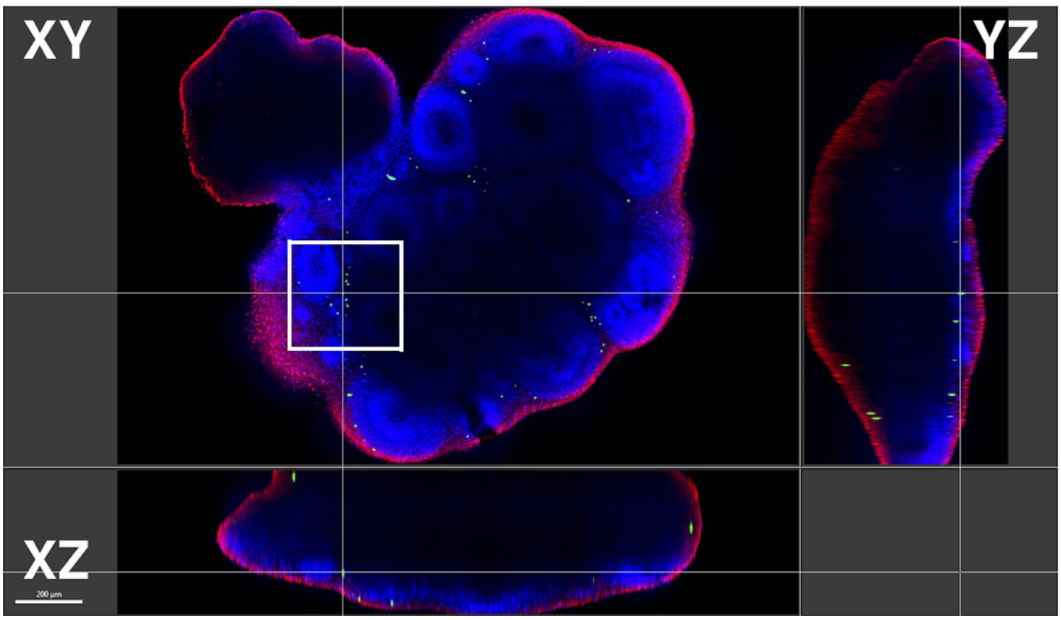

Figure 10: Orthogonal Viewing Viewing Tool - Reconstruction of tissue slices has been a common research practice; however, a significant downside has pushed researchers to record larger tissues in 3D[1].

(ex.: 561 nm, em.: 570 nm-620 nm), carboxyfluorescein diacetate succinimidyl ester (CFDA-SE) (ex.: 488 nm, em.: 500 nm-540 nm). All were performed at room temperature, and 3D organoid samples were mounted in Ethyl-3-phenylprop-2-enoate (table 8).

2.7.2 color Images of H&E Stainings

color Images of H&E Stainings: Microscope: Leica Aperio AT2. Objective: 40X (10-times magnification), i.e. 400X zoom. Acquisition parameters apply to all figures unless specified otherwise.

2.7.3 Incucyte Live-Cell Imaging

As described above, cells were stained with CFDA-SE. 1000 cells were plated in multiple wells of a 96-well suspension plate (clear plastic, Greiner) with or without a day 30 cerebral organoid. The vessel was imaged in an Incucyte S3 (Sartorius) by standard whole-well imaging over 48 hours. Magnification: 4x. Image Channels: Phase, Green.

2.7.3.1 Cell Movement Tracking (TrackMate Plugin)

Still, images captured in the time-lapse imaging mentioned above were processed using the TrackMate[130,131] plugin on ImageJ. Images were: i) imported, ii) converted to a stack, iii) converted to 8-bit iv) imported and processed using TrackMate.

2.8 Image Analysis Pipeline

2.8.1 Generation of High Quality 2D Scatter Visualizations 3D Image Data

2.8.1.1 Step 1: Image Processing and Positional Data

Bitplane Imaris V9.1 software ($RRID$: $SCR_0 07370 Oxford Instruments$ `http://www.bitplane.com/imaris/imaris` tools were used to process and quantify organoid co culture images (fig. 11A). Whenever cells were counted, the dot replacement tool was adopted, creating a mask of the cells to provide a total cell count. The position of these cells within 3D space was exported as a set of cartesian coordinates.

2.8.1.2 Step 2: Data Import and Filtering

Pandas and NumPy are well-established open-source libraries for Python. The former is generally favored for data analysis and visualization, while the latter is used for numerical calculations. Positional data were generated using the dot replacement tool in Imaris software. The files include, amongst others, cartesian coordinates represented by an x-, y-, and z-component (μm). They were imported as dataframes into Matplotlib and cleaned to only relay the x-, y-, and z-coordinates in μm. Every organoid consisted of a pair of dataframes i) CFSE (cells) and ii) MAP2 (MAP2 staining loci), and triplicate data were individualised into a dataframe for downstream processing. Data were filtered to remove -inf "negative Infinity" ie. values not representable by a finite number, numbers which can skew results.

2.8.1.3 Step 3: Co-culture Scatter Plots (Proplot)

Proplot is a Python package that is used for highly detailed data visualizations. It may benefit users to create complex figures, including subplots, and greater freedom when designing the aesthetics[132]. This is why the package was chosen to visualize the positional data, mainly due to the many events that need to be displayed. After importing and filtering data, every x-, y-, and z-coordinate of each cell type and organoid

analyzed is given their ID. A simple subplot generates a 2D scatter plot for each XY-, YZ-, and XZ-axes. To allow the reader to distinguish cells better between each 2D image, a "colorbar" for CFSE is represented according to the z-coordinate of the data points in the data frame. This reveals single or clusters of leukemia cells and determine whether they were near the organoid surface or within. For co-culture assays involving PDX, cell lines, and healthy control cells, dataframes were created for both the detected leukemia cells, as well as the organoid staining (see section 2.3.1 - *CodeDataAvailability/organoid_leukaemia_analysis/notebooks/Scatter_Plots_Leukaemia_Healthy.ipynb*). For all experimental conditions, the coordinates had to be declared manually. Then, the coordinates were plotted with the "ProPlot" package documentation. A custom "colorbar" was made that would help localize cells more efficiently in each row. By declaring the color (c) of the colorbar to anneal to the z-coordinate (z), the color hue changes according to the z-position (z-axis) value of a coordinate.

2.8.2 Generating Detailed Organoid Surface Reconstructions from Confocal Image Data Data

Open3D is an open-source library valuable for implementing 3D data in software development[133]. It was intended to use this documentation to develop a new method for examining and visualizing organoids. Positional data given by the dot replacement tool in Imaris software was imported into Python v3.1 by matplotlib[134] packages. Other packages, including numpy[135] and pandas[136], were used (please refer to the GitHub repository (repository/requirements.txt)). Every organoid consisted of a pair of data frames i) CFSE (cells) and ii) MAP2 (MAP2 staining loci). A novel computer pipeline was used to create smooth, highly detailed renders of organoid (fig. 11B). This was accomplished using Open3d, an open-source package created to create, amongst others, 3D renders using point data. Using the original implementation, a notebook was written with code to create a triangle mesh from an oriented PointCloud (pcd) using the "Screened Poisson Reconstruction" method proposed by Kazhdan and Hoppe in 2013[137]. This method requires a *pointcloud* as an input. A pointcloud is a collection of points in 3D space following the cartesian coordinate system (x, y, z), typically representing the external surface of objects. Each point may have attributes attached for visual appearance, such as color values (RGB), and their reflectivity. Pointcloud data are usually contained inside multi-dimensional arrays known as *tensors*, which provide efficiency when performing demanding transformations or filtering calculations.

More critically, they also contain the orientation and relative position of each point in space. This provides the critical information needed for rendering, detection of features, and comparing multiple pointclouds[138]. A poisson surface reconstruction is named such, as "poisson" refers to the elliptic partial differential equation, named after the French mathematician and physicist Simeon Denis Poisson. The MAP2 loci served as the basis for the pointcloud. The poisson surface reconstruction creates a continuous 3D mesh from oriented pointclouds by solving an equation that interpolates the points while fitting a smooth surface through them, ensuring both accuracy and smooth curvature[133].

2.8.2.1 Distance Queries using Raycasting Scenes (Open3D Library)

Following up, *distance queries*, an integral tool of the *RaycastingScene* class in Open3D, was used to query the distance between leukemia cells and organoid meshes (fig. 11C). It places 3D objects in a virtual space and uses artificial "rays" to determine their appearance. A *closest distance* calculation was used to find the minimum distance between points of two datasets[133]. The program returned the distances for each leukemia cell in the image data relative to the reconstructed organoid surface, producing a large dataset. The resulting data were categorized for triplicate repeats and then used to build a dataframe containing the distances and to which cell type it belongs. These results were then plotted using the seaborn[139] package, a data visualization tool for Python.

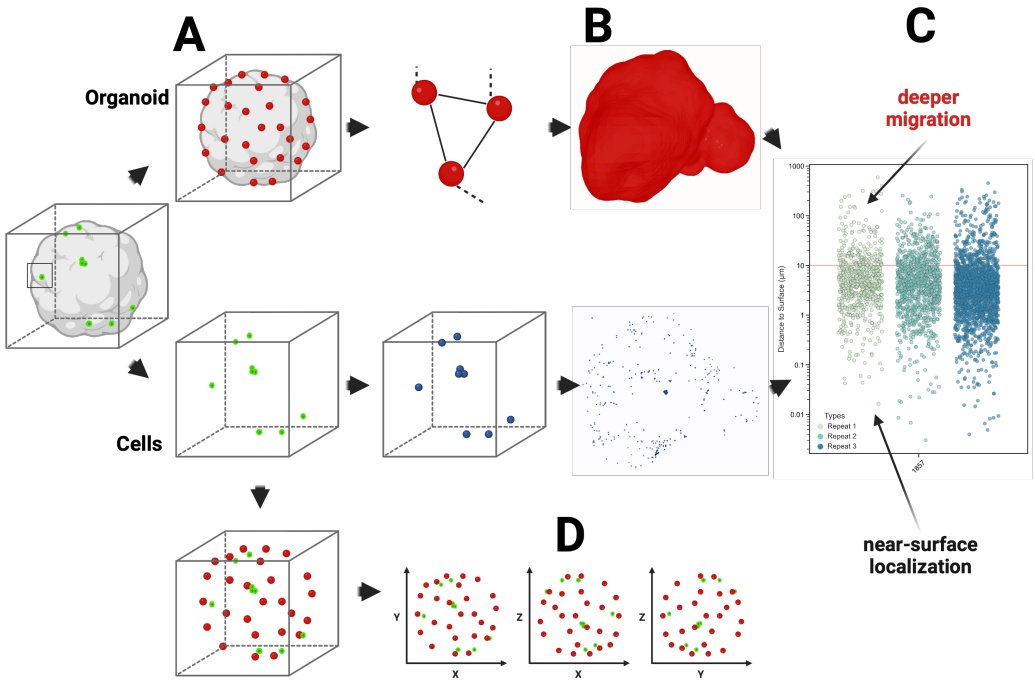

Figure 11: Workflow: Informatics-based Processing of Image Data and Quantification of Invasion Events - Workflow for visualization and quantification of image data. (A) Organoids and CFSE immunofluorescence signals are quantified into individual foci whose xyz location can be exported for further processing. (B) Both organoid and CFSE positional data are used to create a mesh which is then used to reconstruct the organoid surface. (C) Finally, the distance between CFSE cells and the organoid surface is quantified and plotted. A logarithmic scale helps divide the extensive data into those cells bound near the surface and those having invaded below the surface. (D) The positional data could also be plotted in 2D as scatter plots. This would help localize 3D events in a 2D environment.

2.8.3 Data and Code Availability

The code used for distance analysis and generating plots can be found at `https://github.com/BIOGOAT/organoid_leukaemia_analysis.git`. The imaging data used for plotting is at `https://figshare.com/articles/dataset/data_zip/23515965`.

2.9 RNA Sequencing

2.9.1 Isolation of Engrafted Cells from Pooled Organoids

Following the manufacturer's instructions, the Dynabeads™ CD19 Pan B (table 6) selection kit was used to isolate CD19+ cells from the organoid/leukemia cell suspension. The DETACHaBEAD CD19 kit (table 6) was used to separate beads from the suspension of positively isolated cells. The maximum total yield of isolated cells was 1.1 million (M) from organoids and 400,000 from suspension (Positive Selection from Organoids: 1.1M cells (90.2% Viability), positive Selection from Suspension: 0.39M cells (86.4% Viability). To validate the effectiveness of the isolation kit, 697 WT cells from the culture flask (5 million) were used and isolated according to the manufacturer's protocol. After using de-attachment of the beads, cells were visible in suspension. FACS analysis using CD19 Pacific Blue antibody (2.5 μl) showed a clear population for CD19, indicating that the kit is functional. Flow cytometry was then used to stain co-cultured cells isolated from organoids and suspension, revealing in a purity of 98% and viability of 99%. RNA extraction was performed using the miRNeasy Micro Kit (50) (table 5).

2.9.2 Sample Preparation

Protocol by Service Provider "Biological and Medical Research Center (BMFZ), Medical Faculty, Heinrich-Heine-University, Universitätsstraße 1 & Transcriptomics Labor"
Due to sample limitation, capillary gel electrophoresis was performed as a quality analysis and a 'Total RNA High Sensitivity Assay' (Agilent Technologies) on the FragmentAnalyser System was implemented. The library preparation was performed according to the manufacturer's protocol using the 'Illumina Stranded Total RNA Prep, Ligation with Ribo-Zero Plus' (Illumina Inc.) kit. The following steps were performed: rRNA depletion, fragmentation, cDNA synthesis, adapter ligation and library amplification. Bead-purified libraries were normalized and sequenced on the NextSeq2000 system (Illumina Inc.) with a read setup of SR 1x101 bp. The bcl2fastq2 tool (v2.20.0.422) was used to convert the bcl files to fastq files for adapter trimming

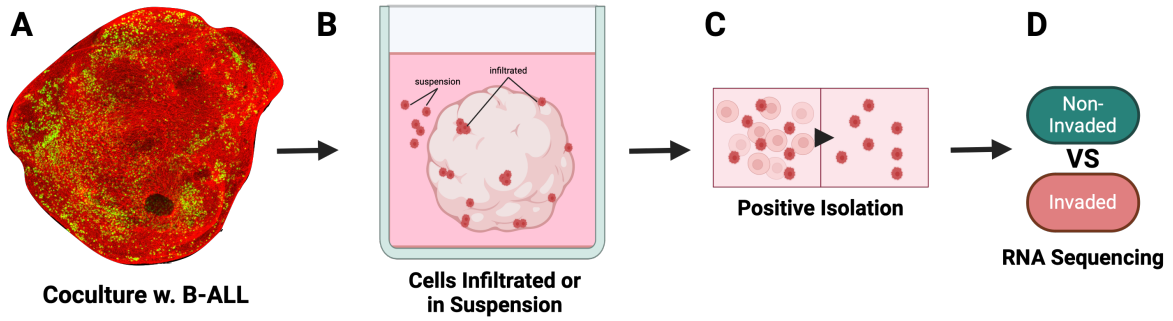

Figure 12: Workflow: Isolation of Highly Infiltrated and Non-Infiltrated Leukemic Cells for RNA Sequencing- (A) Matured cerebral organoids are co-cultured with BCP-ALL cells for 4 weeks (**Note!** Image is not representative as CFDA-SE staining is omitted for downstream RNA sequencing). (B) Leukemic cells are be classified into infiltrated (within organoid) or non-infiltrated (remaining in suspension). (C) Magnetic bead-based isolation of leukemic cells from organoids and suspension is required to have pure suspensions. (D) RNA Sequencing is performed to compare infiltrated to non-infiltrated BCP-ALL.

and demultiplexing. Sequenced read depth was well above 30 Million clusters per sample. The raw sequencing data were uploaded to Galaxy software, and initial quality control was performed by FastQC and aggregated via MultiQC. After cutting the adapters with FASTQ Trimmer, the reads were aligned to the reference genome GRCh38 with RNA STAR. FastQC determined that at least 85% of all reads were uniquely mapped. To quantify the gene expression *featureCounts* was used, followed by *edgeR* to normalize the data to the sequencing depth. Differentially expressed genes were determined by an absolute log2 fold change of >1 / < -1 and an FDR < 0.05. Differentially expressed genes with a low log2CPM (normalized log2CPM < -1) were treated preferentially. The analysis pipelines and plots generated in fig. 35 were provided by the colleague *Julian Schliehe Diecks* (Universitätsklinikum Düsseldorf).

2.10 Proliferation Assay between CD79a/Igα Knockdown and shRNA-miR30 Control

A proliferation assay was prepared for a CD79a knockdown and shRNA-miR30 control cells. Cells were counted using an automated cell counter, and 250,000 cells/ml were seeded per well. The cell count in cells per milliliter was measured every 48 hours for 14 days.

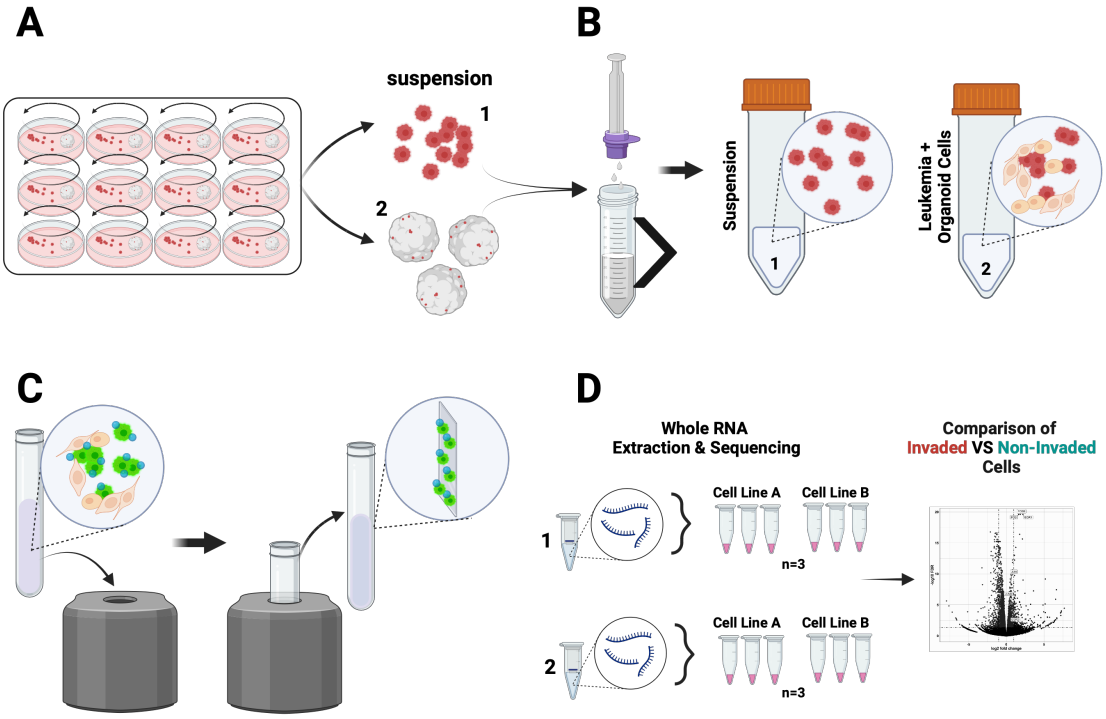

Figure 13: Workflow: Post-Co-culture Positive Isolation of Invaded and Non-Invaded Cells - (A) Up to 48 organoids are co-cultured with 100,000 cells for four weeks. CFSE is not added to cells in this step. (B) 70 μm strainers are used to mash and filter whole organoids and suspension cells to create a suspension. (C) Using magnetics beads, CD19+ leukemic cells were isolated from the organoid/leukemia suspension. The exact process is used for leukemia suspension cells. FACS analysis is performed to check the percentage of CD19+ cells in the isolated suspensions. (D) RNA extraction is performed, and RNA is prepared for "infiltrated" i.e. from mashed organoids, and "non-infiltrated" i.e. from leukemia suspension.

2.11 Flow Cytometry

2.11.1 Validation of CD79a/Igα Knockdown Model

CD79a Knockdown and shRNA-miR30 Control cells were gated with Viability dye (table 6). Next, intracellular staining was performed according to manufacturer instructions and stained with CD79a or isotype antibodies (table 6).

2.11.2 Validation of CFDA-SE-stained Leukemia Engraftment in Organoids

Organoids were gently dissociated by pipetting, and cells were stained with Viability dye (table 6). Next, intracellular staining was performed according to manufacturer instructions and stained with FosB or cFos antibodies (table 6) overnight at 4°C. Next, leukemia cells were washed and stained with secondary anti-rabbit Cy3 antibodies (table 6). Leukemia cells were incubated only with isotype and secondary antibodies as a staining control. Leukemia cells carried CFDA-SE to gate the cells inside the organoid or suspension properly. Analysis was performed with FlowJo software, gating CFSE-positive as organoid infiltrating cells.

2.12 Statistical Analysis

The statistical analysis utilized GraphPad PRISM 9.00 and SPSS 22. Normal distribution was assessed via the Shapiro-Wilk test. If the distribution was normal, statistical significance was determined using an unpaired t-test. Otherwise, the Mann-Whitney U test was employed. For normal distribution and multiple groups, ANOVA was utilized. A P-value less than 0.05 was considered significant. Bivariate correlation analysis was conducted as previously described[44].

2.13 Inhibitors used for Co-culture Assays

The compound Plerixafor (AMD3100) (selleckchem.com catalogue No.S8030) is an antagonist for chemokine receptors CXCR4 and CXCL12, which mediate chemotaxis. The use of plerixafor is to mobilize hematopoietic stem cells. Its purpose is to stimulate the immune system by encouraging the release of stem cells from the bone marrow into the blood of patients with non-Hodgkin lymphoma or multiple myeloma. Plerixafor (table 8) is a type of bicyclam derivative that acts by blocking the CXCR4 receptor. It attaches to three acidic residues in the receptor's binding pocket, specifically Asp171, Asp262, and Glu288[122]. Plerixafor (AMD3100) was used to pre-treat the 697 cel line for 12 hours at a final concentration of 44nM from a stock solution at 10 mg/μl.
T-5224 (table 10) is a molecule that inhibits the activity of a transcription factor called c-Fos/activator protein (AP)-1. It has anti-inflammatory properties and specifically targets the DNA binding activity of c-Fos/c-Jun without affecting other transcription factors. In co-culture, using only the 697 cell line, cells were pre-treated with either

1 μl or 5 μl final concentration T-5224 (including DMSO control) and co-cultured with mature cerebral organoids according to the standard protocol (10,000 cells per organoid).

2.14 Tables of Human iPS Cells, Devices and Consumables

Table 3: List of Human iPS cell Lines Used for Cerebral Organoid Cultivation

Cell Line	**Supplier**	**Catalog Nr.**	**Source Type**	**Donor**	**Reprogramming Method**
Cellartis Human hiPS cell Line 12 (CiPSC12)	Takara Bio	Y0080	Skin Fibroblast	Healthy 24-year-old male (European/North African)	Defective polycistronic retrovirus technology (stable integration of Oct-4, SOX2, KLF-4, and c-Myc)
HW8 iPSC	Lab of Zhengping Zhuang (National Cancer Institute, NIH)		Skin Fibroblast	Healthy male	Sendaivirus (non-integrating RNA virus, transcription factors: Oct-4, SOX-2, KLF-4, and c-Myc)
mTag-RFPt	Coriell Institute (NJ, USA)	AICS-0031-035		WTC parental line (Conklin Laboratory, J. David Gladstone Institute)	

Table 4: List of Devices Specific to Cerebral Organoid Culture

Device	**Manufacturer**	**Catalog Nr.**
Titramax 1000	Heidolph Instruments	600-650
Intelli-Mixer	ELMI	10-30
CELLSPIN complete	PFEIFFER	183001
Spinner Flask 250ml	PFEIFFER	182026

Table 5: List of Kits Required for CD34+ Selection from Human Cord Blood

Product Name	**Manufacturer**	**Catalog Nr.**
EasySepTM Human Cord Blood CD34 Positive Selection Kit II	StemCell Technologies	17896
EasySepTM Magnet	StemCell Technologies	18000
miRNeasy Micro Kit (50)	Qiagen	1071023
RNASE-Free DNase Set(50)	Qiagen	79254

Table 6: List of Antibodies/Dyes Used for Cell Culture/IF Staining

Product	**Manufacturer**	**Catalog Nr.**	**Dilution**	**Host**
Anti-MAP2	Abcam	ab5392	1:1000-1:10000	Chicken polyclonal
Anti-Beta-Tubulin III, Clone TUJ1	StemCell Technologies	#60052	5 μg/ml	Mouse monoclonal IgG2a
Anti-Human Nestin, Clone 10C2	StemCell Technologies	#60091	5 μg/ml	Mouse monoclonal IgG1
SOX2 (D6D9)	CellSignalling	#3579S	1:200	Rabbit monoclonal
S100b	Abcam	#ab11178	1:100	Mouse monoclonal

Continued from previous page

Product	**Manufacturer**	**Catalog Nr.**	**Dilution**	**Host**
PAX6	BioLegend	#901302	1:50	Rabbit Polyclonal IgG
AlexaFluor 488GAM	Invitrogen	#A32723TR	5-10 μg/ml	Goat
AlexaFluor 488DAR	Invitrogen	#A32790TR	5-10 μg/ml	Goat
AlexaFluor 594 GAM	Invitrogen	#A11005	5-10 μg/ml	Goat
AlexaFluor 594DAR	Invitrogen	#A32754	5-10 μg/ml	Goat
AlexaFluor 700GAM	Invitrogen	#A-21036	5-10 μg/ml	Goat
DAGP633	Sigma	N.A.	1:100	N.A.
DAPI	StemCell Technologies	#75004	1:600 of 8 μM stock	N.A.
CFDA-SE (CFSE)	N.A.	N.A.	20 μM (final conc.)	N.A.
PE anti-human CD79a	BioLegend	N.A.	N.A.	N.A.
FosB (5G4) mAb	Cell Signalling	2251	1:800	Rabbit
c-Fos (9F6)	Cell Signalling	2250	1:3200	Rabbit
c-Jun (60A8) mAb	Cell Signalling	9165	1:200	Rabbit
Viability Dye	eBioscience	65-0863-14	Manufacturer Protocol	N.A.
FOXP3 Transcription Staining Buffer Set	ThermoFisher Scientific	00-5523-00	Manufacturer Protocol	N.A.

Continued from previous page

Product	**Manufacturer**	**Catalog Nr.**	**Dilution**	**Host**
IgG1κ isotype	BioLegend	400119	Manufacturer Protocol	Mouse
secondary anti-rabbit Cy3 antibodies	BioLegend	406402	Manufacturer Protocol	Donkey
ProLong Gold Antifade	Invitrogen	P36934	Manufacturer Protocol	N.A.

Table 7: List of Chemicals

Product	**Catalog Nr.**	**Manufacturer**
Sodium Pyruvate	11360070	ThermoFisher Scientific
P300 Reagent	L3000001	ThermoFisher Scientific
Dorsomorphin	P5499	Sigma Aldrich
Insulin Solution Human	I9278-5ML	Sigma-Aldrich
NaN (Sodium Azide)	8223350100	Sigma-Aldrich
Tris Base	T1503-250G	Sigma-Aldrich
Tri-ethanolamine	90279-100ML	Sigma-Aldrich
2-mercaptoethanol	31350010	Gibco
NaCl (Sodium Chloride)	7647-14-5	Avantor (VWR)
1-Propanol	71-23-8	Avantor (VWR)
EtOH (Absolut)	64-17-5	Avantor (VWR)
Xylol	1330-20-7	Avantor (VWR)
Triton X-100	AAA16046AE	Fisher Scientific
2-Propanol	11304817	Fisher Scientific

Table 8: List of Cell Culture Media and Supplements

Product	**Catalog Nr.**	**Manufacturer**
GelTrexTM	A1413302	ThermoFisher Scientific

DMEM-F12	21331046	ThermoFisher Scientific
1XPBS (Phosphate-Buffered Saline)	J61196.AP	ThermoFisher Scientific
Opti-MEM™	31985062	ThermoFisher Scientific
Lipofectamine 3000	L3000001	ThermoFisher Scientific
STEMdiff™ Neural Induction Medium	05835	StemCell Technologies
Neurobasal Medium	21103049	StemCell Technologies
L-Glutamine	25030081	Gibco
B27 Supplement (50x)	12587010	Gibco
N2 Supplement (100X)	17502048	Gibco
MEM-NEAA (MEM, Non-essential amino acids)	11140035	Gibco
Penicillin-Streptomycin (10,000U/mL)	15140122	Gibco
RPMI1640 GlutaMAX	61870036	Gibco
FBS	F9665-500ML	Sigma-Aldrich
Goat Serum	G9023	Sigma-Aldrich
Donkey Serum	D9663	Sigma-Aldrich

Table 9: List of Laboratory Equipment and Consumables

Product	**Catalog Nr.**	**Manufacturer**
isopropanol freezing container	1535050	ThermoFisher Scientific
Mr. Frosty™ Freezing Container	5100-0001	ThermoFisher Scientific
Bio-One CELLSTAR	10536952	Greiner
Bottle top vacuum filtration systems, SFCA membrane	513-1551	Nalgene
Accutase	00-4555-56	Sigma Aldrich
Ficoll-Paque Plus	GE17-1440-03	Cytiva

Red Blood Cell Lysis Buffer	N/A	Zentralapotheke Uniklinik Düsseldorf
Eppendorf (Round-bottom)	0030123620	Eppendorf
Lenti-X Packaging Single Shots	631276	Takara
LentiX Concentrator	631231	Takara
24x50mm	1.5	Menzel-Glaeser
FOXP3/Transcription Staining Buffer Set	00- 5523-00	eBioscience

Table 10: List of Inhibitor Compounds

Compound	**Catalog Nr.**	**Manufacturer**
SB431542	S1067	Selleckchem.com
Rock Inhibitor (Y-27632)	S1049	Selleckchem.com
Plerixafor (AMD3100)	S8030	Selleckchem.com
T-5224	HY-12270	MedChemExpress
Dorsomorphin	P5499	Sigma-Aldrich

Chapter 3

Results

3.1 Project Stages Overview

This section outlines the various stages of the project. The characterization of cerebral organoids and the workflow to produce them has been addressed in previous chapters. This thesis proposes cerebral organoids, a form of iPSC-derived 3D culture system, as a novel tool in CNS-leukemia research. In brief, cerebral organoids initiate from cell aggregates termed "neurospheres" which mature to organoids by an expanding neuroectoderm and stratified neuroepithelium. Immunofluorescence and immunochemical staining of organoids and subsequent imaging is used to characterize the organoids. To this end, the workflow was separated into stages. In summary, the cerebral organoid cultivation protocol is established by confirming that the structural and cellular features are consistent with the literature (fig. 14A). A novel implementation to co-culture ALL leukemia with organoids is then developed and tested with high-risk CNS leukemia along with less neurotropic leukemia and healthy human stem cells (fig. 14B). This is followed by a first-of-its-kind implementation of computer analysis to reveal deep leukemia engraftment into organoids (fig. 14C). To further test the specificity of the model, known molecular pathways implicated in CNS-leukemia are targeted via cell knockdown models or inhibitors to document their effect on engraftment (fig. 14D). Finally, RNA sequencing is performed to find molecular pathways implicated in the engraftment of leukemia cells into the organoids (fig. 14E). The fulfillment of these stages is key to address the research questions of the thesis.

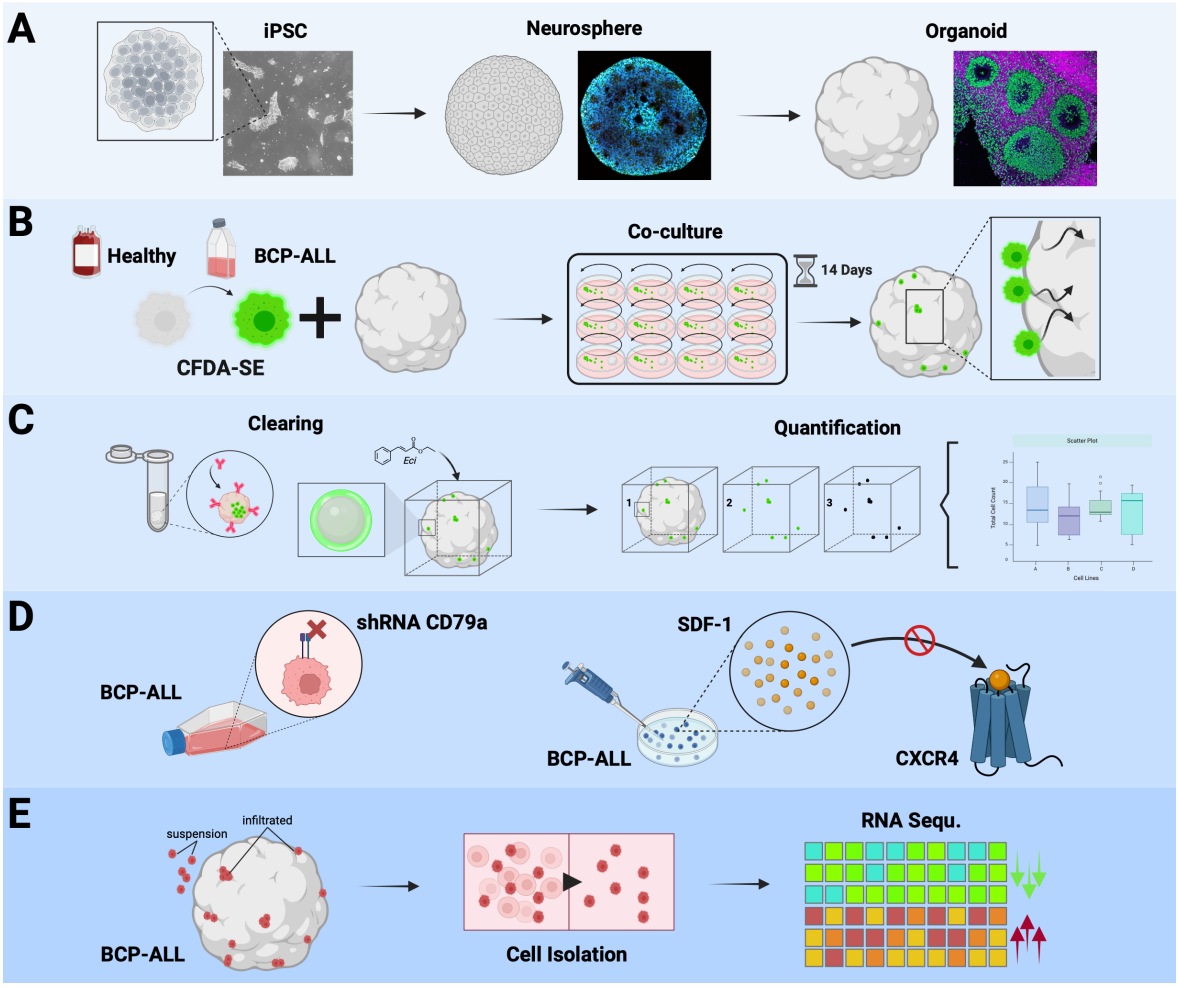

Figure 14: PhD Project in Stages: Co-culture Model and Analysis Schemes - A graphical illustration of the project in several stages (*highlighted by colored backdrop*). (A) Mature cerebral organoids are cultivated and established from human hiPS cell lines. (B) Co-culture assays are tested and modified to select conditions in which cell engraftment is detectable. Leukemia or healthy controls carry a fluorescent dye for tracking and downstream analysis. (C) 3D confocal microscopy of fluorescently-stained organoids is used for cell detection. Image analysis protols (established or novel) are used to process and quantify the fluorescent cells in the organoids. (D) A selection of candidates recently implicated in CNS-invasion of BCP-ALL are tested using the co-culture model. BCP-ALL engraftment is put under further scrutiny by utilizing an established BCP-ALL knockdown model of BCR-signaling, or pre-treatment with a chemokine signaling-inhibitor. (E) The transcriptomic profile of organoid-infiltrating BCP-ALL cells is analyzed via whole RNA sequencing. Infiltrating and non-infiltrating cells are isolated and compared against each other.

3.2 Neurosphere Formation and Characterization

Human induced pluripotent stem cells (iPSCs) can renew and transform into various cell types. Additionally, these cells can organize themselves to form complex 3D structures that mimic the characteristics of tissues found in living organisms. Researchers discovered how cerebral neuroepithelial cells derived from hiPS cells generate various neuronal cell types in a sequence miming corticogenesis in living organisms. Additionally, these cells display a complex, multi-layered structure when cultured in specific floating aggregates[99,123,140]. This has subsequently led to an array of publications introducing protocols for organoid cultivation. Details to the overall protocol was detailed in section 2.1.3.

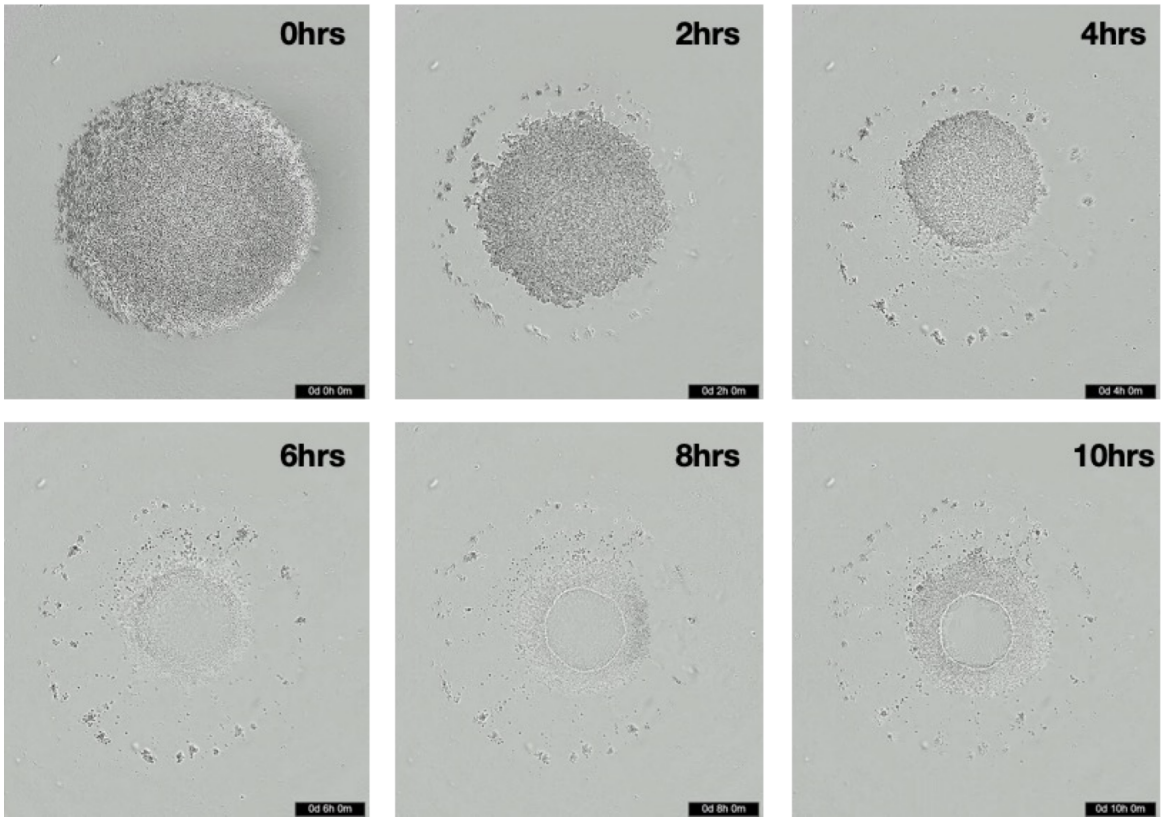

Figure 15: Time-lapse Imaging of Neurosphere Formation and Aggregation Behavior of hiPS Cells - Time-lapse Images of hiPS Pellets Reveal the Formation of Neurospheres. Human iPS cells plated in 96-well ULA plates were imaged over time via the Incucyte S3 live cell imager. Single snapshots are shown for 0-10 hours post-seeding within 2hr gaps. Within the first 4hrs, condensing of the cell pellet is apparent, progressing over the next 6hrs. Timescale - *bottom right*

Culturing human induced pluripotent stem cells (iPSCs) and seeding for neurosphere formation was undertaken according to the workflow in section 2.1.2.2 and section 2.1.3.1 respectively. After seeding, the behavior of hiPS cells was studied via live-cell imaging (fig. 15). This revealed that hiPS cells self-aggregate within a few hours after seeding. Interestingly, some residual cell material remained in the wells after neurosphere formation; however, it is not known whether this is an effect of surplus cells. Some neurospheres were removed from the culture and immunostained to check for neural induction. Small voids in the dense and nuclei-rich spheroid were observed (fig. 16). Moreover, some components were positive for the type IV intermediate filament marker Nestin (acronym: neuroepithelial stem cell protein), consistent for neural progenitor cells. In summary, immunophenotyping of neurospheres induction revealed key neuronal markers.

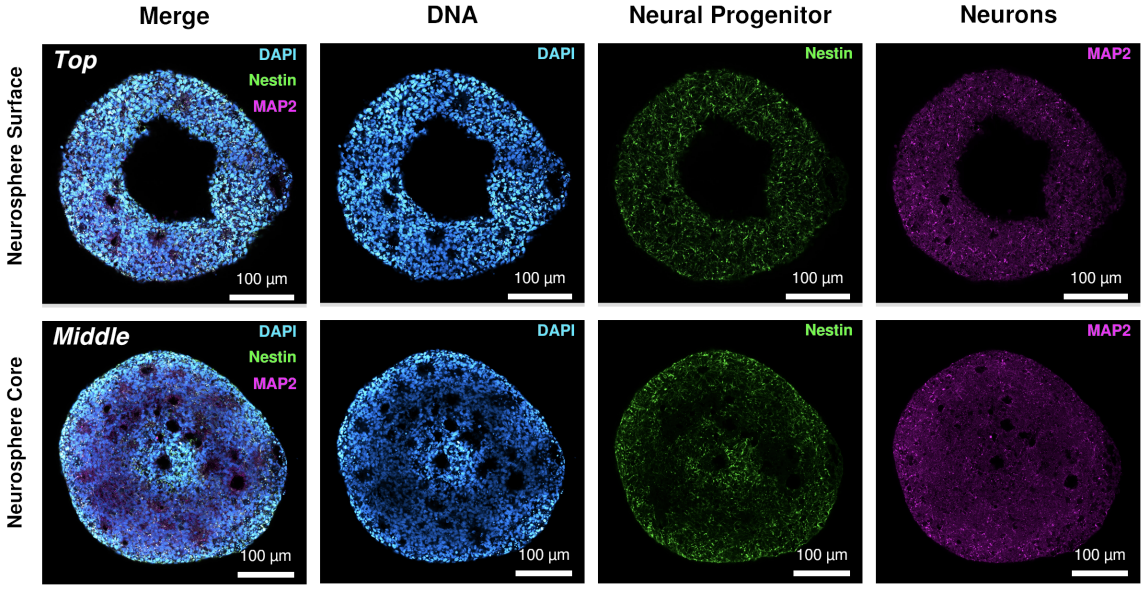

Figure 16: Validation of Abundant Protein Markers in Neurospheres by Fluorescent Immunostaining - Day 4 neurospheres derived from human hiPS cells were stained with Nestin, a neural progenitor marker, and the neuronal marker MAP2 antibody. Two sets of images were produced to show the top surface and inner layer of the neurosphere. Circular or oval-shaped voids were observed, indicating the early development of ventricular structures in early organoids. There was a high abundance of Nestin when overlaid with the nuclear marker DAPI, indicating successful neuronal induction. MAP2 did not reveal axons, dendrites, or other neuronal features typically seen in matured organoids. Scale bars – 100 μm

3.3 Immunophenotyping Key Features of Cerebral Organoids

Neurospheres were expanded without Matrigel according to the workflow (section 2.1.3) in either stationary or dynamic (spinner flask) suspension culture (fig. 17A-C). Over time the semi-translucent structure of the neuroepithelium began to appear (fig. 17, white single arrow). Neuroepithelial formations are expected to form in the maturation phase. As seen under phase contrast microscopy, thick plate-like formations emerged on the outside of organoids (fig. 17D/ROI/single black arrow). Furthermore, an inner lumen beneath the plate-like epithelium became visible (fig. 17D/ROI/double black arrows). Overall, the maturation of neurosphere in suspension culture exhibit features consistent with early cerebral organoid cultures.

The emergence of features in matured organoids as described above are part of a dynamic process. These features are structural and yield a growing array of cell types, introduced in fig. 3. To confirm the presence and arrangement of key neuronal markers and structures, paraffin-embedded sections of 60 day-old cerebral organoids were stained (section 2.6.6). Since an organoid constitutes a milieu of different cell types and connective tubular proteins and filaments, a selection of various markers were available to characterize the organoid. Literature shows 3D or 2D specimens stained for nuclei (DAPI), neuronal precursor cells (SOX2, Nestin), and mature neurons (MAP2, TBR1, Reelin, TUJ1)[116]. The detailed protocol of Gabriel et al. describes a typical ventricular zone organization from the apical (ventricle) to the basal (cortical plate) site. A marker for neuronal precursor cells (NPCs) 'Nestin', was shown to co-localize with a DAPI nuclear stain in these regions. Beta-3-tubulin 'TUJ1' marks neurons within the primitive cortical plate at the basal site. As an option, the space where dividing apical radial glial cells can be marked using 'pVim', which co-localizes with the cilia marker 'Arl13b'[116]. Distinct from other brain region-specific organoid models, the cerebral kind expresses the organizational and cellular features of cortical development. They can be identified by a pseudo-neuroepithelial layer surrounding a lumen[117,141]. Immunostaining tissue slices with markers representing neural progenitor 'paired box protein' (PAX6) and mature neuronal cells 'beta-three-tubulin' (TUJ1) should reveal critical features. The abundance of these markers in cerebral organoid tissue has already been documented[142]. Here, median sections of paraffin-embedded organoids showed the distinct pattern of numerous neural rosettes composed up of a dense, circular- or oval-shaped arrangement of nuclei surrounding a lumen (fig. 18A-B),

separated by a region of neuronal tissue positive for TUJ1, an abundant peptide amongst mature neurons[142]. The black void in the TUJ1 signal containing these ventricles was also apparent and annealed well with previously published literature[143] (fig. 18B, double-headed white arrow), forming a radial outgrowth of nuclei from the lumen towards the cortical plate of the pseudo-epithelium (baso-apical formation) (fig. 18B, single white arrow). Ultimately, the results demonstrate how the cultivated organoids aligned well with previously published protocols and present consistent features of neuroepithelial development. Overall, a basis for reliably cultivating cerebral organoids was achieved. Furthermore, the contrast between these features are clearly visible in H&E stainings of paraffin-embedded slices (fig. 18C) Imaging tissues becomes increasingly difficult with size as they become increasingly optically opaque to light. Tissue transparency decreases due to the higher refraction of incoming light caused by their refractive index, consequently complicating the detection of antibody-labeled proteins. "Refractive index" matching is one technique available to researchers to make larger tissues optically "clear". The term "clearing" is, therefore, used colloquially to render the tissue transparent. Such applications have benefitted researchers in resolving intricate structures such as axonal projections and whole embryos[129,144,145,146]. Here an already established protocol was adopted using non-toxic ethyl cinnamate protocol[129] to rapidly clear organoids (section 2.6.5). A side-by-side comparison reveals the rapid change in opacity after clearing (fig. 9). To confirm the image clarity under IF microscopy, whole organoids were stained for PAX6 or SOX2 'SRY-box 2' (progenitor neurons) and TUJ1 (mature neurons). As a result, a z-stacks recording of an organoid in 3 to 4 fluorescence channels was completed in 45-90 min. The fluorescence signal from all three channels appears bright and sharp across the tissue (fig. 18D). Critically, there is adequate visibility of intricate neuronal structures as well as immediate progenitor cell types (fig. 18E). Accordingly, utilizing ethyl cinnamate as a mounting medium for 3D confocal imaging provided an excellent basis. This approach was subsequently adopted for co-culture experiments with leukemia cells.

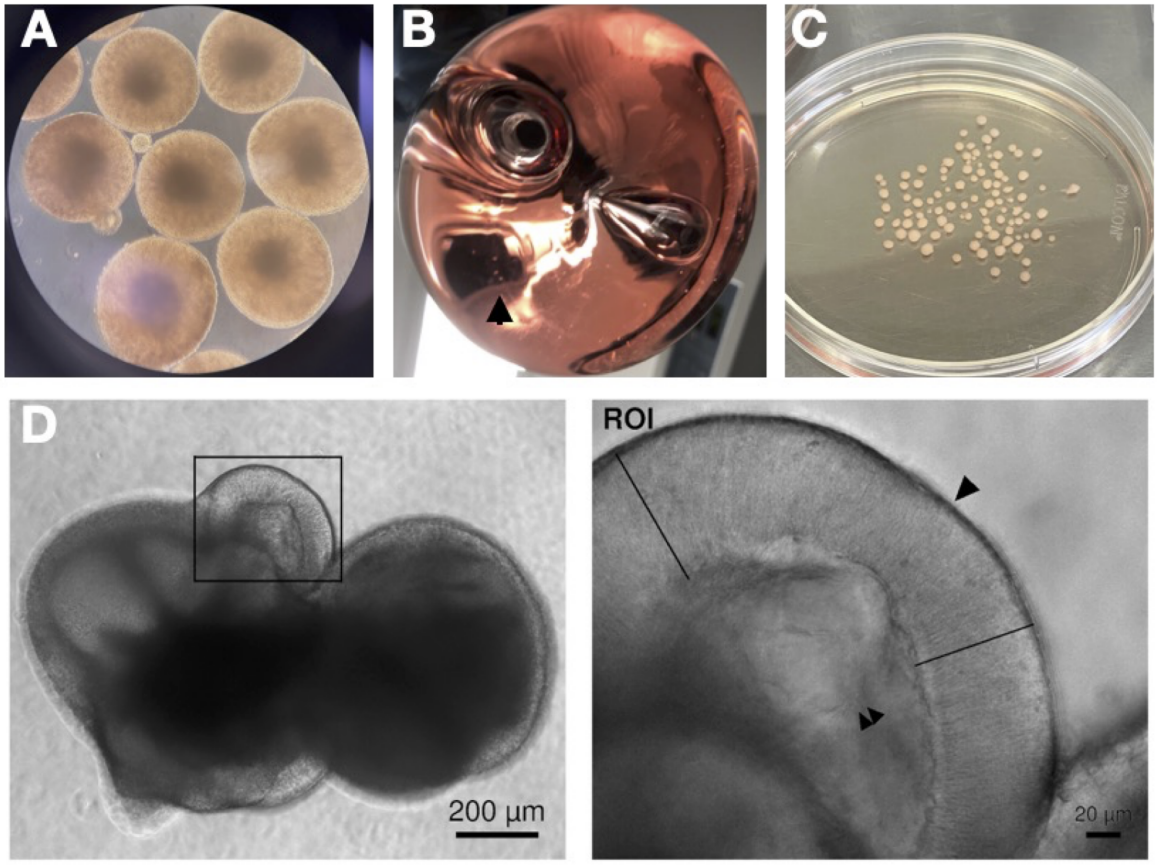

Figure 17: Transition from Early to Matured Organoid Identified by Brightfield Microscopy of Key Structural Features - Several weeks to a few months may pass between seeding hiPS cells to harvesting matured organoids. (A) Neurospheres appear as spheroids in suspension culture as seen under brightfield microscopy—neuronal differentiation and growth progress during cultivation in spinner flasks (B). Phase-contrast brightfield microscopy of a mature organoid reveals the emergence of the neuroepithelium (D). (ROI) The neuroepithelium (black lines) bears a smooth surface (single black arrow) and surrounds a lumen on the apical side (double black arrows).

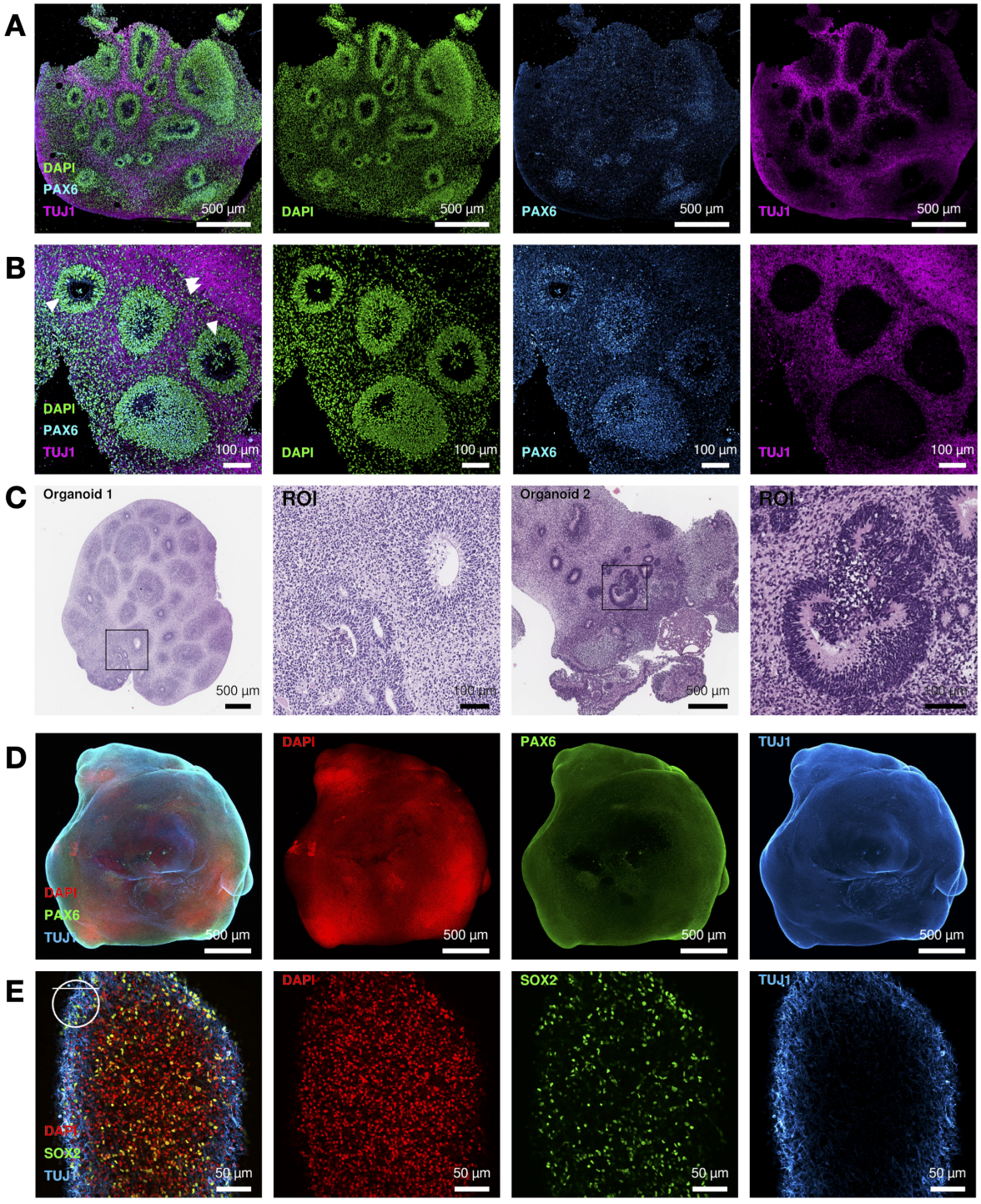

Figure 18: Immunochemical and Tissue Stainings to Reveal Key Structural and Cellular Features of Cerebral Organoids - (A-B) Immunocytochemical stainings of (paraffin-embedded) fixed cerebral organoids. Median sections of 60DOA ChiPSC12 cerebral organoids were stained for intermediate neuronal progenitor cells via anti-PAX6 and mature neurons via anti-TUJ1 and all nuclei via DAPI nuclear stain. Confocal imaging reveals rosette-like formations of radially organized neurons, and baso-apical formations form the core structures.

*continued from previous page...*Neural rosettes appear heterogeneous in shape and size (a combination of round and oval), with a dense ring of nuclei surrounding a lumen. Mature neurons marked by TUJ1 (double white arrows) are not expected to localize with the dense ring of nuclei of the rosettes (single white arrows). Therefore, dark voids can be seen where the neural rosettes reside. (C) Hematoxylin and eosin staining of paraffin-embedded 60DOA cerebral organoids. (D-E) Anti-PAX6 and anti-SOX2 primary antibodies to label neuronal progenitor cells, and an anti-TUJ1 antibody to label mature neurons. The introduction of 99.9% ethyl cinnamate resulted in a gradual increase in tissue transparency. A cerebral organoid, denoted as 60DOA, was captured as a z-stack and presented as a maximum intensity projection image. Furthermore, a higher magnification 30X silicone objective was employed to capture images of the two top layers of the same organoid. In the top left corner, a horizontal line indicates the z-position of the image acquisition with respect to the organoid (sphere). The scale bars are 500 μm, 100 μm, and 50 μm. Specifically, the imaging involved 405nm for DAPI, 488nm for SOX2/PAX6, and 597nm for TUJ1.

3.4 Investigating Leukemia Co-cultivation with Cerebral Organoids

3.4.1 Optimisation of Culturing Conditions and Analysis

Having an *in vitro* model delivering the means to study cancer engraftment into human tissues with a three-dimensional microenvironment would be beneficial. Furthermore, a model to study cancer in the CNS niche *in vitro* has gained traction recently[115,119]. Early cerebral organoid studies focused mainly on achieving features resembling early corticogenesis[100,105,142,102,147]. Within time, the first publications studying glioblastoma engraftment into cerebral organoids emerged, revealing some specificity in the model[113,114,115]. No study has yet introduced a co-culture system combining leukemia cells and brain organoids, making this project's core novelty to develop first-of-its-kind co-culture assay between cerebral organoids and BCP-ALL cells. BCP-ALL cells with the t(1;19) translocation leading to the TCF3::PBX1 fusion protein is known to be associated with an increased risk for CNS relapse[13]. Therefore, the *TCF3::PBX1*$^+$ BCP-ALL cells were used as the model subgroup for these experiments. *TCF3::PBX1*$^+$ PDX cells (PDX1) were utilized for co-culture experiments after staining with CFDA-SE dye. Confocal microscopy images of cleared organoids were recorded and displayed as maximum-intensity projections of the recorded channels. In addition, an orthogonal viewer tool was used to separate the 3D images into three separate 2D images (section 2.7.1.1). When scrolling through a z-stack, the tool provides a 2D image for each

coordinate in each z-slice.

During 3-day co-culture, PDX1 cells localized with the organoid in the maximum intensity projections (MIP) images; however, they did not appear below its surface, and thus the inner regions of the cerebral organoid (fig. 19A). This, in turn, led to the assumption that the engraftment process may require more time; therefore, the duration of the co-culture assay was extended up to 7 or 14 days. Although the patch of leukemic cells appeared visibly larger after seven days of co-incubation, more engraftment of the leukemia cells was noticed after 14 days of co-culture (fig. 19B-C). Moreover, under high magnification, the overlap of organoid nuclei and complex axonal/dendritic networks clearly shows the dissemination of leukemic cells under the surface (fig. 19D-E). Preserving the structural integrity of the organoid tissue architecture is essential for conducting post-engraftment analysis. This was a primary factor leading to the adoption of confocal imaging for analysis over tissue mashing and flow cytometry analysis. To examine changes to the organoid architecture as a results of leukemia engraftment, a 14-day co-culture with the PDX1 cells was conducted. Focussing on areas with and without leukemia, the expression of key neuronal markers MAP2 (neuronal) and Nestin (intermediate progenitor) appeared unaltered (fig. 20). In essence, most prominent leukemia engraftment occurs after 14-days, preserving the structural integrity of the organoid.

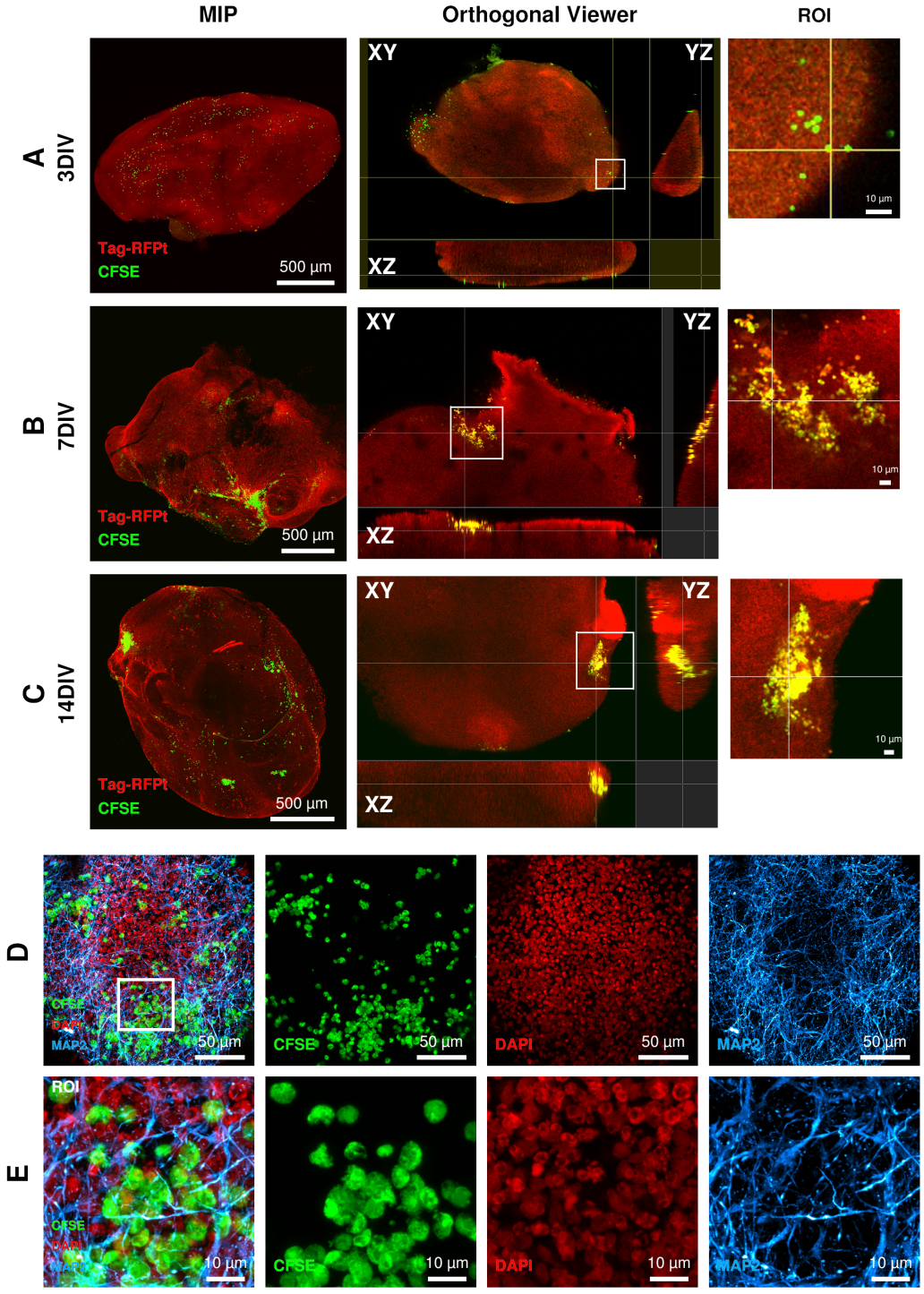

Figure 19: Validation of BCP-ALL Invasion into Cerebral Organoids after 14DIV - The cerebral organoids were cultured together with CFSE-stained *TCF3::PBX1*$_+$ (PDX1) leukemia cells for a period of 14 days. In the left-hand column, maximum intensity projections (MIP) show the colocalization of DAPI and mtag-RFPt with the CFSE signal of the cells. On the right-hand column, orthogonal views illustrate the spatial orientation of the cells, as marked by white arrows, by visualizing the organoid in three dimensions (XY, ZY, ZX).

continued from previous page... The orthogonal viewer displays areas of leukemia cells located on the surface or within the organoid, which are further highlighted by the region of interest (ROI) image. Additionally, sub-surface CFSE-stained leukemia cells are observed to be in proximity to other neuronal cell types. (D, E) The cleared organoids were captured using a 60x oil objective to observe the uppermost layer containing infiltrated leukemic cells. The stacked images were combined, showing CFSE, DAPI, and anti-MAP2 staining. Enlarged images highlight leukemic cells closely associated with the organoid volume (ROI), suggesting that they are situated within an intricate network of neurons and their axonal/dendritic connections. Fluorophores: mtag-RFPt (Tag-RFPt), CFSE, DAPI, MAP2 (AF647). Scale bars – 50 μm, 10 μm.

Organoids are a dynamic *in vitro* system, maturing over a period of weeks to months in culture. The effect of organoid age was tested briefly by co-culturing cerebral organoids at 10, 30, or 60 days of age (DOA) with 10,000 leukemia cells. The results show similar images of cell aggregates engrafting into the organoid across the three age timepoints (fig. 21). Similarly, leukemia cell concentration in the vicinity of organoids needed adjustment. To avoid oversaturating the system, and having too high cell density in microscopy samples affecting readability of the samples, a range of concentrations were tested. Clinically, the detection of CNS disease in BCP-ALL is classified according to WBC count in the CSF via traumatic lumbar puncture. The current classification of CNS1-3 lists cell concentrations in the single digits per microlitre of CSF. Therefore, to assess the clinical relevance of the model, the minimum number of leukemic cells required to engraft into the cerebral organoids was evaluated. To accomplish this, co-culture experiments were carried out with a limiting dilution (50, 100, 5000, and 10000 cells) of PDX1 cells for 14 days. The IF results identified progressively increasing engraftment of leukemia cells in a concentration-dependent manner. More importantly, the invasion was noticed with as low as 50 leukemia cells (fig. 22). Subsequently the stability of CFSE as a fluorescent staining dye in the same time frame was studied. To this end, the 697 BCP-ALL line was stained with CFSE and co-cultured for 14 days, mashed and stained for flow cytometry analysis (workflow anneals that of section 2.11.2 with a change in antibody to anti-human CD19 FACS antibody, table 6). Green cells (FITC) were checked for their overlap with human CD19 (C5.5-A). The analysis showed that more than 90% of CD19-positive events (lymphocytes) are positive for CFSE after 14 days of co-culture (fig. 23). Even though some leukemic cells are expected to loose a portion of the CFSE signal during the 14 days of co-culture with the organoids, this decrease is not

significant enough for them to become undetectable in the immunofluorescence images. In summary, BCP-ALL engraftment in organoids is a reliably detectable event after two weeks in co-culture. Ultimately, BCP-ALL leukemia engraftment into organoids occurred irrespective of organoid age or significant dilution of leukemia in co-culture. Furthermore, labelling with CFDA-SE is suitable for tracking leukemia cells engraftment into organoids after 14 days of co-culture.

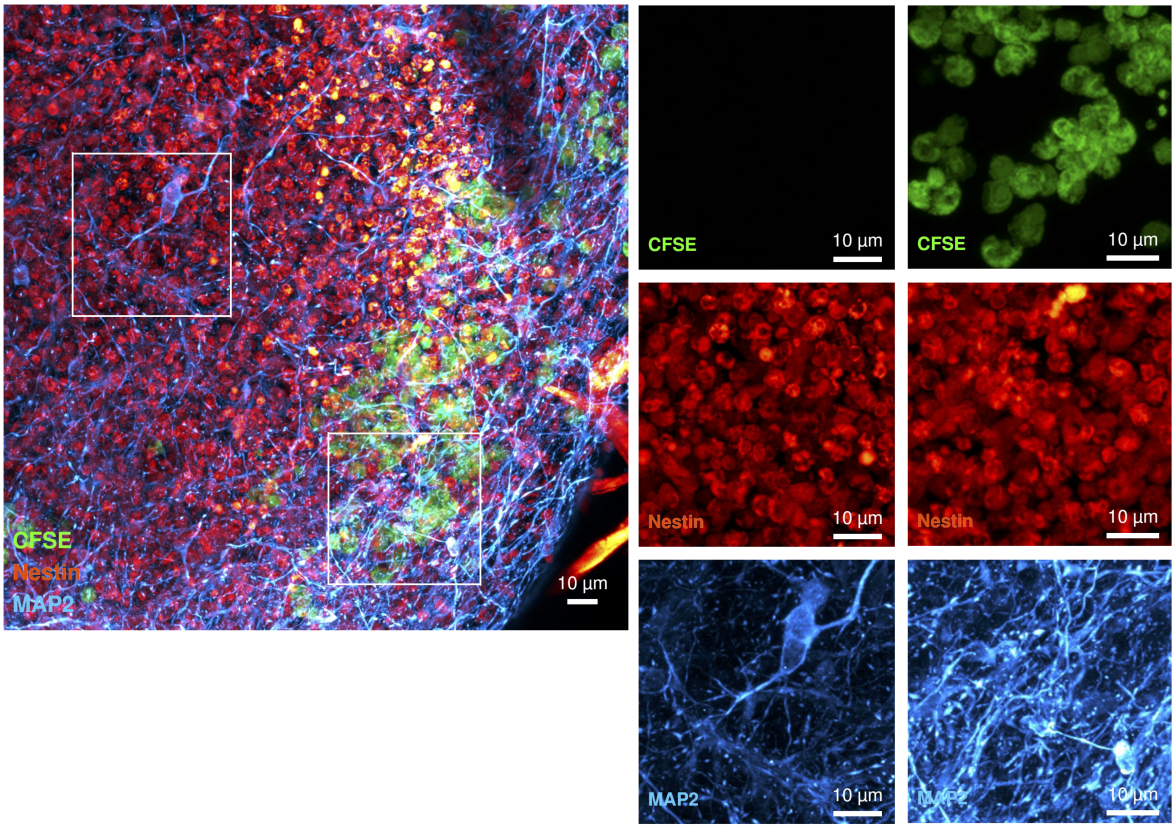

Figure 20: Study of Expression of Key Neuronal Markers of Organoid Tissues after Engraftment - Organoids were co-cultured with the CFSE labeled (TCF3::PDX1+) PDX1 cells for 14 days. Subsequently, infiltrated organoid was stained with intermediate progenitor cell marker anti-Nestin (a neuroepithelial stem cell protein) and anti-MAP2 (a microtubule-associated protein). Left - A MIP displays a portion of organoid infiltrated by PDX1. Right – Two ROIs (from Left) show areas with/without infiltration and the presence of Nestin and MAP2. Scale bars: 10 μm. 488nm: CFSE (green), 596nm: Nestin (red), 647nm: MAP2 (blue).

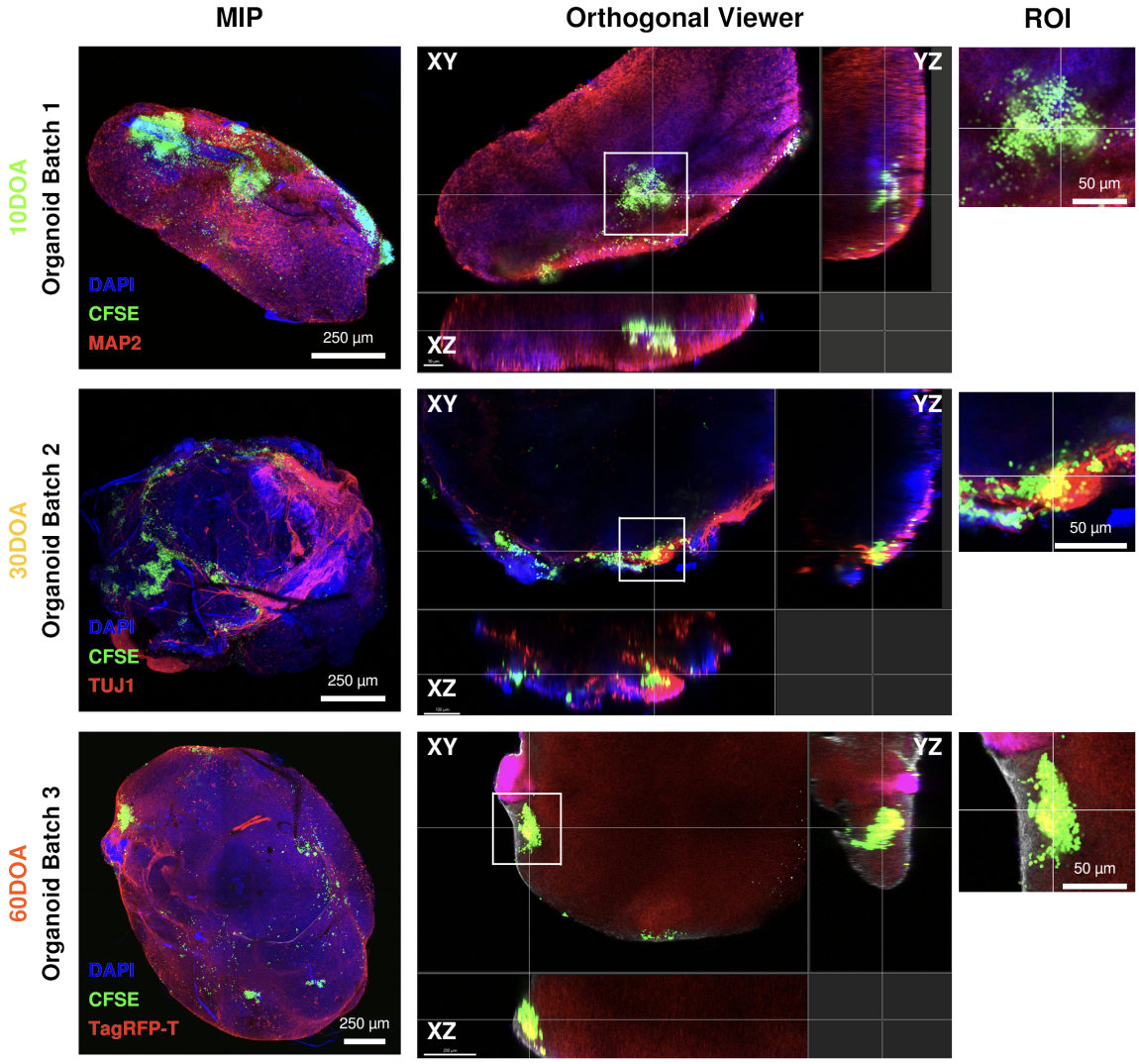

Figure 21: BCP-ALL Leukemia Engraftment across Different Organoid Ages - Cerebral organoids were cultured for 10, 30, and 60 days and then co-cultured with 10,000 BCP-ALL cells (PDX1). These organoids were then stained with either TUJ1 (beta-three-tubulin) or MAP2 (microtubule-associated protein 2) unless they were derived from the mtag-RFPt-expressing hiPS cell line (table 3). Z-stacks were displayed as MIPs, and orthogonal views of the organoids were shown in combination with ROIs of single cells or clusters. Scale bars – 250 μm, 50 μm. Fluorophores: mtag-RFPt (Tag-RFPt), CFSE, DAPI, MAP2 (AF647), TUJ1 (AF594)

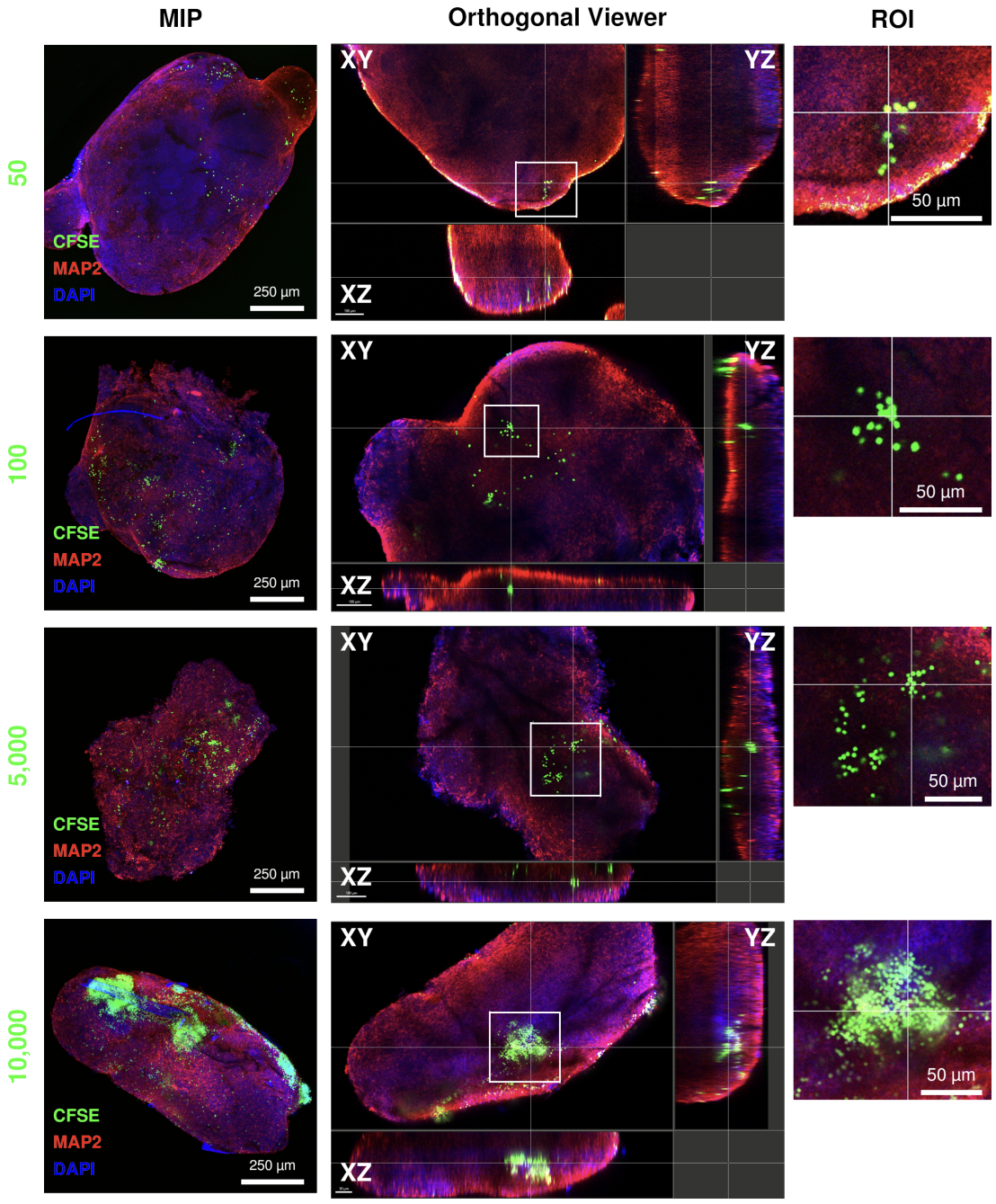

Figure 22: Cell Invasion across a Series of Dilutions - Cell engraftment was assessed by reducing the cell concentration in co-culture by up to 200-fold. Cerebral organoids were co-cultured with CFDA-SE-stained TCF3::PBX1+ PDX cells. A-D show 50, 100, 5000, and 10000 cells (PDX) per organoid. The cerebral organoids were labeled with anti-MAP2 (microtubule-associated protein 2) (table 6) and presented as MIPs using the orthogonal viewer tool. The orthogonal views of the organoids are displayed in conjunction with ROIs of individual cells or clusters. Scale bars – 250 μm, 50 μm. Fluorophores: CFSE, DAPI, MAP2 (AF647).

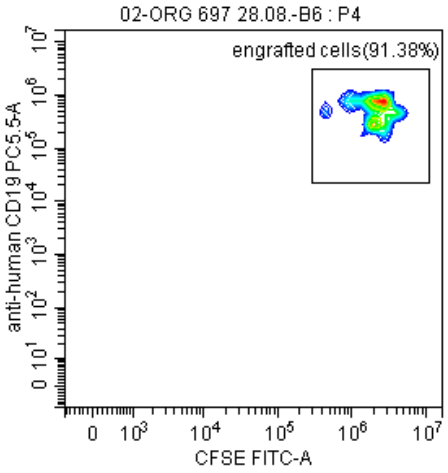

Figure 23: CFSE Signal Remains Visible as a Co-Stain with human CD19 marker for BCP-ALL - To determine the persistence of CFSE signal of cells engrafted in organoids, organoids were mashed and suspensions were co-stained for human CD19 surface protein. BCP-ALL 697 cell line were co-cultured for 14 days. Organoid mashing and FACS staining procedure was followed according to section 2.11.2. Populations double-positive for FITC (CFSE) and CD19 (C5.5-A) are highlighted. The percentage of green cells was shown for both engrafted cell types.

3.4.2 Cell Migration of BCP-ALL leukemia in Co-culture

The broader literature on the invasion and migration of leukemia cells confirms that cell motility is inherent due to their lymphoid identity[148]. Next, it was investigated whether leukemia cells show motility towards organoids. Healthy controls in thr form of CD34+ HSPCs (sourced from cord blood) and BCP-ALL 697 were co-cultivated with cerebral organoids or as suspension only in triplicates. Time-lapse imaging was performed using an Incucyte S3 microscope, and cell migration patterns were quantified for all cell types according to the methods described in section 2.7.3. Visualization using the trackmate[130] visualized BCP-ALL cells moving towards the organoid in suspension culture. The same behavior was not seen for HSPCs (fig. 24). These findings were consistent across experimental triplicates (not shown). Although some HSPCs appear to rotate towards their organoid, similar movement is seen for other cells in the well homing away from the organoid (fig. 25 white arrows). Quantifying these tracks for both BCP-ALL and HSPCs across triplicates revealed significantly higher distances covered by BCP-ALL compared HSPCs (fig. 26).

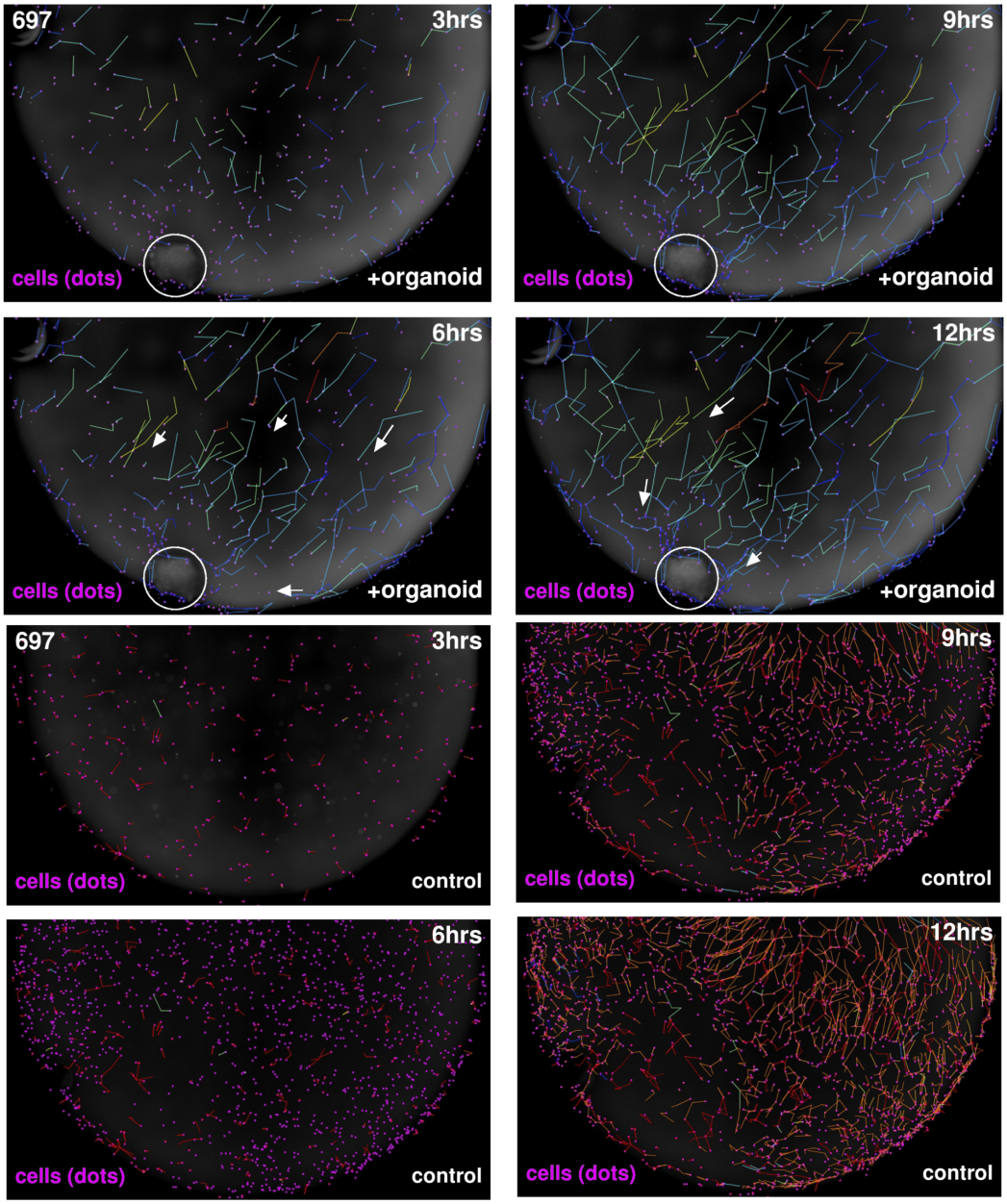

Figure 24: Time-lapse Imaging of BCP-ALL in Co-culture with Cerebral Organoids - Leukemia cells laballed with CFDA-SE were plated at a density of 1000 cells per well shown as "cells (dots)", with or without a single cerebral organoid (n=3). Time-lapse imaging was performed over 24 hours at 3-hour intervals to monitor the movement of leukemia cells (indicated by white arrowheads). The two conditions were labeled as "+organoid" and "control" for CFSE-stained cells only. The analysis was carried out using the TrackMate plugin on ImageJ (section 2.7.3). The movement paths of the cells over time was traced, revealling movement (single white arrow) towards the cerebral organoid (indicated by the white oval), originating from the perimeter of the center of the well.

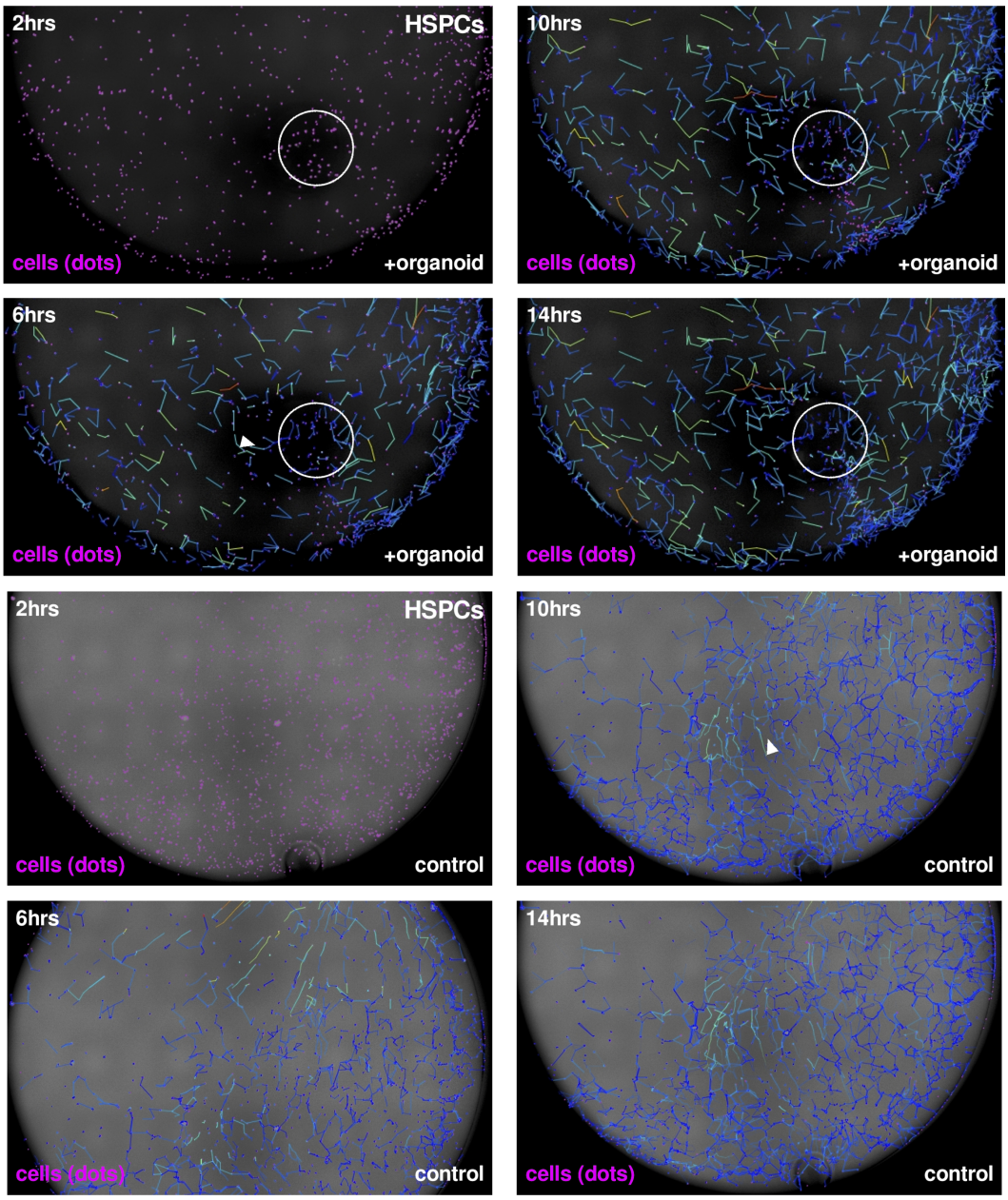

Figure 25: Time-lapse Imaging of HSPCs in Co-culture with Cerebral Organoids - HSPC cells labeled with CFDA-SE were seeded at a density of 1000 cells per well shown as "cells (dots)", with and without a single cerebral organoid per well (n=3). Time-lapse imaging was conducted over a 24-hour period with images taken every 3 hours to monitor the movement of leukemia cells (indicated by white arrowheads). The two experimental conditions are referred to as "+organoid", and "control" for CFSE-stained cells only. The analysis was carried out using the TrackMate plugin on ImageJ (section 2.7.3). The movement of HSPCs in co-culture and suspension was traced over time (single white arrow).

*continued from previous page...*Analysis was carried out using the TrackMate plugin on ImageJ (section 2.7.3.1) to identify and trace the paths of cell movement over the time-lapse. Leukemia cells were observed migrating towards the cerebral organoid (depicted as a white oval), originating from the perimeter of the well. Cells surrounding the organoid at the early stage of the experiment exhibited minimal, irregular movement around the organoid, as indicated by green arrowheads.

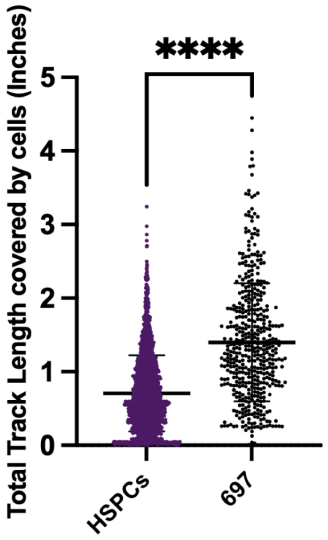

Figure 26: Quantification of Cell Migration during Time-lapse Imaging unveils Higher Movement of Leukemia Cells- The total track length covered by the *TCF3::PBX1*$^{+}$ 697 cells and cord blood-derived HSPCs in co-culture with mature cerebral organoids, was measured by time-lapse imaging for 12h, and analysis was performed via TrackMate plugin. The results depicting the total track length covered by the cells. Statistical analysis was performed using the unpaired two-tailed t-test (HSPCs vs 697, n=3, $P < 0.0001$).

3.4.3 Mitotic Inactivation of BCP-ALL Cells

Next, the effect of mitosis inhibition was studied using the co-culture model to investigate the role of BCP-ALL cell proliferation during cell infiltration. 697 cells were exposed to a non-cytotoxic concentration of Mitomycin-C (30nM) for a duration of three hours and subsequently co-cultured with cerebral organoids. Cells pre-treated with inhibitor still engrafted; however, engraftment of cells within the cerebral organoids relative to the corresponding vehicle control (DMSO)-treated cells was visibly reduced (fig. 27A). Furthermore, total cell counts for treated cells was notably reduced (fig. 27B). These findings support the notion that organoid infiltration is driven by the migration

of BCP-ALL cells; however, upon reaching the organoid, they subsequently proliferate within the organoid microenvironment.

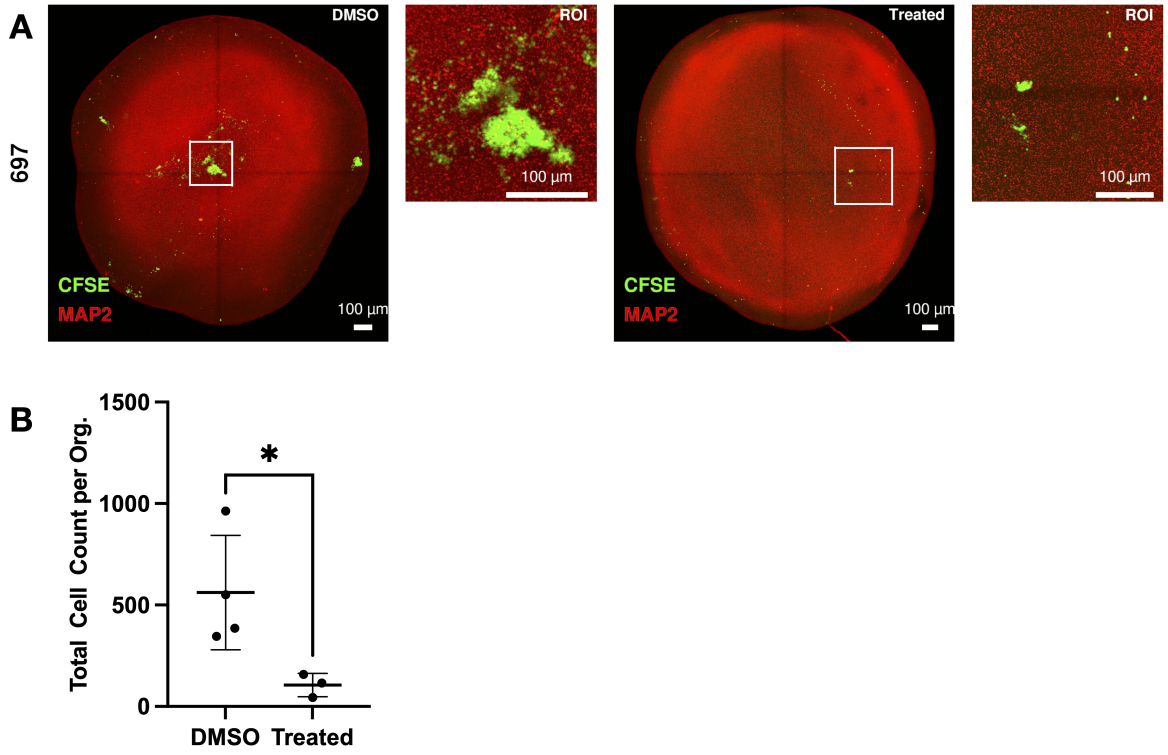

Figure 27: Mitotic Inactivation of BCP-ALL Leukemia in Organoid Co-cultures - The 697 cell line was treated with Mitomycin-C and co-cultured with mature organoids, according to the methodology in section 2.2.6. The organoids were subsequently stained using anti-MAP2 primary and anti-chicken 647 secondary antibodies. (A) Confocal images depict leukemic cells (CFSE) co-localizing with the organoid (MAP2). Regions of Interest (ROIs) highlight differences in the clustering/aggregation of leukemic cells under different conditions. Scale bars - 100 μm (B) Total cell count comparison was made between DMSO and treated cells. Statistical analysis involved comparing the treated and DMSO control 697 cell lines using the unpaired two-tailed t-test (n = 3 replicates). Treated vs DMSO (P=0.0432)

3.4.4 Quantification of Infiltration of Leukemia Cells Across High-risk BCP-ALL and non-ALL Subtypes

To distinguish the engraftment potential between leukemia subtypes, cells imaged inside organoids were counted. To this end, common image analysis tools were adopted to identify and count individual leukemia cells within each 3D organoid image (section 2.8.1.2). Cord-blood-derived HSPCs were incorporated as healthy cell controls. HSPCs did not form large aggregates in the organoids after 14 days compared to PDX1 leukemia cells (fig. 28A-B). Healthy buffy-coat-isolated B-lymphocytes were added as a control in the subsequent analysis. Moreover, *TCF3::PBX1*$^{+}$ 697, and Kasumi2 exhibited a significantly ($P<0.05$) higher engraftment over CD34+ HSPCs (fig. 28C). High-risk BCP-ALL subgroups cell lines (*TCF3::HLF*; HAL01 and *BCR::ABL1*; SUPB15) were included, revealing higher engraftment over HSPCs (fig. 28C). Moreover, 697 and SUPB15 engraftment was significantly higher than that of B-lymphocytes (B-Cell). In addition, two more *BCR::ABL1*$^{+}$ chronic myeloid leukemia (CML) cell lines, K562 and KCL22, were incorporated into the co-culture assay as a non-BCP-ALL subtype, which are not typically associated with CNS-leukemia, as further controls. However, despite comparable growth kinestics to *TCF3::PBX1*$^{+}$ leukemia, K562 and KCL22 exhibited low engraftment similar to HSPC controls (fig. 28C). Moreover, the analysis was extended to include more PDX-ALL samples. These represent high-risk ALL subgroups including KMT2A-rearranged (*KMT2A-r*$^{+}$), *TCF3::PBX1*$^{+}$, and *BCR::ABL1*$^{+}$ ALL. Here, *TCF3::PBX1*$^{+}$ PDX1 counts were significantly higher than HSPC and CML controls (fig. 28D). Interestingly, *BCR::ABL1*$^{+}$ PDX3 was only on par with B-lymphocytes, but significantly higher than HSPCs. Of note, leukemia cells recovered from the suspension after co-culture exhibited high viability (around 80% or above) (fig. 29). Altogether, these co-culture assays revealed differential organoid engraftment kinetics in different PDX-ALL samples, all of which significantly exceeded the organoid engraftment of HSPCs and K562, KCL22 cells.

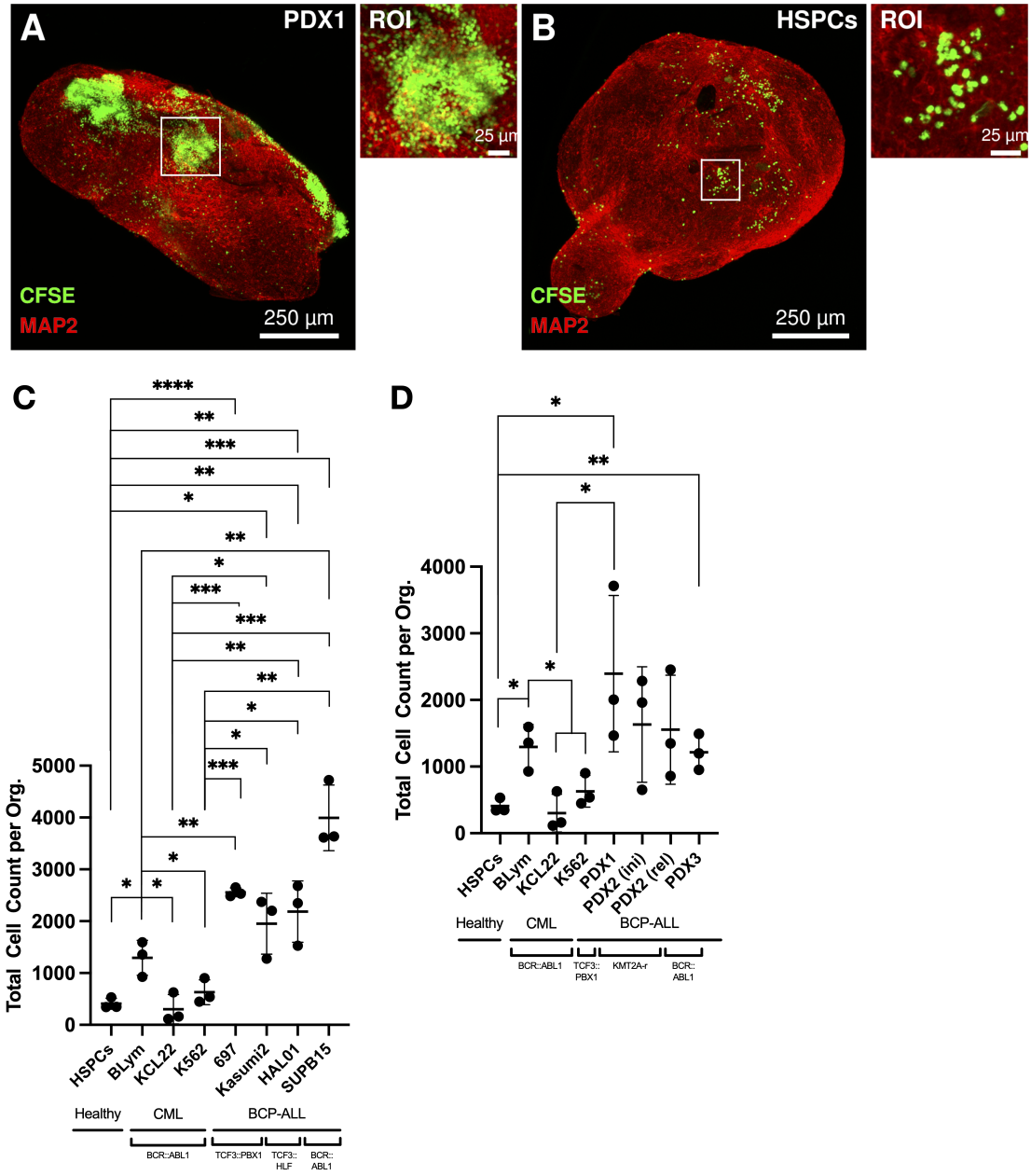

Figure 28: Quantification of Cell Engraftment after Co-culture - A total cell count of invaded cells reveals BCP-ALL as significantly more aggressive over healthy controls. (A-B): Cerebral organoids were co-cultured with *TCF3::PBX1*$^{+}$ (PDX1) cells and cord blood-isolated CD34+ cells (healthy control). Enlarged images of cell clusters are shown by white squares (ROI). Scale bars – 25 μm and 250 μm. (C-D): A quantitative analysis of total cell count of leukemia cell lines, PDX (Patient-derived Xenograft), HSPCs and B-lymphocytes (BLym). Statistical analysis compared the HSPC, CML, and B-lymphocytes to every other condition using the unpaired two-tailed t-test (n = 3 replicates): *TCF3::PBX1* vs HPSC - 697 ($P < 0.0001$), Kasumi 2 ($P = 0.0111$), PDX1 ($P = 0.0433$). *TCF3::PBX1* vs B-lymphocytes (B-Lym) - PDX1 ($P=0.0124$), 697 ($P = 0.0033$). *TCF3::HLF* vs HSPCs: HAL01 ($P = 0.0070$). *BCR::ABL1* vs HSPCs - SUPB15 ($P = 0.0006$), PDX3 ($P=0.0086$).

continued from previous page... BCR::ABL1 vs B-Lym - SUPB15 (P = 0.0029), KCL22 (P = 0.0176), K562 (P = 0.0498). HSPCs vs B-lymphocytes (P = 0.0124) [*Note: For simplicity, only statistically significant comparisons are shown*] Fluorophores: CFSE, DAPI, MAP2 (AF647).

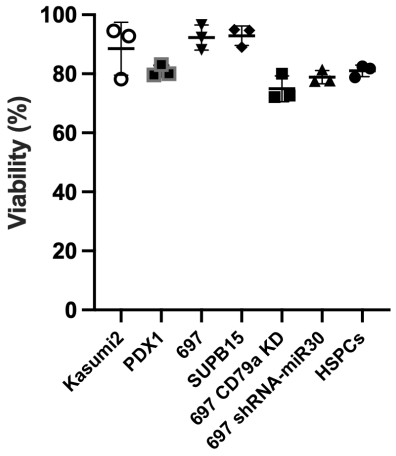

Figure 29: Cell Viability of Cells Recovered from Co-culture Suspension Leukemia cells were recovered from 14-day coculture suspensions and stained with DAPI fluorochrome, after which they were analyzed using FACS. The percentage of viable cells is shown for commercial cell lines (Kasumi2, 697, SUPB15), PDX, cell line models (shRNA-miR30), and healthy controls (HSPCs).

3.5 Novel Implemention of Data Science Tools for Pinpointing BCP-ALL Engraftment

3.5.1 Validation of Cell Infiltration using 2D Scatter Visualizations

The critical characteristics of cerebral organoids for structural and cellular features are commonly shown using fluorescence images. Although significant progress has been made in the quality of 3D organoid imaging[129,149], typical histological or single-cell analysis needs more spatial information within whole organoid tissues. Modern analysis pipelines, such as multiscale comparative analyses for organoids, have unlocked new potential in studying 3D organoids[121]. Python has become an increasingly attractive program for scientific applications, next to other systems such as R, MATLAB, Stata, and SAS. Pandas[136] and NumPy[135] libraries introduced and organized the coordinate data exported from Imaris (section 2.8.1.2). Imaris uses built-in software tools to detect single events/shapes in 3D images, however a tool

was needed to routinely analyzelarge datasets of organoids. Here, a novel computer pipeline to analyze3D co-culture images is introduced. CML controls (KCL22, K562) were analyzed alongside *BCR::ABL1*$^{+}$ PDX3 and *TCF3::PBX1*$^{+}$ PDX1. In brief, Imaris-based image analysis was used to extract „positional data" from CFSE-stained cancer cells (green), as well as foci (e.g. somas stained via anti-MAP2 staining) from neuronal staining (fig. 11). The positional data were converted to an array of [x, y, z] coordinates, e.g. [845.777, 664.661, 3675.28] section 2.8.1.2. 2D scatter plots of MAP2 and CFSE positional data were created using the matplotlib package, mapping the relative position along the z-axis according to their positional data section 2.8.1.3. This showed a clear overlap of CFSE (colorbar) with MAP2 (red) (fig. 30). Moreover, the difference in cell dissemination between CML and BCP-ALL was apparent (fig. 30A-D). Due to the configuration of the colorbar, cell aggregates were easily localized across the 2D plots of each condition. In summary, this visualization provides an enhanced assessment of cell engraftment and sub-surface localization.

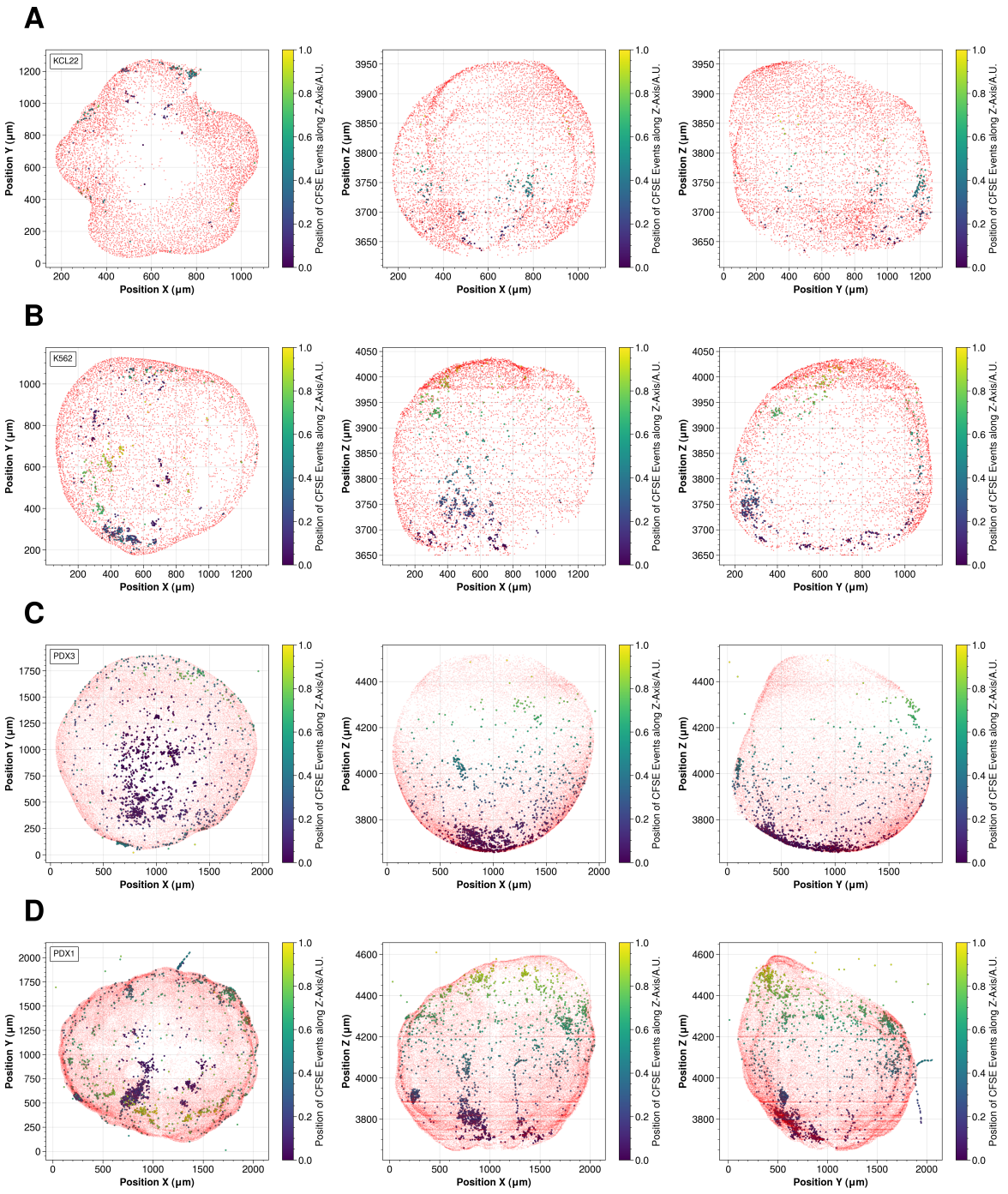

Figure 30: Relative Position and Distance of Leukemia and Healthy Controls to Organoid Surfaces - (A-D) The cerebral organoids used in the leukemia/organoid co-culture assay are largely composed of mature neurons and long, developed axonal and dendritic networks. The use of an anti-MAP2 primary antibody shows their distribution across the entire volume of the organoid. This distribution could be used to better interpret the position and clustering of leukemia cells engrafted within the organoid tissue...

continued from previous page... The number and relative position of MAP2-positive loci and CFSE-positive cells within each organoid were extracted as *positional data*. These are cartesian coordinates given by an x-, y-, and a z-component, extracted from confocal image channels for MAP2 foci and CFSE-positive leukemic cells. Scatter plots were created by employing numpy, pandas, and matplotlib packages (section 2.8.1.2). A 2D plot visualizes any two axes at a time with MAP2 in red, and CFSE in green. A custom gradient colorbar is used for each channel to illustrate the relative position of both axes with respect to the third axis, in this case the z-axis. Python's libraries Matplotlib and Seaborn were leveraged to visualize these data. Specifically, the organoids volume (as red dots) were overlayer on each axis with a scatter plot of CFSE-positive leukemia cells (green).

3.5.2 Generation of Detailed Surface Reconstructions of Cerebral Organoids from Image Data

Confocal image data was used to convert leukemia and organoid foci into coordinate data ie. pointclouds. 3D modeling of organoids may pose a solution to quantify positional relationships between CFSE-stained cancer cells and the brain organoid volume. The development of modern computer graphics has extensively researched the problem of reconstructing 3D surfaces from point samples[133]. Furthermore, the idea of segmenting whole organoids for spatial analysis has previously been demonstrated[121]. Here, a novel approach to spatial organoid analysis is introduced. The confocal images of organoids (section 2.3.1) illustrated the smooth surfaces of organoids; however, peaks and troughs add a layer of complexity. The two-dimensional evaluation was created to provide a qualitative, intermediate assessment of co-culture (fig. 30). To quantify positional relationships between CFSE-stained cancer cells and the brain organoid volume, a manipulable 3D model was created from whole organoid confocal images (fig. 31A). Firstly, the previously-mentioned positional data (section 2.8.1.1) were converted into pointclouds (section 2.8.2). *Open3D* is a python/C++-based package capable of producing detailed surface reconstructions which require pointcloud data as an input. The reconstruction is achieved by performing a 'poisson surface reconstruction'[137]. To elaborate, pointclouds are unstructured and require a triangular mesh to produce a an accurate surface reconstruction. This method produces a 'triangle mesh' with 'points' and 'triangles' which, in addition to smoothing algorithms, aims to produce an incredibly detailed representation of the original image. Indeed, both MAP2- and CFSE-based image data were successfully converted to pointclouds overlapping with the original image (fig. 31B-C/**ROI**). Furthermore, the reconstruction using the

MAP2 pointcloud closely resembled to original structure (fig. 31A,D/**ROI**). In summary, immunostained organoid can be readily and accurately converted into digital models. Its practical use for spatial analysis will be elaborated in the subsequent section.

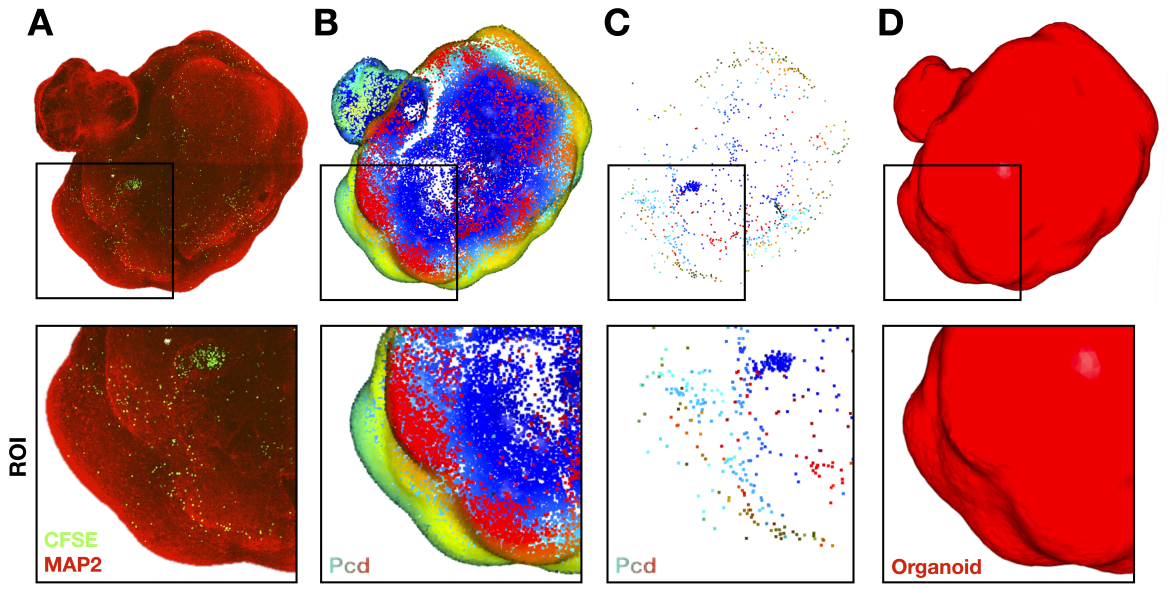

Figure 31: Study of High Resolution Reconstructions of Organoid Surfaces from Immunofluorescence Image Data - (A) Confocal images taken from day 60 organoids co-cultured with leukemia or HSPCs were analyzed using Imaris image analysis software (see section 2.7.1). (B-C) The Open3D package was used to create an accurate reconstruction of the organoid volume, based off MAP2 foci, to perform distance calculation of leukemia cells to the organoid surface. Here, the positional data are represented as a *pointcloud* (Pcd). (D) The MAP2 pointcloud is used to create a detailed polyhedron *mesh* representing the organoid surface. Bulbous/convex and concave details on the surface are seen.

3.5.3 Calculating Relative Depth BCP-ALL Engraftment into Organoids

Section section 3.5.2 could demonstrate how highly detailed surface reconstructions of organoids are possible. Next, the distance between leukemia cell dots to the surface render were measured. Cerebral organoids have been reported to harbor hypoxic conditions. It was thus hypothesized that the depth with which BCP-ALL cells migrate into organoids correlates with their ability to adapt to unfavorable conditions known in the literature. To be able to measure these variations in distance on the micron level, another function built into Open3D was used in an attempt to accurately measure the penetration distance of leukemia or control cells into the organoids. The *RaycastingScene*

class provided by Open3D is a valuable tool for users looking to transform their triangle meshes into functions[133]. The tool offers a convenient way to work with 3D models and explore their properties. Here, it was adopted to calculate the distance of cells to the surface of the organoid mesh. Image data from *TCF3::PBX1*$^+$ PDX1, *BCR::ABL1*$^+$ PDX3, CML, B-lymphocytes and HSPCs were used in this instance. The program returned the distances for each leukemia cell in the image data relative to the reconstructed organoid surface, producing many data points. The data were illustrated on a logarithmic scale to better differentiate between "near-surface" and "below-surface" cells. The resulting dataset was plotted and demonstrated a clear difference between the leukemia cells (PDX1) and healthy controls HSPCs (fig. 32A). Upon closer inspection, engrafted cells appeared to be distributed along a range of distances, clearly dominated by surface-bound cells. PDX1 appeared to show more consistent invasion into deeper parts of the organoids than healthy and CML controls, as well as PDX3. The data were filtered to better compare cells engrafted beyond the surfaces. Engraftment distance beyond 10 μm was chosen as a cutoff to distinguish between surface-bound and deep engraftment. This revealed a significantly higher number of deeply engrafted PDX1 cells over healthy HSPCs and B-lymphocytes. This was also seen when comparing to CML subtypes KCL and K562. Interestingly PDX3, a *BCR::ABL1*$^+$ PDX3 sample, shows significantly less engraftment compared to *TCF3::PBX1*$^+$ PDX1, being on the level of CML controls (fig. 32B). Both healthy and CML controls, exhibited relatively similar engraftment to each other. To summarize, closest distance calculations on surface-reconstructed organoids reveals differential engraftment between CML and BCP-ALL, re-affirming the higher engraftment of BCP-ALL-PDX over CML control cells.

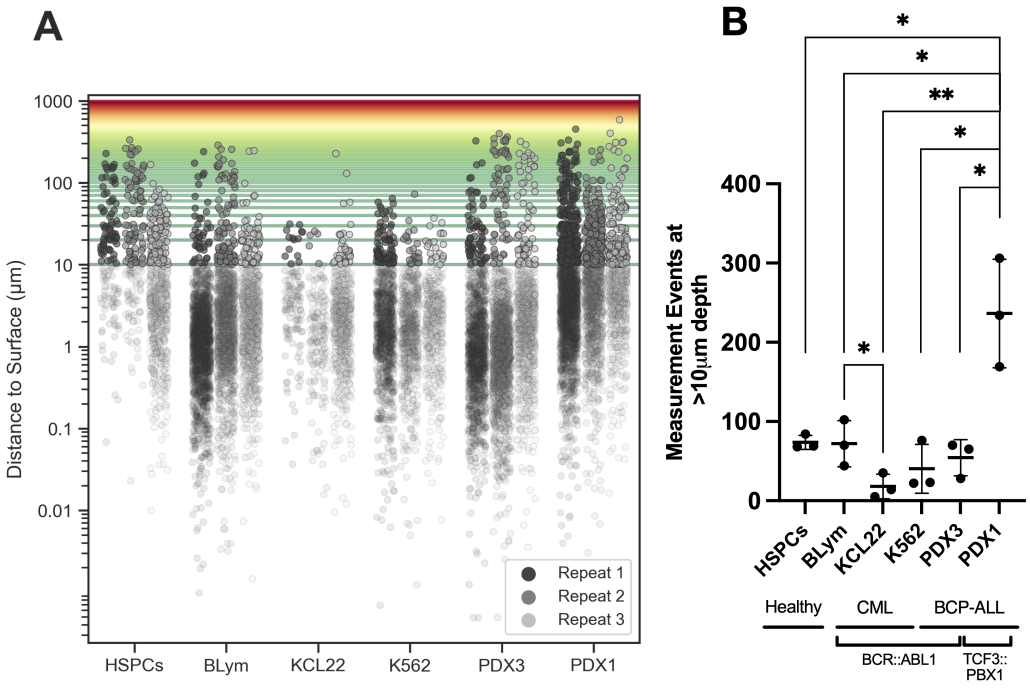

Figure 32: Quantification of Engraftment Distances into Organoids (A-C) - Healthy controls HSPCs and B-lymphocytes (BLym) were tested alongside CML controls (KCL22, K562), as well as both PDX3 and PDX1. The distances of engraftment of cells are shown along the y-axis on a logarithmic scale. Cells measured to be 10 microns or deeper within the organoid with respect to its surface are highlighted by a green to red gradient backdrop. Cells concentrated around the surface are lighter in tone. Triplicates are displayed as different levels of grayscale. (D) Sub-surface detection of leukemia and healthy control cells. The Python analysis pipeline was used to determine the distance of cells below the surface of organoids they were co-cultured with. It was estimated that distances above 10 μm would be considered a boundary for deep invasion. As such, the sum of measurements beyond this boundary is displayed for *TCF3::PBX1*entities. Statistical analysis compared the PDX1 against all other entities using the unpaired two-tailed t-test (n = 3 replicates). PDX1 vs HSPCs (P=0.0151), PDX1 vs B-lymphocytes (P=0.0187), PDX1 vs KCL22 (P=0.0058), PDX1 vs K562 (P=0.0107), PDX1 vs PDX3 (P=0.0120), BLym vs KCL22 (P=0.0466)

3.6 Manipulating BCR-and Chemokine Signaling Function in *TCF3::PBX1*$^+$ Leukemia Co-cultures

The key mediators of CNS involvement in BCP-ALL are yet unclear. Recent efforts to unveil the role of preBCR signaling in CNS invasion identified CD79a/Igα as a crucial mediator in leukemia cells' infiltration[65]. A short-hairpin RNA (shRNA) mediated knockdown (KD) of CD79a in a *TCF3::PBX1*$^+$ cell line 697 (shCD79a) lead to significantly lower CNS engraftment in murine models[65]. A preliminary assessment of the model was conducted before incorporating it in the co-culture procedure. Flow cytometry was conducted to measure the surface expression of CD79a to the representative miR30 and isotype controls (fig. 33A). Testing their proliferation in organoid media revealed comparable growth characteristics (fig. 33B). The model was subsequently seeded at 10,000 cells per organoid for 14 days. Strikingly, CD79a knockdown impeded the engraftment of 697 cells into cerebral organoids compared to shRNA-miR30 control cells (fig. 34A, graph). Of note, both cells previously demonstrated high viability after co-culture (fig. 29).

The chemokine receptor CXCR4 and respective ligand stromal-derived factor-1 (SDF-1) are considered important in CNS relapse both in BCP-ALL and T-ALL[45,49,150]. Specifically, their interaction led to the assumption that SDF-1 in the CSF may be a promoter of CNS tropism. A prior study inhibited CXCR4-SDF-1 signaling via the small- molecule inhibitor Plerixafor in mice, preventing the dissemination of BCP-ALL blasts into the skull, vertebral bone marrow, and subarachnoid space[49]. Therefore, Plerixafor (table 10) was evaluated for inhibiting the CXCR-SF1 axis to prevent the engraftment of leukemia cells into cerebral organoids. To validate the expression of SDF-1, immunostainings were performed on whole organoids revealing high expression of SDF-1. Moreover, the expression pattern closely overlapped with the well-established neuronal marker MAP2. SDF-1 expression remains stable across various brain regions postnatal, including the hippocampus, and persists throughout the organism's lifespan[50]. Plerixafor was used at a final concentration of 44nM based on the IC_{50} value published by the supplier[151], and toxicity was not observed in 697 cells even after 72 hours of exposure (fig. 34C). Subsequently, Plerixafor or vehicle control (12h) pre-treated 697 cells were washed and co-cultured with the cerebral organoids. The visual burden and absolute quantification of leukemic cells into the organoids identified a significant reduction in the engraftment of leukemia cells as

compared to vehicle-treated controls, as confirmed by total cell count analysis (fig. 34D). Taken together, attenuation of CD79a/Igα or CXCR4-SDF-1 signaling attenuated *TCF3::PBX1*$^{+}$ leukemia cell engraftment into cerebral organoids, annealing with the previously published results in murine models[152,49].

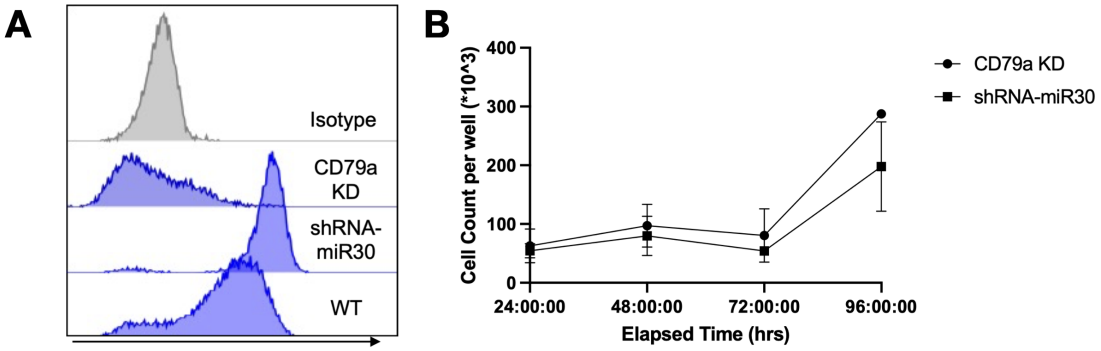

Figure 33: B-cell Receptor Knockdown (CD79a Igα) Validation- Intracellular Staining of CD79a α in Knockdown (KD), Empy Vector (EV). (A) FACS analysis of CD79a KD, shRNA-miR30, and WT 697 cells was stained for intracellular expression of CD79α. Lower levels of CD79α are seen towards the left-hand side of the histograms. (B) Cell proliferation was tested by seeding 50,000 cells per well, measuring cell concentration every 24hrs.

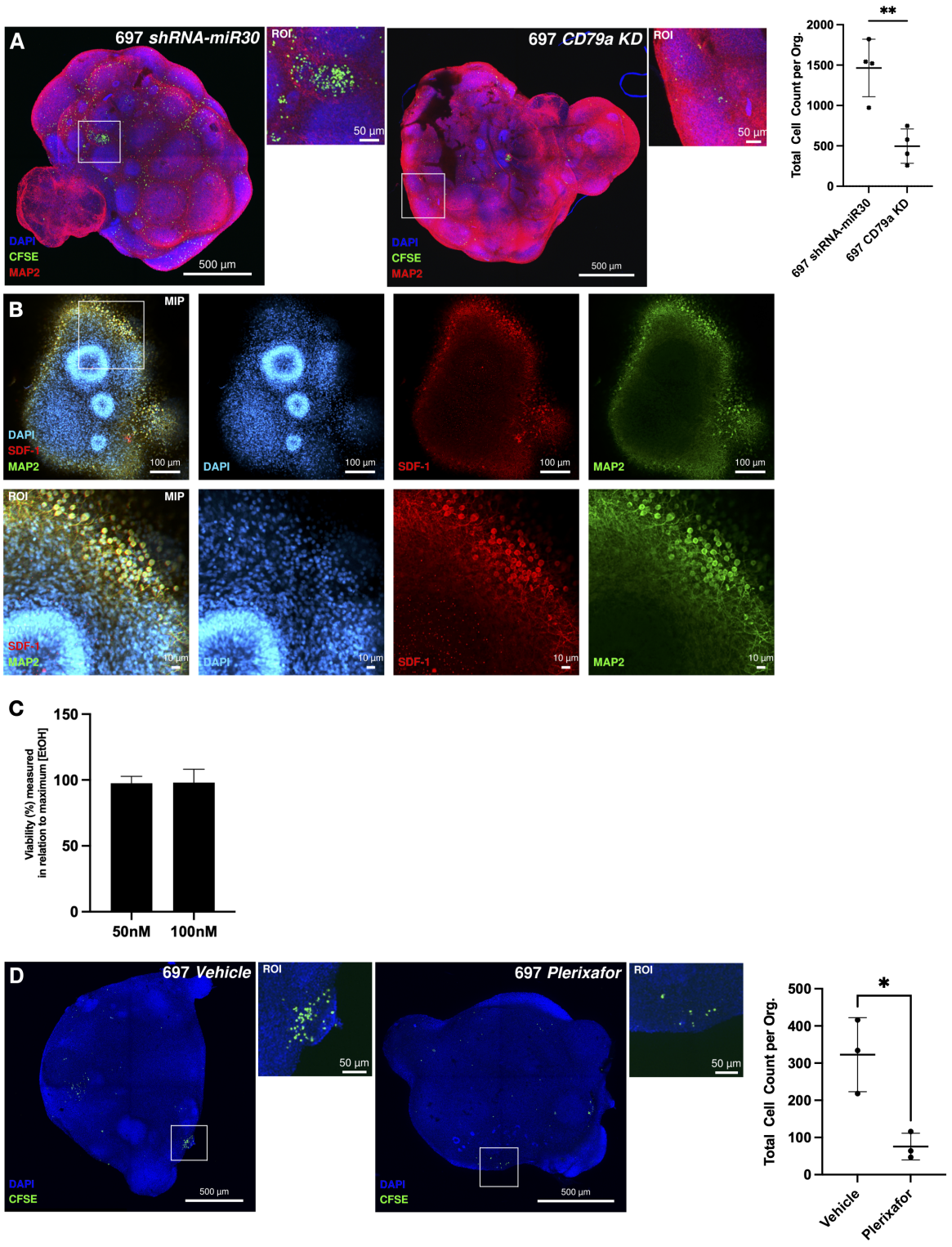

Figure 34: CD79a/Igα Knockdown and inhibition of CXCR4-SDF-1 Interaction (A) *TCF3::PBX1*$^{+}$ shRNA-mediated CD79a...

*continued from previous page...*knockdown (KD) or empty vector (E.V.) control 697 cells (10,000 cells) were seeded in a co-culture assay with (day 30) cerebral organoids for 14 days. Both conditions were analyzed using the unpaired two-tailed t-test, 697 CD79a vs. 697 E.V. ($p = 0.0034$). Scale bars – 500 μm, 50 μm. (B) To demonstrate the expression of SDF-1 in cerebral organoids, day 30 cerebral organoids were stained. A single z-slice of a complete 3D stack is shown above, including a portion of the image in the ROI. Immunofluorescence staining revealed co-localization with anti-MAP2 signal in cerebral organoids, and the expression of SDF-1 significantly increased in neurons, including a portion of the image in the ROI. Scale bars – 100 μm, 10 μm. (C) Toxicity screen was performed according to section 2.5 at 50nm and 100nm and percentage viability was plotted for the 697 and SUPB15 cell lines after 72hrs. (D) 697 wild-type (10,000) cells pre-treated for 12h with (44nM) Plerixafor or with vehicle control in a co-culture assay with (day 30) cerebral organoids for 14 days were seeded in each condition. Both conditions were analyzed using the unpaired two-tailed, Vehicle vs. 697 +Plerixafor ($p = 0.0155$). Scale bars – 500 μm, 100 μm, and 50 μm.

3.7 Transcriptome Profile of Cerebral Organoid-infiltrating *TCF3::PBX1*$^{+}$ Leukemia

It has been reported that BCP-ALL cells can undergo transcriptional/metabolic adaptations when reaching the CNS niche[39,153]. To test this, a co-culture assay was used to identify new pathways and molecules relevant to CNS infiltration of BCP-ALL. Cerebral organoids were co-cultured with cell lines 697 and Kasumi2, respectively, and infiltrating versus non-infiltrating cells were collected after dissociation and sorting and then subjected to RNA-sequencing (section 2.9.1). Differential RNA expression analysis identified upregulation of FOS, FOSB, and EGR1 with consistent and significant (FDR < 0.05; log2(FC) $<$ -1 or log2(FC) > 1) altered expression in invaded leukemia cells as compared to a non-invaded fraction (fig. 35A-B). Fast gene set enrichment analysis (fGSEA) identified significant enrichment in gene clusters regulated by NF-κB in response to TNF and stem cell-related signatures in the invaded leukemia cells compared to non-infiltrated cells. In comparison, the oxidative phosphorylation-, ribosome biogenesis-, reactome translation- and mitochondrial proteins-related gene signatures were downregulated in the invaded leukemia cells compared to non-infiltrated cells (fig. 35). Subsequent validation was performed by repeating the same assay; however, intracellular FACS staining was performed according to the protocol described in section 2.11.2 on the invaded and non-invaded leukemia cells, revealing a consistent upregulation of FOS and FOSB (fig. 35). Further, immunofluorescence staining was performed on suspension (non-infiltrated), paraffin-embedded organoid slices, as well as WT BCP-ALL cells, according to section 2.6.6. The difference in localization of these AP-1 members was tested by staining for FOSB, JUN, and FOS. All three exhibit strong co-localization with the nucleus, while the distribution is mostly diffuse within WT cells (fig. 36). Previous evidence points to the involvement of AP-1 signaling deregulation in hematological cancer, particularly ALL[74,75]. In summary, increased activity of AP-1 is prominent in BCP-ALL maintained inside organoids.

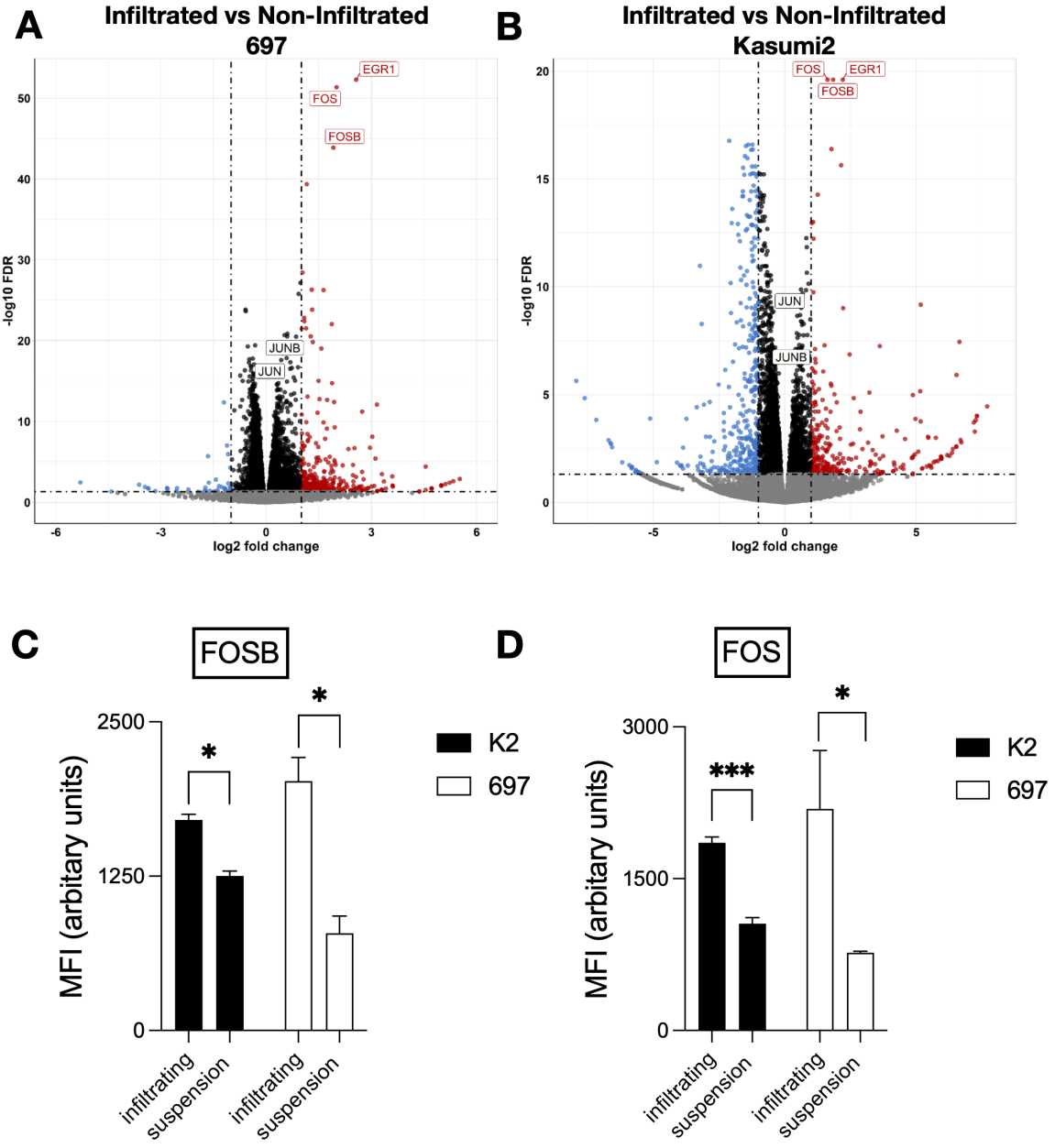

Figure 35: Study of Gene Expression Levels in Infiltrating and Non-Infiltrating TCF3::PBX1+ Leukemia Cells Isolated from Cerebral Organoids - (A-B) Volcano plot showing significantly (FDR < 0.05; log2(FC) < -1 or log2(FC) > 1) up- or down-regulated genes from RNA-seq data of cerebral organoid-infiltrated 697 (A) and Kasumi 2 (B) cells compared to non-infiltrated fraction. (C-D) 697 and Kasumi 2 (K2) cell lines isolated from organoid co-cultures were stained for FOSB and FOS and measured using flow cytometry. The mean fluorescence intensity (MFI) is plotted for both infiltrating (leukemia cells inside organoids) and suspension (non-infiltrated) cells. Statistical analysis was performed using the unpaired two-tailed t-test (FOSB n = 3, FOS n = 4).

3.7.1 Monitoring AP-1 Involvement at Onset of Co-culture using BCP-ALL/AP-1 Reporter Models

It is yet unclear if the AP-1 pathway plays an extensive role in facilitating migration, homing, and overall biological fitness of BCP-ALL cells (or subclones) for CNS invasion. It is also uncertain whether the primary function of the pathway is to promote the survival of BCP-ALL cells within the hostile environment of the CNS niche. It could not be fully elucidated whether adaptations, such as AP-1 member upregulation, occur i) to migrate and engraft into the organoid or ii) as a response to the organoid microenvironment. To establish a functional link between and AP-1 signaling and CNS-involvement in BCP-ALL, *TCF3::PBX1*$^{+}$ 697 cells were stably transduced with an AP-1-GFP reporter construct (section 2.2.4). This construct included transcriptional response elements (TRE) upstream of the mCMV promoter, which allowed for GFP expression in response to AP-1 transcriptional activity. To test the effects of the AP-1 construct, *TCF3::PBX1*$^{+}$ 697 cells which were transduced with the construct or a negative control were co-cultured with and without organoids. All conditions of AP-1 and negative control were normalized to a non-fluorescent 697 wild-type (WT). Live cell imaging, using the Incucyte (section 2.7.3), measured GFP-fluorescence over time. Interestingly, fluorescence in AP-1-carrying 697 cells was significantly ($P<0.0001$) higher when in co-culture compared to suspension only (fig. 37). This was not seen in control cells. In summary, these findings suggest that the microenvironment plays an important role in modulating AP-1-mediated transcriptional responses.

3.7.2 Targeted Inhibition of the AP-1/cFos Axis in BCP-ALL Co-cultures

To further elucidate the functional role of AP-1 signaling in the engraftment of leukemia cells within the organoids, an experiment was conducted by employing an AP-1-specific inhibitor. T-5224 inhibits the AP-1 complex (section 2.13) by blocking the DNA-binding ability of the c-Fos/c-Jun dimer specifically, with minimal impact on other transcription factors[154,75]. In the literature, the ability to inhibit invasion and metastasis of other cancer forms has been documented in *in vivo* studies[127,155]. The toxicity range of the compound was tested according to the method described in section 2.5. Then, the BCP-ALL cell line 697 was treated at 5 μM or DMSO and co-cultured with organoids and live cell imaging was performed to reveal the migration of cell in either condition. Interestingly, migration of cells towards an

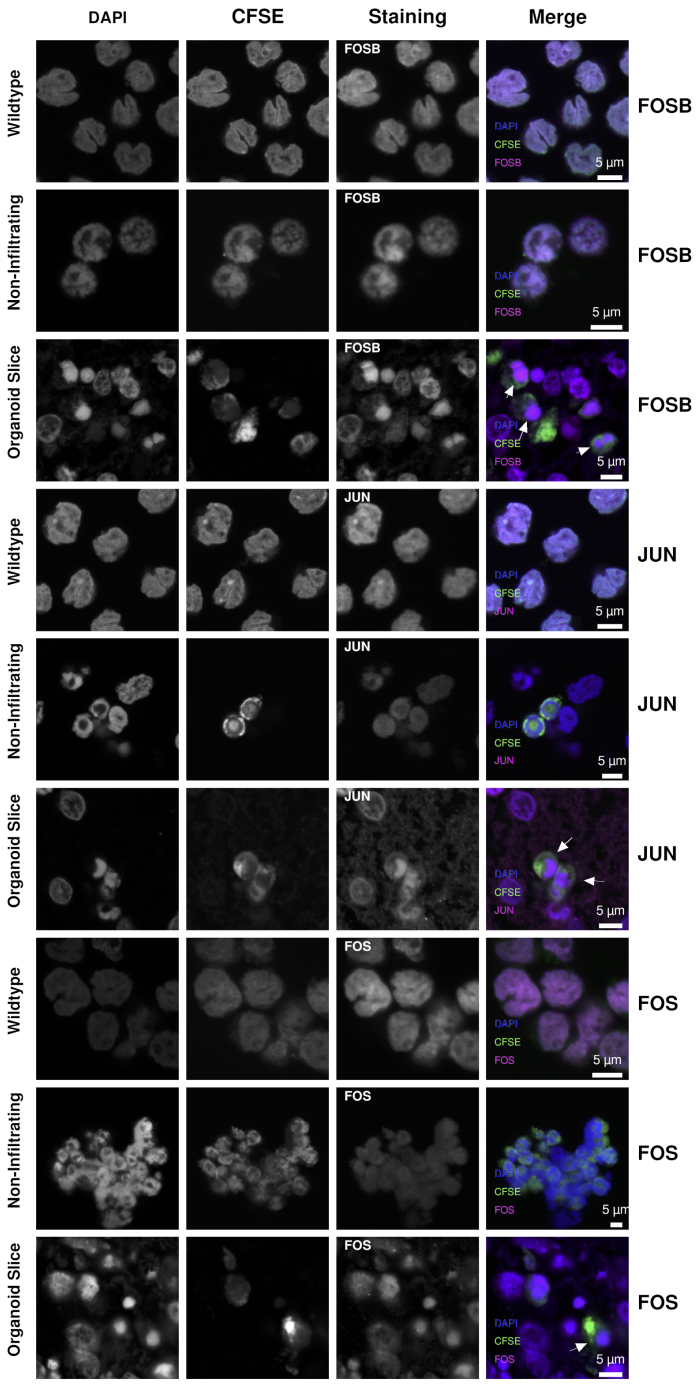

Figure 36: Pinpointing AP-1 Member Localization in Infiltrated and Non-Infiltrated BCP-ALL - A repeat of the assay in fig. 35 with the BCP-ALL cell line 697. Paraffin-embedded slices bearing infiltrated, suspension (non-infiltrated), and wildtype cells were isolated for immunofluorescence staining. All samples were stained for FOSB, JUN, and FOS. Images are grouped in grids of 3 by 4 with the marker for all rows display above, as well as **Wildtype**, **Non-Infiltrating**, and **Organoid Slice** for columns. Immunofluorescence signals are shown in greyscale and color merge in the column along the far right. In **Organoid Slice** columns the overlap of all color channels display the localization of AP-1 members (*white arrows*). Scale bars – 5 μm

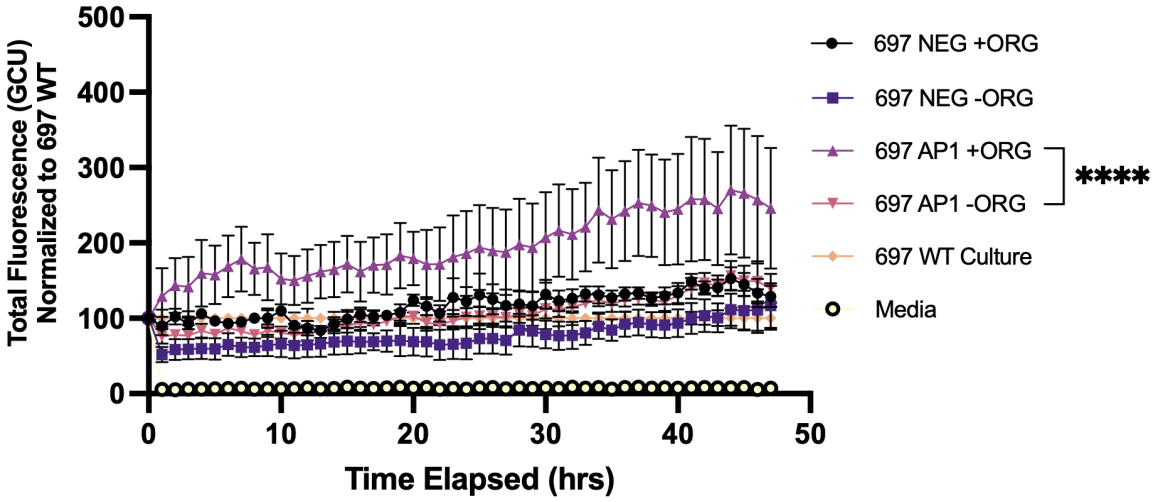

Figure 37: Detection of AP-1 Upregulation of AP-1 via Reporter Construct in BCP-ALL- 697 transduced with either the AP-1 construct (697-AP1) or a corresponding negative control (697-Neg) were co-cultured in the presence (+ ORG) or absence (- ORG) of organoids, respectively. 10,000 cells were seeded from each condition in triplicate. Live cell imaging using revealed an early and consistent rise in GFP fluorescence exclusively within the 697-AP1 TRE cells when co-cultured with organoids. 697 wild-type cells (697 WT culture) and normal culturing media were included as a non-fluorescent controls. Significance between 697 AP1 +ORG vs. 697 AP1 +ORG was calculated using the unpaired two-tailed t-test (697 AP1 +ORG vs 697 AP1 -ORG, n=3, $P<0.0001$).

organoid was visibly different (fig. 38, fig. 39). Upon quantification, cells treated with T-5224 showed significantly attenuated migration towards cerebral organoids (fig. 40). Collectively, the involvement of the AP-1 pathway in CNS leukemia and potential candidate for pharmacological inhibition is further supported by these findings.

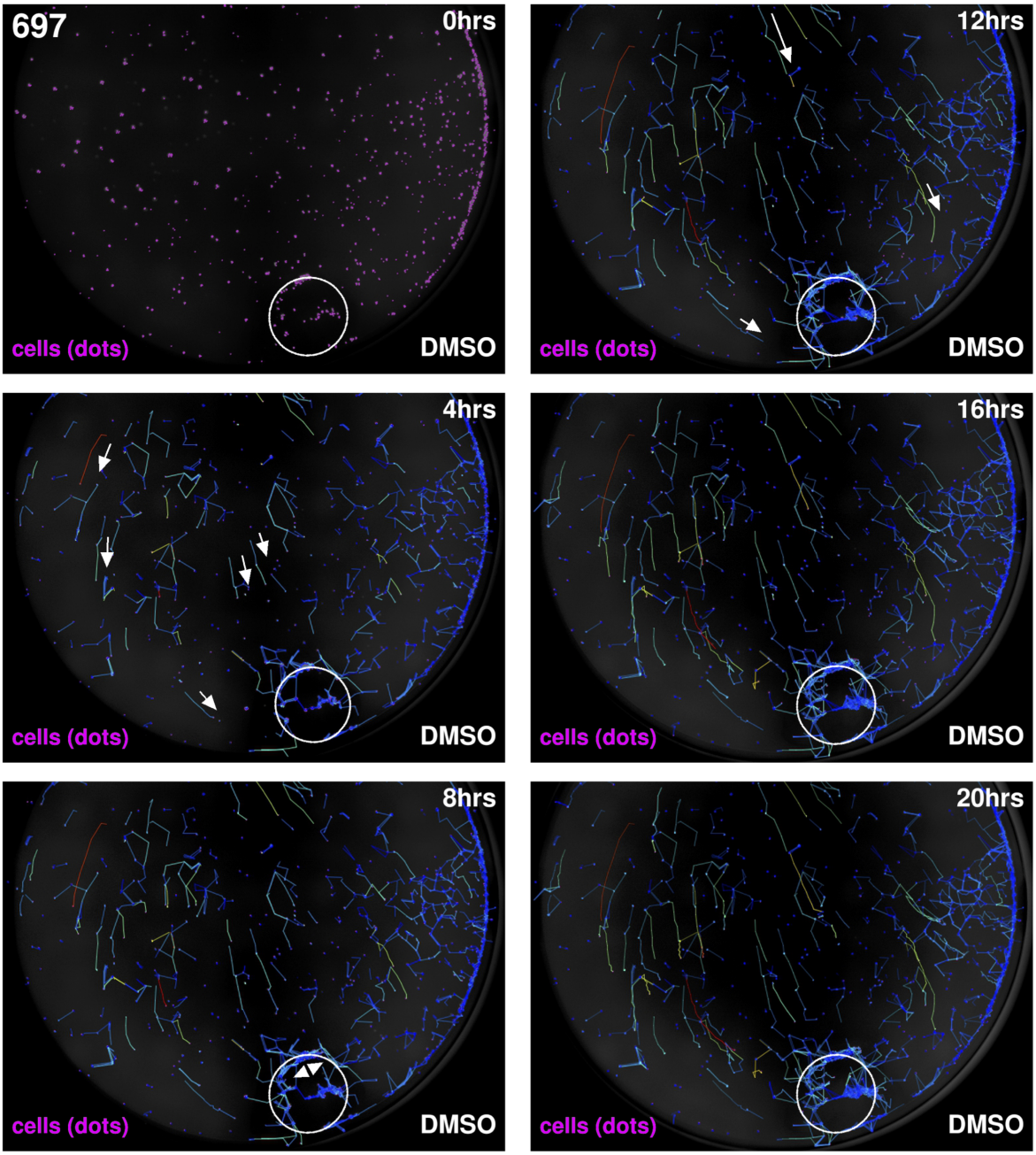

Figure 38: AP-1/c-Fos Targeted Inhibition: Time-lapse Imaging of Leukemia DMSO-treated Control - The 697 leukemia cell line was stained with CFDA-SE treated with DMSO as a control and platted at 1000 cells with one organoid (n=3), shown as "cells (dots)". Time-lapse imaging over 24 hours (every 4 hrs, here displayed 0hrs-20hrs) track the movement of leukemia cells (white arrowhead). Motion of cells in and around the organoids is noticeable (opposite white arrowheads). Analysis performed via the TrackMate plugin on ImageJ (section 2.7.3) identified and traced lines along the movement path of the cells over the time-lapse.

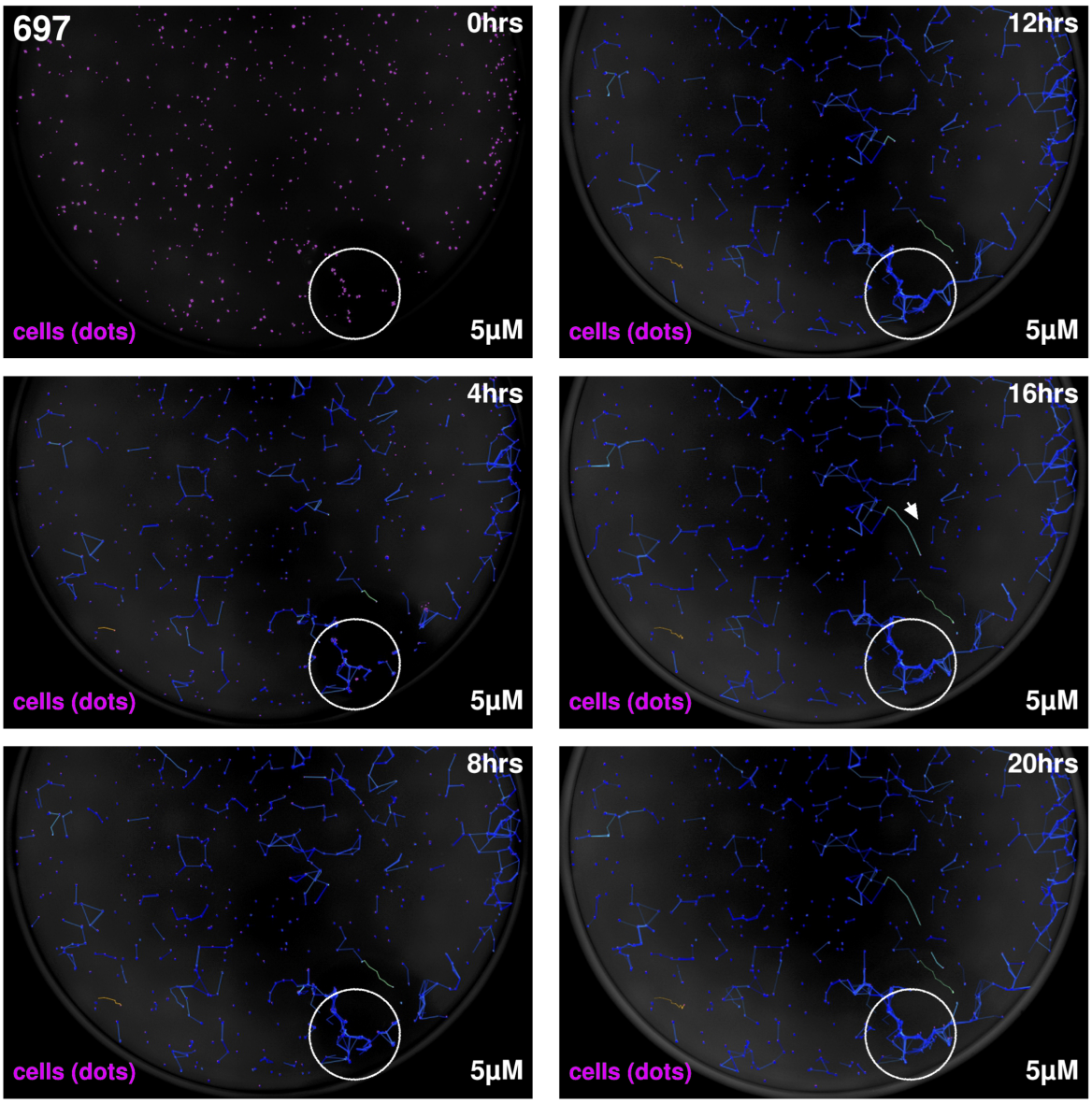

Figure 39: AP-1/c-Fos Targeted Inhibition: Time-lapse Imaging of Leukemia treated with T-5224 - The 697 leukemia cell line was stained with CFDA-SE and treated with the AP-1 inhibitor T-5224 at a final concentration of 5 μM and platted at 1000 cells with one organoid (n=3), shown as "cells (dots)". Time-lapse imaging over 24 hours (every 4 hrs, here displayed 0hrs-20hrs) track the movement of leukemia cells (white arrowhead). Analysis performed via the TrackMate plugin on ImageJ (section 2.7.3) identified and traced lines along the movement path of the cells over the time-lapse.

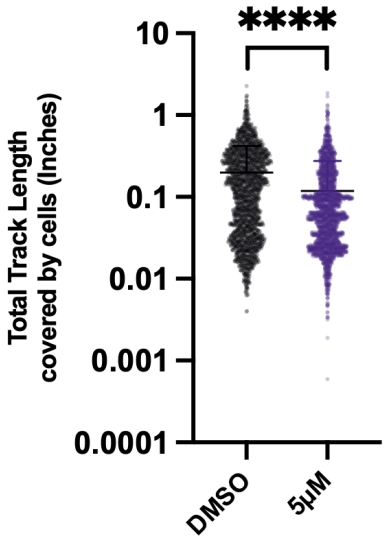

Figure 40: AP-1/c-Fos Targeted Inhibition: Quantification of Total Cell Movement in Co-culture - The total track length covered by 697 cells, with or without T-5224 treatment was measured by time-lapse imaging for 20h, and analysis was performed via TrackMate plugin. The results depicting the total track length covered by the cells. Statistical analysis was performed using the unpaired two-tailed t-test (DMSO vs 5 μM, n=3, $P < 0.0001$).

Chapter 4

Discussion

4.1 Background

The engagement of the central nervous system (CNS) during acute lymphoblastic leukemia (ALL) at the initial diagnosis or relapse stage remains a major clinical challenge. Efforts are being undertaken to elucidate the underlying biological mechanisms of CNS invasion and develop less-toxic yet highly efficacious therapies to treat CNS-leukemia[32,49]. Yet, robust models to faithfully recapitulate components of human pathophysiology still need to be completed. Although still in development, brain organoids are gaining popularity in cancer research, attributable to considerable advantages over 2D *in vitro* or *in vivo* models. This thesis discussed the importance of reliable *in vitro* cancer research models, focusing on organoids' potential in leukemia research. A new set of procedures for creating and testing co-culture assays between cerebral organoids and BCP-ALL cells was proposed to address the need for leukemia-specific applications for this model.

4.2 BCP-ALL-cells invade robustly into cerebral organoids in comparison to non-ALL-cells

A robust concept for a co-culture assay involving organoids and leukemia was designed. Co-culture assay between mature hiPS cell-based cerebral organoids and leukemia were employed. Over several iterations of the assay cell seeding, assay duration, and organoid age were altered to study their effect on engraftment. Critical differences exist in this organoid/leukemia assay analysis to previously published image-based

assessments of cancer dissemination in cerebral organoids (section 1.5.4.1). Here, the orthogonal view tool was adopted to initially prove that cell engraftment occurred, which cannot be faithfully illustrated in two-dimensional images, addressing a potential pitfall common in the field. Investigating how time affects the interaction of the two showed that *TCF3::PBX1*$^+$ leukemia cells engraft deep into cerebral organoids within a 14-day of co-culture compared to healthy control, as single cells or even forming large cell aggregates (fig. 19). Engraftment was also shown to occur irrespective of organoid age, showing large sub-surface cell clusters (fig. 21). Next, the leukemia cell concentration was limited up to 200-fold. Here, as little as 50 cells lead to visible infiltration of the organoid (fig. 22). A closer investigation into the migratory propensity of ALL-cells was conducted using live-cell imaging of ALL-cells in the early stages of the co-culture. Time-lapse imaging of 697 (BCP-ALL) and CD34$^+$ HSPCs reveals direct migration of 697 cell towards the organoid, a behavior not seen in isolated suspension (fig. 24). By contrast, migration was vastly reduced in HSPCs (fig. 25); moreover, 697 significantly outperformed HSPCs in distance covered during the assay (fig. 26). This aligns with the well-established role of chemotaxis and invasion in both liquid and solid tumor metastasis, in part driven by chemokine signaling[62,156]. It was decided to isolate the proliferative component in ALL-cells via mitotic inhibition, testing the role of migration and proliferation in colonization of leukemia cells in the organoid microenvironment. This revealed a significant reduction in cell engraftment in treated cells (fig. 27), supporting the notion that cell migration is a core driver of organoid engraftment; however, cell division is essential to colonise the organoid.

To better understand the propensity of leukemia subtypes to engraft, BCP-ALL leukemia, non-ALL and healthy controls were quantified by counting all cells from confocal images. Several high-risk BCP-ALL leukemia entities were investigated alongside HSPCs and two CML cell lines KCL22 and K562. This showed significantly higher engraftment of *TCF3::PBX1*$^+$ leukemia after 14-day co-cultures compared to other non-ALL cells. While other high-risk-ALL cell lines *TCF3::HLF*$^+$ and *BCR::ABL1*$^+$ cell lines showed differential engraftment, they too significantly exceeded HSPCs and CML cell lines. The significantly lower level of HSPCs within the organoids post-co-culture further supports a diminished early migratory propensity as seen in live-cell imaging. PDX-ALL cells of high-risk ALL subgroups *TCF3::PBX1*$^+$ and *BCR::ABL1*$^+$ showed exhibited differential engraftment characteristics, while

significantly exceeding that of CML and HSPC cells. Similarly, *BCR::ABL1*$^{+}$ PDX cells significantly exceeded HSPC and KCL22 engraftment. As previously described, CNS involvement in CML rarely occurs, occasionally detailed in case reports[157,158,159]. Of note, two PDX-ALL candidates of high-risk KMT2A-rearranged (*KMT2A-r*) implicated in CNS-leukemia, were added (initial and relapse) as an isogenic control; however, no differences in their engraftment potential were apparent. Future assays may include further replicates as well as *KMT2A-r*$^{+}$-PDXs in part to address the large spread seen in the data. Surprisingly, healthy B-lymphocytes isolated from buffy coats exceeded both HSPC and CML cell counts. In general, lymphocyte may enter the CNS in low concentration under healthy physiological conditions. This behavior may increase in during inflammatory events such as multiple sclerosis or viral infections[160,161]. Interestingly, BCP-ALL lymphocytes are known to retain the chemokine signaling capabilities, particularly for homing and retention within the bone marrow microenvironment. A higher level of interaction of B-lymphocytes in co-culture may thus not come as a surprise, but may be directed by the migratory capabilities by B-cells. More donor blood samples need to be tested to account for errors. Furthermore both HSPCs and B-lymphocytes require specialized media to thrive *in vitro*. The decision to include CMLs with growth characteristics comparable to BCP-ALL cells was made as they are not commonly associated with CNS relapse would thus represent a more comparable control to BCP-ALL. Furthermore, both exhibit similar growth kinetics *in vitro*. Live-cell analysis of KCL22 and K562 co-cultures could test the assertion whether leukemic engraftment in cerebral organoids is steered solely by inherent migratory properties.

4.3 Spatial Analysis Reveals Deep Dissemination of BCP-ALL Into Brain Organoids

In recent years, a vast body of literature has contributed to the idea that 3D culture system are superior to 2D culture system in reflecting the cell microenvironment[89,90,91,92,93]. Here, it was postulated that precise spatial detection of engraftment can be achieved. Previous publications on organoid co-culture differ significantly in their representation and analysis, specifically using microscopy data[115]. Collapsed z-stack representations do not accurately reflect the relative position of fluorescent or dyed cells, and reliable interpretation of imaging-based analysis is crucial to trust the model's specificity to its research application. Initially, confocal images were analyzed based on a "total cell

count" basis. This was illustrated in orthogonal images showing how cells could reside near the surface or deeper within organoid tissue (fig. 19). This ostensibly limited the analysis of cell behavior within these 3D tissues.

Spatial analysis in organoids has been seen in other recent examples of brain organoid co-cultures with other cancers or entirely different organoid types[115,119]. However, computational pipelines have only been used to characterize brain organoid development[121]. This project introduced a novel pipeline featuring established Python packages to analyze leukemia-organoid assays. Cell infiltration could be reliably detected using image analysis software; however, little could be known about the relative position of cells to the organoid, and therefore the depth of cell invasion. Such quantification could further elucidate the difference in engraftment between leukemia subtypes. To better interpret the localization of leukemia, scatter plots used cartesian coordinates isolated from confocal images. This visualized the distribution of both organoid structures against leukemic cells helps interpret where the leukemia cells tend to localize with respect the organoid volume, especially by showing all three dimensions (fig. 30A-D). This demonstrated an accurate representation by plotting the cartesian coordinates. To convert these data into full 3D models, pointclouds were created for both organoid and leukemia stainings (fig. 31B-C). By employing a poisson-surface reconstruction, watertight polyhedrons were successfully created for all organoid data. Furthermore, the distance between leukemia cells within organoids was determined by animating whole organoids in 3D. The broader literature on organoid/cancer co-cultures does not provide similar analyses using automated imaging analysis tools. This is where this project differentiates strongly from previous 2D illustrations of co-cultures. In this regard, more details were uncovered on how leukemia cells engraft organoids.

The co-culture image data for *TCF3::PBX1*$^{+}$ PDX1, *BCR::ABL1*$^{+}$ PDX3, low-CNS propensity KCL22 and K562, healthy HSPCs and B-lymphocytes were analyzed to further elucidate their spatial distribution. It was discovered that the measurements of distances within organoids is spread out (fig. 32A), with the majority of cells residing near the organoid surface. This indicated that cells are distributed along a length from the surface of the organoid to the deepest measurable part of the organoid. The data were filtered to differentiate between the surface-bound majority and the sub-surface cell clusters. Here, *TCF3::PBX1*$^{+}$ PDX1 cells frequently and significantly migrate deeper than *TCF3::PBX1*$^{+}$ PDX3 which anneals to the CNS engraftment seen for

PDX3 in xenotransplanted mice (data not shown). PDX1 engraftment also exceeded HPSC, B-lymphocytes (fig. 32B). Although the depth of engraftment across CML, HSPCs, and B-lymphocytes appeared similar, B-lymphocytes travelled significantly deeper than KCL22 (CML) (fig. 28). Similar to total cell count, CML entities KCL and K562 exhibited depth of invasion closer to HSPCs, and significantly less than *TCF3::PBX1*$^{+}$ PDX1 (fig. 32B). Interestingly, BCP-ALL PDX3 cells demonstrated a comparatively lower depth of invasion than PDX1 cells. These findings are consistent with the CNS engraftment status observed in a murine model, where PDX1 cells exhibited higher CNS involvement (CNS++) compared to PDX3 cells (CNS+), based on semi-quantitative scoring. Although these are preliminary observations, they suggest that CNS organoids could potentially serve as an *in vitro* model to replicate the CNS engraftment characteristics of ALL cells observed *in vivo*. Although K562 and KCL22 CML cell lines are established in their growth characteristics, the discrepancy in engraftment suggest that factors other than proliferation are responsible. CNS involvement in CML is seen as a rare manifestation of relapse. The robust growth but limited migration of K562 and KCL22 CML cell lines in cerebral organoids suggest they are effective as a non-migratory control in studies of CNS leukemia. This underscores disparities in the spatial distribution within organoids which reaffirms the extent to which migration drives engraftment rather than proliferation. Future studies ought to show if the ability of ALL-cells to invade CNS organoids (either in absolute number or depth) correlates with their propensity to invade the murine or human CNS as suggested by our data. Overall, this method clearly demonstrates differences in engraftment between high-risk-BCP-ALL and comparative non-ALL with low propensity to relapse to the CNS. This further supports the cerebral organoid as a complementary tool to investigate potential therapeutic targets.

4.4 BCP-ALL Engraftment is Reduced by Ablation of Chemokine-/and BCR-Receptor Signaling

The key mediators of CNS relapse are yet to be fully revealed. Some have been previously elucidated in murine models and cell lines. The role of preBCR in CNS malignancies had been shown in this regard, as ablation of the CD79a Igα signaling component significantly reduced BCP-ALL engraftment in organoids (fig. 34). Introducing this specific knockdown in an organoid co-culture setting revealed a reduction in engraftment. This result stands in agreement with the previous published

murine studies involving this model[65]. Further regulators of CNS-metastasis are found in the chemokine receptor-ligand interaction. Specifically, the role of the receptor-ligand interaction of CXCR4-SDF-1 is relevant in both BCP-ALL and T-ALL. The inhibitor Plerixafor (AMD3100) had previously been associated with reduced CNS metastasis. Similarly, pre-treated *TCF3::PBX1*$^+$ BCP-ALL cells co-cultured with organoids lead to a significant decrease in engraftment. However, the variance in total cell count compared to the data acquired in section 3.4.4 and fig. 28 was noticeable. The observed difference may result from employing ethanol as a solvent for Plerixafor and the subsequent washing procedures, which might have influenced the engraftment of 697 cells into the organoids. Taken together, knockdown of CD79a/Igα or inhibition of CXCR4-SDF-1 signaling attenuates *TCF3::PBX1*$^+$ leukemia cells' engraftment into cerebral organoids, annealing with the previously published results in murine models and further validates this approach as a model system to investigate CNS disease. These established candidate pathways were selected to test the relevance and reproducibility of the co-culture model. Taken together, the co-culture model recapitulated the signaling mechanisms shown previously to attenuate CNS engraftment[31,40] *in vivo* findings.

4.5 AP-1 Genes are Selectively Upregulated in Cerebral Organoid-infiltrating *TCF3::PBX1*$^+$ Leukemia Cells

Transcriptomic analysis of organoid-infiltrating leukemia revealed significant upregulation of AP-1 pathway components FOS and FOSB, not seen in non-infiltrating controls (fig. 35A,B). Repetition of the experimental setup and flow cytometry analysis of FOS and FOSB confirmed an increase in expression over non-infiltrating cells (fig. 35C-D), supporting the role of AP-1 signaling involvement in engraftment of leukemia cells into cerebral organoid. Furthermore FOS, FOSB and JUN were shown to colocalize with the nucleus of engrafted BCP-ALL compared to suspension or wildtype cells (fig. 36). This is compounded by a recently published study which revealed AP-1 involvement in CNS+ T-ALL patient cohorts, linking FOS and FOSB to poor prognosis in high-risk groups. In particular, AP-1 candidate genes were significantly more elevated in CNS-isolated ALL cells compared to both spleen and bone marrow compartments of PDX-mice[162]. Apart from AP-1 expression, significant enrichment in the hypoxia-related gene signature was observed in the RNA sequencing data of cerebral organoid-infiltrated leukemia cells. Notably, oxidative phosphorylation was

strongly downregulated in infiltrated compared to non-infiltrated cells. In fact, AP-1 signaling is frequently associated with hypoxia signaling[163], reported as a crucial pathway BCP-ALL cells utilize for their CNS interactions[38]. This is supported by evidence from BCP-ALL patient xenograft models in recipient mice[66]. Transcription factors of the AP-1 family were previously shown to regulate genes associated with survival in acute and chronic myeloid leukemia[164,165]. Leukemic cells in the CNS have been shown to acquire a state of quiescence for which continuous survival signals, provided by the microenvironment, are required[166,167]. More so, the increased number of AP-1 member genes shown to negatively regulate cell proliferation, which may address the low proliferation phenotype associated with ALL cells in the CNS[166,66]. In fact, specific configurations of AP-1 transcription factors can control cell survival, proliferation, apoptosis and chemoresistance[74,168]. AP-1-driven therapy resistance and relapse is supported by recent data, revealing the JNK/JUN axis as a critical factor for steroid resistance in T-ALL. More critically, FOSB rather than JUN held the highest association with CNS-involvement in patients[76]. Overall, there appear to be multiple modes through which AP-1 signaling is regulated in both BCP-ALL and T-ALL. To provide an example, a breakdown of the phenotypic effects of AP-1 knockdown (KO) in gene-knockout mice has been documented. These include lethality during the embryonic stage, sterility, abnormally dense bone (osteopetrosis), and nurturing defects[169,170]. Thus, AP-1 machinery actively regulates a multitude of processes during development. This highlights the need for deeper understanding of AP-1 in regards to future cancer therapies. To summarize, BCP-ALL organoid co-cultures successfully identified AP-1 candidate genes known in CNS involvement in both *in vivo* and patient data. Furthermore, metabolic adaptations to hostile conditions such as the CNS were identified.

4.6 Targeted Inhibition of AP-1 Signaling Components

Involvement of AP-1 was seen in organoid-infiltrating BCP-ALL; however, whether the upregulation of the AP-1 pathway primarily contributes to mechanisms that facilitate migration, or to foster the survival of BCP-ALL cells within the hostile environment of the CNS niche, was unknown. The role of the microenvironment was tested by using *TCF3::PBX1*$^{+}$ 697 cells stably transduced with an AP-1-GFP reporter construct in co-culture. Live-cell imaging revealed significantly higher AP-1-GFP fluorescence signal

in co-cultures compared to suspensions, suggesting that the microenvironment plays a role in AP-1 activation (fig. 37) . This was further tested via targeted inhibition of the FOS/JUN component of the AP-1 pathway with T-5224 (section 3.7.2). Inhibition with 5 μM T-5224 visibly reduced cell migration (fig. 38, fig. 39). Quantifying distance covered by cells confirmed this (fig. 40). The findings further confirm the involvement of the AP-1 pathway in leukemia engraftment and endorse the possibility of targeting the AP-1 pathway in leukemia through pharmacological inhibition. In line, evidence from prior pharmacological assessment of *KMT2A-r*$^{+}$ ALL demonstrated reduced proliferation specifically when treating with the T-5224 AP-1 inhibitor *in vitro*[75].

4.7 Cerebral Organoids as a Complementary Model to CNS-Leukemia

Organoids were introduced as an emerging tool in biomedical research, inherently capable to address limitations of well-established mouse xenograft or 2D monolayer cultures. Capable of simulating the architecture and function of organs[171], they permit *in vitro* investigation of physiological events. Organoids have been reported as suitable for biobanking given their genomic stability. This is compounded by its established use in high-throughput screens[171]. In direct contrast with animal models, several advantages are well-documented. Organoids carry lower experimental complexity given the regulatory aspects and long-term planning required for *in vivo* models. Real-time imaging of single-cell events is possible given the comparatively smaller size. Most of all, and in the context of this project, organ development can differ vastly between species. The development of the human neocortex is a prime example; organoids can introduce critical steps in differentiation to more accurately reflect the 3D tissue microenvironment[147,100,99]. Although early examples of organoid co-cultures existed, they severely underperform in fully utilizing the 3D aspect. This PhD project introduces several novelties in the context of BCP-ALL leukemia were introduced and previously published ways of investigating cell invasion were challenged. Leukemia engraftment were detectable using flow cytometry (section 2.11.2) and confocal microscopy (section 2.3.1). In addition, the computer-analysis pipeline introduced in section 2.8.2.1 provides a new tool for research applicable beyond CNS-leukemia. Chemokine-receptors such as CXCR4 remains a highly prevalent chemokine receptor in hematological malignancies, including metastasis and adaptation to chemotherapy (in AML). Here, inhibiting the binding of its ligand SDF-1 showed significant impact on cell engraftment. The first

demonstration of organoid-infiltrating cells emabled the comparison of infiltrated and non-infiltrated cells from organoids to perform RNA sequencing. This revealed that a known potential therapeutic target in AP-1 is involved in leukemia dissemination into organoids. Furthermore, investigating the onset of AP-1 involvement during co-culture pointed towards a role in leukemia migration. In summary, the above mentioned novelties may support organoids as a preclinical model for screening potential therapeutics, including those that inhibit pathways or target specific targets.

Chapter 5

Outlook

5.1 Applicability of Brain Organoids as a Preclinical Model

There is a clear interest in finding alternative disease models to animal testing. To this day, these models are associated with significant time investments, extensive bureaucracy to approve studies, and often a failure to faithfully predict outcomes from human clinical trials. Failure of therapeutics developed through these models significantly undermines the number of available and effective drugs to patients, affecting healthcare costs. Increasing public pressure to move away from animal testing is partly reflected by the United States Food and Drug Administration (FDA) Modernization Act 2, signed in 2021, loosening the reliance on animal models[118,172].

Here, the cerebral organoids model demonstrated effectiveness as a surrogate system for studying signaling pathways implicated in CNS-leukemia. However, it is crucial to acknowledge that cerebral organoid technology currently serves as a complementary model, augmenting existing models for studying the involvement of ALL cells in the CNS. Animal models were briefly introduced and contrasted with novel 3D culture systems. Neither are they a perfect model of human biology nor can the ethics of their use be ignored for long. Organoid assays can benefit in their scalability and generation from patient material, as previously shown[102].

5.2 Limitations and Recommendations for Improvement

The field of organoid research is becoming ever more attractive as a complementary research model. Yet, the establishment of novel techniques seldom meets a few issues. This project was no exception in this regard. This is a foundational project for its institute, building on limited expertise and equipment. In hindsight, some areas for improvement will be addressed in this chapter.

5.2.1 Live-cell and Lightsheet Microscopy Imaging

This project could not delve much into a live-cell approach for co-cultures, as technological limitations and time had to be considered. Organoids will remain turbid without any clearing applications to the tissue. This would be only possible for fixated samples. Referring back to how cells appear when traversing into the organoid in the co-cultures, single cells or larger aggregates of cells are consistent observations. It is unclear, however, whether single cells seed a more extensive aggregate growth within the organoid. In other words, analyses of co-cultures need to give more insight into the clonal behavior of cells. Real-time/live-cell analysis of organoids in co-culture can be developed to detect unseen events. These could include detecting single events, division and migration of cells, and changes to the organoid. The issue of performing 3D live-cell imaging on large tissues has yet to be solved. Similarly, during the project, it was discovered that the type of microscopy used for organoids would broadly impact the quality and usability of the image data. The organoid-leukemia pipeline can be medium throughput, with a range of 12-48 organoids per experiment. Due to material and time constraints, advanced imaging systems such as light-sheet microscopy were not adopted. These limitations may lead into downstream analysis such as the computational analysis pipeline. The wider research field may benefit from novel tools delivering better spatial analysis. This is not limited to cancer engraftment in brain organoids, but may expand to organoid application. This advanced method offers enhanced spatial analysis capabilities, aligning with the project's innovative objectives. It ought to be mentioned that this transition from simple detection to spatial analysis poses a change in the analytical approach. Previous adoptions of spatial analysis of organoids were limited to characterization of organoid development [121]. Since this is the first-of-its-kind implementation with regards to leukemia-organoid co-cultures, it should aim to enrich the comprehension of the subject rather than a repudiation of the

previous method's value. Furthermore, this analysis concept ought not to be limited to a leukemia setting, but may be used for other organoid assays. If parts or all of the methodology shown in this thesis are used, their active development is recommended. There is unexploited potential in using computer analysis pipelines for medium-and high-throughput experiments, including live-cell imaging analysis.

5.2.2 Critical Assessment of Organoid Cultivation Protocols

To their disadvantage, organoids still need to be developed to reflect human tissue closer rather than mimicking a part of them. Overall, they only approximate the structure and function of organs. There is yet to be a protocol to generate highly complex and intricate morphologies, such as leptomeninges. The leptomeninx is crucial in leukemia metastasis into the CNS (section 1.3.3), as involvement of brain parenchyma is recurrently observed in ALL[86]. As such, an organoid incorporating a functional meningeal layer may pose insightful. The cerebral organoid presented in this thesis does not yet yield these intricate compartments and is yet to be developed. A recent study has explored enhancing the cytoarchitectural complexity of organoids by incorporating cultivated meningeal precursors already maturing organoid in culture. This yielded marginal improvements in corticogenesis over previously established protocols[173]. Such an approach does not activate any intrinsic cellular mechanisms of spheroid bodies or neurospheres but rather adds further complexity to the production process of organoids. The system itself is conceptualised as a co-culture model. This thesis' protocol thus serves a more reproducible, but less time-intensive co-cotulture system. The assays conducted revealed phenotypic and transcriptional characteristics of engrafting ALL cells overlapping with those of engrafted in murine CNS settings. It would be intriguing to explore whether the ability of ALL cells to adapt and survive, for example under hypoxic conditions, is more crucial for effective CNS colonization than their migration and homing capabilities. This could be adressed by testing ALL engraftment in CNS organoid models with organoids of other leukemia-relevant organs, like the bone marrow[119]. Although showing promise for the progression of organoid complexity, further investigation is warranted to achieve a truer replication of the tissue. As such functional vascularisation does not exist in the organoids used in this project. These commonly rely on the perpetual flow of nutrient-rich media to sustain themselves. Having a usable vascularisation of organoids can positively affect parts of this model. Firstly, human brain organoids without microcirculation rely solely on

culturing equipment to deliver oxygen and nutrients to deeper regions. This is often quoted to limit the growth period of organoids in suspension culture, leading to necrotic formations in their core. Of note, some organoid protocols enable the development of vascular systems by introducing pericytes and endothelial cells. However, these systems mainly function as part of the structure rather than actively promoting the flow of nutrients[174,175]. Fluidic/microfluidic devices, such as the organ-on-chip system, can mitigate this issue by providing some control over nutrient flow and oxygenation. Microfluidics refers to the scientific and technological field that involves the precise manipulation and processing of fluids at a microscale level[37,176]. However, these systems require scalability to accommodate a realistic throughput of leukemia co-culture assays. In a first, Pellegrini et al created CNS organoids that generated a fluid resembling CSF and exhibited features of barrier formation[177]. It will be interesting to see if similar results as obtained in this thesis by studying the barrier function of such organoids. It must be stressed that meningeal and vascular formations are lacking in this model with regard to CNS dissemination, which is also a missing component in this thesis. Secondly, cell-protein interactions at the microvasculature are relevant in CNS-leukemia, as was shown for integrins mediating the invasion of leukemia cells (section 1.3.4.1). Transmigration is the process by which leukocytes can leave the blood vessels (extravasate) by squeezing between the cells that make up the blood vessel walls, a process called "paracellular route" or "diapedesis". They use membrane protrusions to feel their way around the surface of the blood vessels and find the junctions between the cells (cell-cell junctions). Adding complex endothelial vessel fenestrations to brain organoids could allow researchers to investigate this interaction since an array of integrins, proteases and signaling pathways are known to mediate this process. Numerous groups have tackled this issue of vascularisation in organoids. One published approach to create a vascularisation, be it non-functional *ex vivo*, involves transplanting organoids into mice[174]. Furthermore, evidence suggests that a continuous epithelium could support the structural and functional integrity of the brain[175]. This approach requires *in vivo* models and approvals to perform these invasive experiments. The existing literature on organoid-cancer interaction has yet to show other organoid types, such as colon or pancreatic organoids, to study whether engraftment is CNS-specific. This is also true for previous publications on organoid-GSC models[115]. It would be worth conducting an experiment where BCP-ALL cells are made to compete with various types of organoids, including neural and colon organoids, to determine if they

preferentially migrate to brain/neural organoids but not to colon organoids, which would be a more accurate representation of the clinical scenario. However this has never been attempted for co-culture assays in the wider literature. A fundamental limitation to this approach is the capacity and expertise of research groups to create such diverse organoid cultures. This project introduced key novelties for leukemia research with 3D *in vitro* systems. Their use as a complementary approach to examine CNS engagement of ALL cells while highlighting the importance of further preclinical validation should be explored. New CNS organoid systems are constantly being developed and improved. It will be interesting to see if similar results as obtained in our organoid model will be observed when adding additional layers of complexity.

5.3 The Role of Synthetic Matrigels to Optimize Organoid Maturation

Initially, the issue of heterogeneity represents a significant obstacle in organoid culture systems. Achieving consistent and optimal growth within and across batches is crucial for co-culture experiments. Today, many protocols to generate complex cerebral organoids exist with complex structural and cellular organization[102,123,178,179]. This is in part due to advancements in matrix technologies. Differences exist in media recipes and the use of tough hydrogel or fibrous matrices, which may lead to even larger and more complex structures[105,141]. The use of matrigel-embedding using matrigel (generated from Engelbreth-Holm-Swarm (EHS) mouse tumor) embedding step is adbsent in this project. The necessity to use Matrigel for cultivation is strongly argued in the field. In principle, extracellular matrices such as matrigel influence growth and development of organoids by forming a surrounding micronenvironment[180]. Several limitations of their use ought to be considered. Organoid cultivation requires extensive optimization of the input steps (iPS cultivation, spheroid/neurosphere expansion) to ensure minimal intra- and inter-batch heterogeneity, as well as optimal differentiation. Matrigel has been reported to consist of at least 1800 unique proteins, whose gross contribution to organoid maturation is difficult to pinpoint. Overall, protein composition may or may not affect cellular processes in organoid development[181]. The presence of these proteins could impact various aspects of organoid biology, requiring careful consideration during experimental design. Batch-to-batch variability in Matrigel production only adds to this uncertainty. The mechanical properties of the cell tissue micronenvironment have a profound effect on key parameters. This has been exemplified in intestinal

and pancreatic organoids, in which the tissue formation, viability, and differentiation and maturation was depenendet on matrix stiffness. Synthetic hydrogels or matrigels can help alleviate this concern by providing a standardized environment that is conducive to uniform organoid development. Properties such as degradation of the matrix and their mechanical properties e.g. stiffness are manipulable. Indeed the ability to modulate stiffness can influence various cellular behaviors such as survival, proliferation, and differentiation[181]. The mechanical properties of hydrogels, including the shear modulus that correlates with stiffness, exhibit heterogeneity within Matrigel formulations. It is significant to note that while synthetic hydrogels hold promise for fine-tuning the mechanical properties of the culture environment, there is currently a lack of agreement regarding an optimal hydrogel formulation that significantly benefits cerebral organoid development. Despite ongoing research efforts in this direction, a hydrogel system that outperforms Matrigel in supporting the growth and maturation of cerebral organoids has yet to be established in the literature. To provide an example of organoid cultivation without basal matrices, a recent publication addressed the above points using a new approach. Cheng Chen and colleagues cultivated brain organoids using a 3D printing approach without matrigel, focusing mainly on optimising shape and coating of their culturing wells[182]. Sakaguchi and colleagues had previously recapitulated human hippocampal formations and their functional neurons, without the use of matrigel[105]. To conclude, matrix development remains a major role in organoid research and requires sincere attention for their benefits and drawbacks.

5.4 Concluding Remarks

In recent years the vast expansion in experimental tools has genuinely changed the game for experimentally tailored *in vitro* systems to fit the needs of research groups[105,117,102,183,103]. As a tool, organoid technology introduces reproducibility and analytical depth while studying human tissue, on par with the flexibility only previously known amongst other model organisms. This thesis presented the novel application of organoid to co-culture high-risk BCP-ALL leukemia. This was accomplished with the development of new confocal microscopy-based analyses to capture the dissemination of leukemia. Organoid tissue complexity will remain a hurdle in the short-term. Recent work in developing accurate barrier systems, connective tissue, and fully functional vascularization systems will help develop the next generation of organoids[177,173,174,175].

Finally, organoids can be made from biopsies derived from any individual in question, providing a way to "tailor" this model to that particular individual. Ultimately, scientists can generate lab-grown, complex tissues and organs for various applications, incl. tissue engineering, drug design/screening, and regenerative medicine. Besides, by generating patient-specific cerebral organoids, this technology can open a new avenue for personalised medicine[184,185].

Bibliography

[1] Maria Thastrup, Alasdair Duguid, Christian Mirian, Kjeld Schmiegelow, and Christina Halsey. Central nervous system involvement in childhood acute lymphoblastic leukemia: challenges and solutions. *Leukemia*, 36(12):2751–2768, December 2022. ISSN 0887-6924, 1476-5551. doi: 10.1038/s41375-022-01714-x. URL https://www.nature.com/articles/s41375-022-01714-x.

[2] R. J. Aur, J. Simone, H. O. Hustu, T. Walters, L. Borella, C. Pratt, and D. Pinkel. Central nervous system therapy and combination chemotherapy of childhood lymphocytic leukemia. *Blood*, 37(3):272–281, March 1971. ISSN 0006-4971.

[3] Matthew R. Warr, Eric M. Pietras, and Emmanuelle Passegué. Mechanisms controlling hematopoietic stem cell functions during normal hematopoiesis and hematological malignancies. *WIREs Systems Biology and Medicine*, 3(6):681–701, November 2011. ISSN 1939-5094, 1939-005X. doi: 10.1002/wsbm.145. URL https://onlinelibrary.wiley.com/doi/10.1002/wsbm.145.

[4] Sean J. Morrison and Allan C. Spradling. Stem Cells and Niches: Mechanisms That Promote Stem Cell Maintenance throughout Life. *Cell*, 132(4):598–611, February 2008. ISSN 00928674. doi: 10.1016/j.cell.2008.01.038. URL https://linkinghub.elsevier.com/retrieve/pii/S0092867408001396.

[5] J. P. Monteiro. Normal hematopoiesis is maintained by activated bone marrow CD4+ T cells. *Blood*, 105(4):1484–1491, February 2005. ISSN 0006-4971, 1528-0020. doi: 10.1182/blood-2004-07-2856. URL http://www.bloodjournal.org/cgi/doi/10.1182/blood-2004-07-2856.

[6] Craig D. Jude, Justin J. Gaudet, Nancy A. Speck, and Patricia Ernst. Leukemia and hematopoietic stem cells: Balancing proliferation and quiescence. *Cell Cycle*,

7(5):586–591, March 2008. ISSN 1538-4101, 1551-4005. doi: 10.4161/cc.7.5.5549. URL http://www.tandfonline.com/doi/abs/10.4161/cc.7.5.5549.

[7] Thomas R. Jackson, Rebecca E. Ling, and Anindita Roy. The Origin of B-cells: Human Fetal B Cell Development and Implications for the Pathogenesis of Childhood Acute Lymphoblastic Leukemia. *Frontiers in Immunology*, 12:637975, February 2021. ISSN 1664-3224. doi: 10.3389/fimmu.2021.637975. URL https://www.frontiersin.org/articles/10.3389/fimmu.2021.637975/full.

[8] Ching-Hon Pui, Jun J. Yang, Stephen P. Hunger, Rob Pieters, Martin Schrappe, Andrea Biondi, Ajay Vora, André Baruchel, Lewis B. Silverman, Kjeld Schmiegelow, Gabriele Escherich, Keizo Horibe, Yves C.M. Benoit, Shai Izraeli, Allen Eng Juh Yeoh, Der-Cherng Liang, James R. Downing, William E. Evans, Mary V. Relling, and Charles G. Mullighan. Childhood Acute Lymphoblastic Leukemia: Progress Through Collaboration. *Journal of Clinical Oncology*, 33(27): 2938–2948, September 2015. ISSN 0732-183X, 1527-7755. doi: 10.1200/JCO.2014.59.1636. URL https://ascopubs.org/doi/10.1200/JCO.2014.59.1636.

[9] Gabriele Escherich and Martin Schrappe. Aktualisierte AWMF Leitlinie über die Diagnostik und Therapie der akuten lymphoblastische Leukämie im Kindesalter. *Klinische Pädiatrie*, 234(06):363–367, November 2022. ISSN 0300-8630, 1439-3824. doi: 10.1055/a-1936-3077. URL http://www.thieme-connect.de/DOI/DOI?10.1055/a-1936-3077.

[10] Mel Greaves. A causal mechanism for childhood acute lymphoblastic leukaemia. *Nature Reviews Cancer*, 18(8):471–484, August 2018. ISSN 1474-175X, 1474-1768. doi: 10.1038/s41568-018-0015-6. URL https://www.nature.com/articles/s41568-018-0015-6.

[11] Ardine M. J. Reedijk, Jan Willem W. Coebergh, Hester A. De Groot-Kruseman, Inge M. Van Der Sluis, Leontien C. Kremer, Henrike E. Karim-Kos, and Rob Pieters. Progress against childhood and adolescent acute lymphoblastic leukaemia in the Netherlands, 1990–2015. *Leukemia*, 35(4):1001–1011, April 2021. ISSN 0887-6924, 1476-5551. doi: 10.1038/s41375-020-01024-0. URL https://www.nature.com/articles/s41375-020-01024-0.

[12] Erik Ten Boekel, Fritz Melchers, and Antonius G. Rolink. Role of the pre-b cell

receptor in b cell development, repertoire selection, and tolerance. *The Journal of Immunology*, 190(2):745–754, 2013.

[13] S Jeha, D Pei, M Onciu, D Campana, C Cheng, JT Sandlund, RC Ribeiro, JE Rubnitz, JR Downing, WE Evans, MV Relling, and C-H Pui. Increased risk for CNS relapse in pre-B cell leukemia with the t(1;19)/TCF3-PBX. page 4.

[14] Susan Y. Wu, Nicholas J. Short, Lewis Nasr, Bouthaina S. Dabaja, and Penny Q. Fang. Central Nervous System Prophylaxis and Treatment in Acute Leukemias. *Current Treatment Options in Oncology*, 23(12):1829–1844, December 2022. ISSN 1527-2729, 1534-6277. doi: 10.1007/s11864-022-01032-5. URL https://link.springer.com/10.1007/s11864-022-01032-5.

[15] David A. Walker, Lisethe Meijer, Beth Coyle, and Christina Halsey. Leptomeningeal malignancy of childhood: sharing learning between childhood leukaemia and brain tumour trials. *The Lancet. Child & Adolescent Health*, 4(3):242–250, March 2020. ISSN 2352-4650. doi: 10.1016/S2352-4642(19)30333-5.

[16] Sharyu Hanmantgad and Yasmin Khakoo. System Cancer and the Central Nervous System Involvement. In *Swaiman's Pediatric Neurology*, pages 1017–1020. Elsevier, 2017. ISBN 978-0-323-37101-8. doi: 10.1016/B978-0-323-37101-8.00133-8. URL https://linkinghub.elsevier.com/retrieve/pii/B9780323371018001338.

[17] Christina Halsey, Georgina Buck, Sue Richards, Faraneh Vargha-Khadem, Frank Hill, and Brenda Gibson. The impact of therapy for childhood acute lymphoblastic leukaemia on intelligence quotients; results of the risk-stratified randomized central nervous system treatment trial MRC UKALL XI. *Journal of Hematology & Oncology*, 4(1):42, December 2011. ISSN 1756-8722. doi: 10.1186/1756-8722-4-42. URL https://jhoonline.biomedcentral.com/articles/10.1186/1756-8722-4-42.

[18] Ricardo Sanchez, Rosa Ayala, Rafael Alberto Alonso, María Pilar Martínez, Jordi Ribera, Olga García, José Sanchez-Pina, Santiago Mercadal, Pau Montesinos, Rodrigo Martino, Pere Barba, José González-Campos, Manuel Barrios, Esperanza Lavilla, Cristina Gil, Teresa Bernal, Lourdes Escoda, Eugenia Abella, Ma Luz Amigo, Ma José Moreno, Pilar Bravo, Ramón Guàrdia, Jesús-María Hernández-Rivas, Antoni García-Guiñón, Sonia Piernas, José-María Ribera, and Joaquín

Martínez-López. Clinical characteristics of patients with central nervous system relapse in BCR-ABL1-positive acute lymphoblastic leukemia: the importance of characterizing ABL1 mutations in cerebrospinal fluid. *Annals of Hematology*, 96 (7):1069–1075, July 2017. ISSN 1432-0584. doi: 10.1007/s00277-017-3002-1. URL https://doi.org/10.1007/s00277-017-3002-1.

[19] T Terwilliger and M Abdul-Hay. Acute lymphoblastic leukemia: a comprehensive review and 2017 update. *Blood Cancer Journal*, 7(6):e577–e577, June 2017. ISSN 2044-5385. doi: 10.1038/bcj.2017.53. URL https://www.nature.com/articles/bcj201753.

[20] Sarah K. Tasian. TCF3::HLF acute lymphoblastic leukemia: still challenging to cure thirty years later. *Haematologica*, 108(7):1713–1714, July 2023. ISSN 0390-6078. doi: 10.3324/haematol.2023.283148. URL https://www.ncbi.nlm.nih.gov/pmc/articles/PMC10316242/.

[21] S. C. Raimondi, E. Privitera, D. L. Williams, A. T. Look, F. Behm, G. K. Rivera, W. M. Crist, and C. H. Pui. New recurring chromosomal translocations in childhood acute lymphoblastic leukemia. *Blood*, 77(9):2016–2022, May 1991. ISSN 0006-4971.

[22] Monika Lejman. Comprehensive chromosomal aberrations in a case of a patient with TCF3-HLF-positive BCP-ALL. page 7, 2020.

[23] Brice Mouttet, Luciana Vinti, Philip Ancliff, Nicole Bodmer, Benoît Brethon, Gunnar Cario, Christiane Chen-Santel, Sarah Elitzur, Volkan Hazar, Joachim Kunz, Anja Möricke, Jerry Stein, Ajay Vora, Yöntem Yaman, Martin Schrappe, Sema Anak, André Baruche, Franco Locatelli, Arend von Stackelberg, Martin Stanulla, and Jean-Pierre Bourquin. Durable remissions in *TCF3-HLF* positive acute lymphoblastic leukemia with blinatumomab and stem cell transplantation. *Haematologica*, 104(6):e244–e247, June 2019. ISSN 0390-6078, 1592-8721. doi: 10.3324/haematol.2018.210104. URL http://www.haematologica.org/lookup/doi/10.3324/haematol.2018.210104.

[24] Meng-Ju Li, Chih-Hsiang Yu, Shu-Wei Chou, Ying-Hui Su, Kuang-Wen Liao, Hsiu-Hao Chang, and Yung-Li Yang. TCF3-HLF-Positive Acute Lymphoblastic Leukemia Resembling Burkitt Leukemia: Cell Morphologic and Immunophe-

notypic Findings. *JCO Precision Oncology*, 6:e2200236, August 2022. ISSN 2473-4284. doi: 10.1200/PO.22.00236. URL https://www.ncbi.nlm.nih.gov/pmc/articles/PMC9489183/.

[25] Daniel A. Arber. 14 - Acute Myeloid Leukemia. In Eric D. Hsi, editor, *Hematopathology (Third Edition)*, Foundations in Diagnostic Pathology, pages 429–466.e5. Elsevier, Philadelphia, January 2018. ISBN 978-0-323-47913-4. doi: 10.1016/B978-0-323-47913-4.00014-8. URL https://www.sciencedirect.com/science/article/pii/B9780323479134000148.

[26] Trisha Tee, Titine Ruiter, Danique Wajon, Shuiyan Wu, Ahmed Dahaoui, Dorette S van Ingen Schenau, Laurens T van der Meer, and Frank N van Leeuwen. MLL (KMT2A)-rearranged Acute Lymphoblastic Leukemias Are Addicted to S-Adenosyl Methionine (SAM): Implications for Therapy. *Blood*, 140(Supplement 1):6343–6344, November 2022. ISSN 0006-4971. doi: 10.1182/blood-2022-159450. URL https://doi.org/10.1182/blood-2022-159450.

[27] Amanda C. Winters and Kathrin M. Bernt. MLL-Rearranged Leukemias—An Update on Science and Clinical Approaches. *Frontiers in Pediatrics*, 5, February 2017. ISSN 2296-2360. doi: 10.3389/fped.2017.00004. URL https://www.frontiersin.org/articles/10.3389/fped.2017.00004. Publisher: Frontiers.

[28] Firas El Chaer, Michael Keng, and Karen K. Ballen. MLL-Rearranged Acute Lymphoblastic Leukemia. *Current Hematologic Malignancy Reports*, 15(2):83–89, April 2020. ISSN 1558-822X. doi: 10.1007/s11899-020-00582-5.

[29] H. O. Hustu, R. J. A. Aur, M. S. Verzosa, J. V. Simone, and D. Pinkel. Prevention of central nervous system leukemia by irradiation. *Cancer*, 32 (3):585–597, September 1973. ISSN 0008-543X, 1097-0142. doi: 10.1002/1097-0142(197309)32:3<585::AID-CNCR2820320311>3.0.CO;2-K. URL https://onlinelibrary.wiley.com/doi/10.1002/1097-0142(197309)32:3<585::AID-CNCR2820320311>3.0.CO;2-K.

[30] Maria Thastrup, Hanne Vibeke Marquart, Mette Levinsen, Kathrine Grell, Jonas Abrahamsson, Birgitte Klug Albertsen, Thomas Leth Frandsen, Arja Harila-Saari, Päivi Maria Lähteenmäki, Riitta Niinimäki, Cornelis Jan Pronk, Aina Ulvmoen, Goda Vaitkevičienė, Mervi Taskinen, Kjeld Schmiegelow, on behalf

of the Nordic Society of Pediatric Hematology and Oncology (NOPHO), Peder Wehner, Britt-Marie Frost, Ulrika Norén-Nyström, Mikael Behrendtz, Bendik Lund, Jouni Pesola, and Dorota Malgorzata Wojcik. Flow cytometric detection of leukemic blasts in cerebrospinal fluid predicts risk of relapse in childhood acute lymphoblastic leukemia: a Nordic Society of Pediatric Hematology and Oncology study. *Leukemia*, 34(2):336–346, February 2020. ISSN 0887-6924, 1476-5551. doi: 10.1038/s41375-019-0570-1. URL https://www.nature.com/articles/s41375-019-0570-1.

[31] Dalma Deak, Nicolae Gorcea-Andronic, Valentina Sas, Patric Teodorescu, Catalin Constantinescu, Sabina Iluta, Sergiu Pasca, Ionut Hotea, Cristina Turcas, Vlad Moisoiu, Alina-Andreea Zimta, Simona Galdean, Jakob Steinheber, Ioana Rus, Sebastian Rauch, Cedric Richlitzki, Raluca Munteanu, Ancuta Jurj, Bobe Petrushev, Cristina Selicean, Mirela Marian, Olga Soritau, Alexandra Andries, Andrei Roman, Delia Dima, Alina Tanase, Olafur Sigurjonsson, and Ciprian Tomuleasa. A narrative review of central nervous system involvement in acute leukemias. *Annals of Translational Medicine*, 9(1):68–68, January 2021. ISSN 23055839, 23055847. doi: 10.21037/atm-20-3140. URL https://atm.amegroups.com/article/view/59808/html.

[32] Lennart Lenk, Ameera Alsadeq, and Denis M. Schewe. Involvement of the central nervous system in acute lymphoblastic leukemia: opinions on molecular mechanisms and clinical implications based on recent data. *Cancer and Metastasis Reviews*, 39(1):173–187, March 2020. ISSN 0167-7659, 1573-7233. doi: 10.1007/s10555-020-09848-z. URL http://link.springer.com/10.1007/s10555-020-09848-z.

[33] Hisayuki Yao, Trevor T. Price, Gaia Cantelli, Brandon Ngo, Matthew J. Warner, Lindsey Olivere, Sarah M. Ridge, Elizabeth M. Jablonski, Joseph Therrien, Stacey Tannheimer, Chad M. McCall, Anjen Chenn, and Dorothy A. Sipkins. Leukaemia hijacks a neural mechanism to invade the central nervous system. *Nature*, 560 (7716):55–60, August 2018. ISSN 0028-0836, 1476-4687. doi: 10.1038/s41586-018-0342-5. URL http://www.nature.com/articles/s41586-018-0342-5.

[34] Douglas Hanahan and Robert A. Weinberg. Hallmarks of Cancer: The Next Generation. *Cell*, 144(5):646–674, March 2011. ISSN 0092-8674. doi: 10.1016/j.

cell.2011.02.013. URL https://www.sciencedirect.com/science/article/pii/S0092867411001279.

[35] Douglas Hanahan and Robert A Weinberg. The Hallmarks of Cancer. *Cell*, 100 (1):57–70, January 2000. ISSN 0092-8674. doi: 10.1016/S0092-8674(00)81683-9. URL https://www.sciencedirect.com/science/article/pii/S0092867400816839.

[36] Anna C. Obenauf and Joan Massagué. Surviving at a Distance: Organ-Specific Metastasis. *Trends in Cancer*, 1(1):76–91, September 2015. ISSN 2405-8033. doi: 10.1016/j.trecan.2015.07.009. URL https://www.sciencedirect.com/science/article/pii/S2405803315000102.

[37] Nuala Del Piccolo, Venktesh S. Shirure, Ye Bi, S. Peter Goedegebuure, Sepideh Gholami, Christopher C.W. Hughes, Ryan C. Fields, and Steven C. George. Tumor-on-chip modeling of organ-specific cancer and metastasis. *Advanced Drug Delivery Reviews*, 175:113798, August 2021. ISSN 0169409X. doi: 10.1016/j.addr.2021.05.008. URL https://linkinghub.elsevier.com/retrieve/pii/S0169409X21001642.

[38] Vera Münch, Luca Trentin, Julia Herzig, Salih Demir, Felix Seyfried, Johann M. Kraus, Hans A. Kestler, Rolf Köhler, Thomas F. E. Barth, Geertruy Te Kronnie, Klaus-Michael Debatin, and Lüder H. Meyer. Central nervous system involvement in acute lymphoblastic leukemia is mediated by vascular endothelial growth factor. *Blood*, 130(5):643–654, August 2017. ISSN 0006-4971, 1528-0020. doi: 10.1182/blood-2017-03-769315. URL https://ashpublications.org/blood/article/130/5/643/36789/Central-nervous-system-involvement-in-acute.

[39] Angela Maria Savino, Sara Isabel Fernandes, Orianne Olivares, Anna Zemlyansky, Antony Cousins, Elke K. Markert, Shani Barel, Ifat Geron, Liron Frishman, Yehudit Birger, Cornelia Eckert, Sergey Tumanov, Gillian MacKay, Jurre J. Kamphorst, Pawel Herzyk, Jonatan Fernández-García, Ifat Abramovich, Inbal Mor, Michela Bardini, Ersilia Barin, Sudha Janaki-Raman, Justin R. Cross, Michael G. Kharas, Eyal Gottlieb, Shai Izraeli, and Christina Halsey. Metabolic adaptation of acute lymphoblastic leukemia to the central nervous system microenvironment depends on stearoyl-CoA desaturase. *Nature Cancer*, 1(10):998–1009,

September 2020. ISSN 2662-1347. doi: 10.1038/s43018-020-00115-2. URL https://www.nature.com/articles/s43018-020-00115-2.

[40] Lennart Lenk, Dorothee Winterberg, Fotini Vogiatzi, Anna Laqua, Lea Spory, Ahmad Mayar, Anna Dietterle, Gina Münch, Christian Vokuhl, Julia Richter, Andrew G. Polson, Thomas Schüler, Ulf D. Kahlert, Matthias Peipp, Thomas Valerius, Martin Schrappe, Gunnar Cario, Hassan Jumaa, Elias Hobeika, Monika Brüggemann, Ameera Alsadeq, and Denis M. Schewe. Preclinical Evidence for the Efficacy of CD79b Immunotherapy in B-cell Precursor Acute Lymphoblastic Leukemia. *HemaSphere*, 6(8):e754, August 2022. ISSN 2572-9241. doi: 10.1097/HS9.0000000000000754. URL https://journals.lww.com/10.1097/HS9.0000000000000754.

[41] Eloisa Arana, Naomi E. Harwood, and Facundo D. Batista. Regulation of integrin activation through the B-cell receptor. *Journal of Cell Science*, 121 (14):2279–2286, July 2008. ISSN 0021-9533. doi: 10.1242/jcs.017905. URL https://doi.org/10.1242/jcs.017905.

[42] Eva Calpe, Carles Codony, Maria Joao Baptista, Pau Abrisqueta, Cecilia Carpio, Noelia Purroy, Francesc Bosch, and Marta Crespo. ZAP-70 enhances migration of malignant B lymphocytes toward CCL21 by inducing CCR7 expression via IgM-ERK1/2 activation. *Blood*, 118(16):4401–4410, October 2011. ISSN 0006-4971. doi: 10.1182/blood-2011-01-333682. URL https://doi.org/10.1182/blood-2011-01-333682.

[43] Silvia Buonamici, Thomas Trimarchi, Maria Grazia Ruocco, Linsey Reavie, Severine Cathelin, Brenton G. Mar, Apostolos Klinakis, Yevgeniy Lukyanov, Jen-Chieh Tseng, Filiz Sen, Eric Gehrie, Mengling Li, Elizabeth Newcomb, Jiri Zavadil, Daniel Meruelo, Martin Lipp, Sherif Ibrahim, Argiris Efstratiadis, David Zagzag, Jonathan S. Bromberg, Michael L. Dustin, and Iannis Aifantis. CCR7 signalling as an essential regulator of CNS infiltration in T-cell leukaemia. *Nature*, 459(7249): 1000–1004, June 2009. ISSN 0028-0836, 1476-4687. doi: 10.1038/nature08020. URL https://www.nature.com/articles/nature08020.

[44] A. Alsadeq, H. Fedders, C. Vokuhl, N.M. Belau, M. Zimmermann, T. Wirbelauer, S. Spielberg, M. Vossen-Gajcy, G. Cario, and M. Schrappe. The role of ZAP70

kinase in acute lymphoblastic leukemia infiltration into the central nervous system. *Haematologica*, 102:346–355, 2017.

[45] Ameera Alsadeq and Denis M. Schewe. Acute lymphoblastic leukemia of the central nervous system: on the role of PBX1. *Haematologica*, 102(4):611–613, April 2017. ISSN 0390-6078, 1592-8721. doi: 10.3324/haematol.2017.165142. URL `http://www.haematologica.org/lookup/doi/10.3324/haematol.2017.165142`.

[46] S.-S. Chen, B.Y. Chang, S. Chang, T. Tong, S. Ham, B. Sherry, J.A. Burger, K.R. Rai, and N. Chiorazzi. BTK inhibition results in impaired CXCR4 chemokine receptor surface expression, signaling and function in chronic lymphocytic leukemia. *leu*, 30:833–843, 2016.

[47] A. Montresor, L. Toffali, A. Rigo, I. Ferrarini, F. Vinante, and C. Laudanna. CXCR4- and BCR-triggered integrin activation in B-cell chronic lymphocytic leukemia cells depends on JAK2-activated Bruton's tyrosine kinase. *Oncotarget*, 9:35123–35140, 2018.

[48] Roman Crazzolara, Alfons Kreczy, Georg Mann, Andreas Heitger, Günther Eibl, Franz-Martin Fink, Robert Möhle, and Bernhard Meister. High expression of the chemokine receptor CXCR4 predicts extramedullary organ infiltration in childhood acute lymphoblastic leukaemia: High CXCR4 Expression Predicts Organ Infiltration in Childhood ALL. *British Journal of Haematology*, 115(3): 545–553, December 2001. ISSN 00071048. doi: 10.1046/j.1365-2141.2001.03164.x. URL `http://doi.wiley.com/10.1046/j.1365-2141.2001.03164.x`.

[49] Sujeetha A. Rajakumar, Ildiko Grandal, Mark D. Minden, Johann K. Hitzler, Cynthia J. Guidos, and Jayne S. Danska. Targeted blockade of immune mechanisms inhibit B precursor acute lymphoblastic leukemia cell invasion of the central nervous system. *Cell Reports Medicine*, 2(12):100470, December 2021. ISSN 26663791. doi: 10.1016/j.xcrm.2021.100470. URL `https://linkinghub.elsevier.com/retrieve/pii/S2666379121003426`.

[50] Xi Cheng, Huibin Wang, Xiuchun Zhang, Shanshan Zhao, Zhike Zhou, Xiaopeng Mu, Chuansheng Zhao, and Weiyu Teng. The Role of SDF-1/CXCR4/CXCR7 in Neuronal Regeneration after Cerebral Ischemia. *Frontiers in Neuroscience*,

11:590, October 2017. ISSN 1662-4548. doi: 10.3389/fnins.2017.00590. URL https://www.ncbi.nlm.nih.gov/pmc/articles/PMC5662889/.

[51] Julie Gavard and J. Silvio Gutkind. VEGF controls endothelial-cell permeability by promoting the beta-arrestin-dependent endocytosis of VE-cadherin. *Nature Cell Biology*, 8(11):1223–1234, November 2006. ISSN 1465-7392. doi: 10.1038/ncb1486.

[52] Sara Weis, Jianhua Cui, Leo Barnes, and David Cheresh. Endothelial barrier disruption by VEGF-mediated Src activity potentiates tumor cell extravasation and metastasis. *The Journal of Cell Biology*, 167(2):223–229, October 2004. ISSN 0021-9525. doi: 10.1083/jcb.200408130. URL https://www.ncbi.nlm.nih.gov/pmc/articles/PMC2172541/.

[53] H. P. Gerber, A. McMurtrey, J. Kowalski, M. Yan, B. A. Keyt, V. Dixit, and N. Ferrara. Vascular endothelial growth factor regulates endothelial cell survival through the phosphatidylinositol 3'-kinase/Akt signal transduction pathway. Requirement for Flk-1/KDR activation. *The Journal of Biological Chemistry*, 273(46): 30336–30343, November 1998. ISSN 0021-9258. doi: 10.1074/jbc.273.46.30336.

[54] J. Pedro Veiga, Lara F. Costa, Stephen E. Sallan, Lee M. Nadler, and Angelo A. Cardoso. Leukemia-stimulated bone marrow endothelium promotes leukemia cell survival. *Experimental Hematology*, 34(5):610–621, May 2006. ISSN 0301-472X. doi: 10.1016/j.exphem.2006.01.013.

[55] Xiaozhuo Yu, Hua Zhang, Meng Yuan, Ping Zhang, Yang Wang, Mingzhe Zheng, Zhuangwei Lv, Woodvine Otieno Odhiambo, Canyu Li, Chengcheng Liu, Yunfeng Ma, and Yanhong Ji. Identification and characterization of a murine model of BCR-ABL1+ acute B-lymphoblastic leukemia with central nervous system metastasis. *Oncology Reports*, 42(2):521–532, August 2019. ISSN 1021-335X. doi: 10.3892/or.2019.7184. URL https://www.ncbi.nlm.nih.gov/pmc/articles/PMC6610040/.

[56] M. L. Arbonés, D. C. Ord, K. Ley, H. Ratech, C. Maynard-Curry, G. Otten, D. J. Capon, and T. F. Tedder. Lymphocyte homing and leukocyte rolling and migration are impaired in L-selectin-deficient mice. *Immunity*, 1(4):247–260, July 1994. ISSN 1074-7613. doi: 10.1016/1074-7613(94)90076-0.

[57] J. J. Campbell, J. Hedrick, A. Zlotnik, M. A. Siani, D. A. Thompson, and E. C.

Butcher. Chemokines and the arrest of lymphocytes rolling under flow conditions. *Science (New York, N.Y.)*, 279(5349):381–384, January 1998. ISSN 0036-8075. doi: 10.1126/science.279.5349.381.

[58] Klaus Ley, Carlo Laudanna, Myron I. Cybulsky, and Sussan Nourshargh. Getting to the site of inflammation: the leukocyte adhesion cascade updated. *Nature Reviews. Immunology*, 7(9):678–689, September 2007. ISSN 1474-1741. doi: 10.1038/nri2156.

[59] S.M. Akers, S.L. Rellick, J.E. Fortney, and L.F. Gibson. Cellular elements of the subarachnoid space promote ALL survival during chemotherapy. *Leukemia research*, 35:705–711, 2011.

[60] Jeffrey S. Gaynes, Leslie M. Jonart, Edward A. Zamora, Jordan A. Naumann, Nathan P. Gossai, and Peter M. Gordon. The central nervous system microenvironment influences the leukemia transcriptome and enhances leukemia chemoresistance. *Haematologica*, 102(4):e136–e139, April 2017. ISSN 1592-8721. doi: 10.3324/haematol.2016.152926.

[61] Ching-Hon Pui and Scott C. Howard. Current management and challenges of malignant disease in the CNS in paediatric leukaemia. *The Lancet. Oncology*, 9 (3):257–268, March 2008. ISSN 1474-5488. doi: 10.1016/S1470-2045(08)70070-6.

[62] Edward Allan R. Sison, Emily McIntyre, Daniel Magoon, and Patrick Brown. Dynamic chemotherapy-induced upregulation of CXCR4 expression: a mechanism of therapeutic resistance in pediatric AML. *Molecular cancer research: MCR*, 11 (9):1004–1016, September 2013. ISSN 1557-3125. doi: 10.1158/1541-7786.MCR-13-0114.

[63] Reynold Spector, S. Robert Snodgrass, and Conrad E. Johanson. A balanced view of the cerebrospinal fluid composition and functions: Focus on adult humans. *Experimental Neurology*, 273:57–68, November 2015. ISSN 1090-2430. doi: 10.1016/j.expneurol.2015.07.027.

[64] Mark T. S. Williams, Yasar Yousafzai, Charlotte Cox, Allison Blair, Ruaidhrí Carmody, Shuji Sai, Karen E. Chapman, Rachel McAndrew, Angela Thomas, Alison Spence, Brenda Gibson, Gerard J. Graham, and Christina Halsey. Interleukin-15 enhances cellular proliferation and upregulates CNS homing molecules in pre-

B acute lymphoblastic leukemia. *Blood*, 123(20):3116–3127, May 2014. ISSN 1528-0020. doi: 10.1182/blood-2013-05-499970.

[65] Lennart Lenk, Michela Carlet, Fotini Vogiatzi, Lea Spory, Dorothee Winterberg, Antony Cousins, Michaela Vossen-Gajcy, Olta Ibruli, Christian Vokuhl, Gunnar Cario, Omar El Ayoubi, Lisa Kramer, Matthias Ritgen, Monika Brüggemann, Robert Häsler, Martin Schrappe, Stephan Fuhrmann, Christina Halsey, Irmela Jeremias, Elias Hobeika, Hassan Jumaa, Ameera Alsadeq, and Denis M. Schewe. CD79a promotes CNS-infiltration and leukemia engraftment in pediatric B-cell precursor acute lymphoblastic leukemia. *Communications Biology*, 4(1): 73, December 2021. ISSN 2399-3642. doi: 10.1038/s42003-020-01591-z. URL http://www.nature.com/articles/s42003-020-01591-z.

[66] Itaru Kato, Yoko Nishinaka, Masahiro Nakamura, Ayse U. Akarca, Akira Niwa, Hiroki Ozawa, Kenichi Yoshida, Makiko Mori, Dapeng Wang, Makiko Morita, Hiroo Ueno, Yusuke Shiozawa, Yuichi Shiraishi, Satoru Miyano, Rajeev Gupta, Katsutsugu Umeda, Kenichiro Watanabe, Katsuyoshi Koh, Souichi Adachi, Toshio Heike, Megumu K. Saito, Masashi Sanada, Seishi Ogawa, Teresa Marafioti, Akira Watanabe, Tatsutoshi Nakahata, and Tariq Enver. Hypoxic adaptation of leukemic cells infiltrating the CNS affords a therapeutic strategy targeting VEGFA. *Blood*, 129(23):3126–3129, June 2017. ISSN 0006-4971, 1528-0020. doi: 10.1182/blood-2016-06-721712. URL https://ashpublications.org/blood/article/129/23/3126/36040/Hypoxic-adaptation-of-leukemic-cells-infiltrating.

[67] Xinyang Zhong, Xuefeng He, Yaxian Wang, Zijuan Hu, Huixia Huang, Senlin Zhao, Ping Wei, and Dawei Li. Warburg effect in colorectal cancer: the emerging roles in tumor microenvironment and therapeutic implications. *Journal of Hematology & Oncology*, 15(1):160, November 2022. ISSN 1756-8722. doi: 10.1186/s13045-022-01358-5. URL https://doi.org/10.1186/s13045-022-01358-5.

[68] Kevin Rouault-Pierre, Lourdes Lopez-Onieva, Katie Foster, Fernando Anjos-Afonso, Isabelle Lamrissi-Garcia, Martin Serrano-Sanchez, Richard Mitter, Zoran Ivanovic, Hubert de Verneuil, John Gribben, David Taussig, Hamid Reza Rezvani, Frédéric Mazurier, and Dominique Bonnet. HIF-2α protects human hematopoietic stem/progenitors and acute myeloid leukemic cells from apoptosis induced by endoplasmic reticulum stress. *Cell Stem Cell*, 13(5):549–563, November 2013.

ISSN 1875-9777. doi: 10.1016/j.stem.2013.08.011.

[69] Xiao-Wen Liu, Yi Su, Hong Zhu, Ji Cao, Wan-Jing Ding, Yu-Chen Zhao, Qiao-Jun He, and Bo Yang. HIF-1α-dependent autophagy protects HeLa cells from fenretinide (4-HPR)-induced apoptosis in hypoxia. *Pharmacological Research*, 62 (5):416–425, November 2010. ISSN 1096-1186. doi: 10.1016/j.phrs.2010.07.002.

[70] Juliana Benito, Yuexi Shi, Barbara Szymanska, Hernan Carol, Ingrid Boehm, Hongbo Lu, Sergej Konoplev, Wendy Fang, Patrick A. Zweidler-McKay, Dario Campana, Gautam Borthakur, Carlos Bueso-Ramos, Elizabeth Shpall, Deborah A. Thomas, Craig T. Jordan, Hagop Kantarjian, William R. Wilson, Richard Lock, Michael Andreeff, and Marina Konopleva. Pronounced hypoxia in models of murine and human leukemia: high efficacy of hypoxia-activated prodrug PR-104. *PloS One*, 6(8):e23108, 2011. ISSN 1932-6203. doi: 10.1371/journal.pone.0023108.

[71] C. Petit, F. Gouel, I. Dubus, C. Heuclin, K. Roget, and J. P. Vannier. Hypoxia promotes chemoresistance in acute lymphoblastic leukemia cell lines by modulating death signaling pathways. *BMC Cancer*, 16(1):746, December 2016. ISSN 1471-2407. doi: 10.1186/s12885-016-2776-1. URL `http://bmccancer.biomedcentral.com/articles/10.1186/s12885-016-2776-1`.

[72] Peter J. Houghton, Richard Lock, Hernan Carol, Christopher L. Morton, Doris Phelps, Richard Gorlick, E. Anders Kolb, Stephen T. Keir, C. Patrick Reynolds, Min H. Kang, John M. Maris, Amy W. Wozniak, Yongchuan Gu, William R. Wilson, and Malcolm A. Smith. Initial Testing of the Hypoxia-Activated Prodrug PR-104 by the Pediatric Preclinical Testing Program. *Pediatric blood & cancer*, 57(3):443–453, September 2011. ISSN 1545-5009. doi: 10.1002/pbc.22921. URL `https://www.ncbi.nlm.nih.gov/pmc/articles/PMC4304205/`.

[73] Olga Frolova, Ismael Samudio, Juliana Maria Benito, Rodrigo Jacamo, Steven M. Kornblau, Ana Markovic, Wendy Schober, Hongbo Lu, Yi Hua Qiu, Daniela Buglio, Teresa McQueen, Sherry Pierce, Elizabeth Shpall, Sergej Konoplev, Deborah Thomas, Hagop Kantarjian, Richard Lock, Michael Andreeff, and Marina Konopleva. Regulation of HIF-1α signaling and chemoresistance in acute lymphocytic leukemia under hypoxic conditions of the bone marrow microenvironment. *Cancer Biology & Therapy*, 13(10):858–870, August 2012. ISSN 1555-8576. doi: 10.4161/cbt.20838.

[74] Robert Eferl and Erwin F. Wagner. AP-1: a double-edged sword in tumorigenesis. *Nature Reviews Cancer*, 3(11):859–868, November 2003. ISSN 1474-175X, 1474-1768. doi: 10.1038/nrc1209. URL https://www.nature.com/articles/nrc1209.

[75] Juan Ramón Tejedor, Clara Bueno, Meritxell Vinyoles, Paolo Petazzi, Antonio Agraz-Doblas, Isabel Cobo, Raúl Torres-Ruiz, Gustavo F. Bayón, Raúl F. Pérez, Sara López-Tamargo, Francisco Gutierrez-Agüera, Pablo Santamarina-Ojeda, Manuel Ramírez-Orellana, Michela Bardini, Giovanni Cazzaniga, Paola Ballerini, Pauline Schneider, Ronald W. Stam, Ignacio Varela, Mario F. Fraga, Agustín F. Fernández, and Pablo Menéndez. Integrative methylome-transcriptome analysis unravels cancer cell vulnerabilities in infant MLL-rearranged B cell acute lymphoblastic leukemia. *Journal of Clinical Investigation*, 131(13): e138833, July 2021. ISSN 1558-8238. doi: 10.1172/JCI138833. URL https://www.jci.org/articles/view/138833.

[76] Zhijie Zhang, Jiangzhou Shi, Qifang Wu, Zijian Zhang, Xiaoyan Liu, Anqi Ren, Guanlin Zhao, Ge Dong, Han Wu, Jiaxuan Zhao, Yuan Zhao, Jia Hu, Hui Li, Tongcun Zhang, Fuling Zhou, and Haichuan Zhu. JUN mediates glucocorticoid resistance by stabilizing HIF1a in T cell acute lymphoblastic leukemia. *iScience*, 26(11):108242, November 2023. ISSN 2589-0042. doi: 10.1016/j.isci.2023.108242.

[77] Treatment of Acute Lymphoblastic Leukemia | NEJM. URL https://www.nejm.org/doi/full/10.1056/NEJMra052603.

[78] Ching-Hon Pui and William E. Evans. Treatment of Acute Lymphoblastic Leukemia. *New England Journal of Medicine*, 354(2):166–178, January 2006. ISSN 0028-4793. doi: 10.1056/NEJMra052603. URL https://doi.org/10.1056/NEJMra052603. Publisher: Massachusetts Medical Society _eprint: https://doi.org/10.1056/NEJMra052603.

[79] Hagop Kantarjian, Deborah Thomas, Susan O'Brien, Jorge Cortes, Francis Giles, Sima Jeha, Carlos E. Bueso-Ramos, Sherry Pierce, Jianqin Shan, Charles Koller, Miloslav Beran, Michael Keating, and Emil J. Freireich. Long-term follow-up results of hyperfractionated cyclophosphamide, vincristine, doxorubicin, and dexamethasone (Hyper-CVAD), a dose-intensive regimen, in adult acute lymphocytic leukemia. *Cancer*, 101(12):2788–2801, December 2004. ISSN 0008-543X, 1097-

0142. doi: 10.1002/cncr.20668. URL https://onlinelibrary.wiley.com/doi/10.1002/cncr.20668.

[80] Kevin R. Krull, Kristina K. Hardy, Lisa S. Kahalley, Ilse Schuitema, and Shelli R. Kesler. Neurocognitive Outcomes and Interventions in Long-Term Survivors of Childhood Cancer. *Journal of Clinical Oncology*, 36(21):2181–2189, July 2018. ISSN 0732-183X, 1527-7755. doi: 10.1200/JCO.2017.76.4696. URL https://ascopubs.org/doi/10.1200/JCO.2017.76.4696.

[81] Rajiv S. Magge and Lisa M. DeAngelis. The double-edged sword: Neurotoxicity of chemotherapy. *Blood Reviews*, 29(2):93–100, March 2015. ISSN 0268960X. doi: 10.1016/j.blre.2014.09.012. URL https://linkinghub.elsevier.com/retrieve/pii/S0268960X14000812.

[82] Sabina Chiaretti, Antonella Vitale, Marco Vignetti, Alfonso Piciocchi, Paola Fazi, Loredana Elia, Brunangelo Falini, Francesca Ronco, Felicetto Ferrara, Paolo De Fabritiis, Mario Luppi, Giorgio La Nasa, Alessandra Tedeschi, Catello Califano, Renato Fanin, Fausto Dore, Franco Mandelli, Giovanna Meloni, and Robin Foà. A sequential approach with imatinib, chemotherapy and transplant for adult Ph+ acute lymphoblastic leukemia: final results of the GIMEMA LAL 0904 study. *Haematologica*, 101(12):1544–1552, December 2016. ISSN 1592-8721. doi: 10.3324/haematol.2016.144535.

[83] Robin Foà, Antonella Vitale, Marco Vignetti, Giovanna Meloni, Anna Guarini, Maria Stefania De Propris, Loredana Elia, Francesca Paoloni, Paola Fazi, Giuseppe Cimino, Francesco Nobile, Felicetto Ferrara, Carlo Castagnola, Simona Sica, Pietro Leoni, Eliana Zuffa, Claudio Fozza, Mario Luppi, Anna Candoni, Ilaria Iacobucci, Simona Soverini, Franco Mandelli, Giovanni Martinelli, Michele Baccarani, and on behalf of the GIMEMA Acute Leukemia Working Party. Dasatinib as first-line treatment for adult patients with Philadelphia chromosome–positive acute lymphoblastic leukemia. *Blood*, 118(25):6521–6528, December 2011. ISSN 0006-4971. doi: 10.1182/blood-2011-05-351403. URL https://doi.org/10.1182/blood-2011-05-351403.

[84] Yin Ting Cheung, Raja B. Khan, Wei Liu, Tara M. Brinkman, Michelle N. Edelmann, Wilburn E. Reddick, Deqing Pei, Angela Panoskaltsis-Mortari, Deokumar Srivastava, Cheng Cheng, Leslie L. Robison, Melissa M. Hudson, Ching-Hon Pui,

and Kevin R. Krull. Association of Cerebrospinal Fluid Biomarkers of Central Nervous System Injury With Neurocognitive and Brain Imaging Outcomes in Children Receiving Chemotherapy for Acute Lymphoblastic Leukemia. *JAMA Oncology*, 4 (7):e180089, July 2018. ISSN 2374-2437. doi: 10.1001/jamaoncol.2018.0089. URL https://doi.org/10.1001/jamaoncol.2018.0089.

[85] Kjeld Schmiegelow, Andishe Attarbaschi, Shlomit Barzilai, Gabriele Escherich, Thomas Leth Frandsen, Christina Halsey, Rachael Hough, Sima Jeha, Motohiro Kato, Der-Cherng Liang, Torben Stamm Mikkelsen, Anja Möricke, Riitta Niinimäki, Caroline Piette, Maria Caterina Putti, Elizabeth Raetz, Lewis B Silverman, Roderick Skinner, Ruta Tuckuviene, Inge Van Der Sluis, and Ester Zapotocka. Consensus definitions of 14 severe acute toxic effects for childhood lymphoblastic leukaemia treatment: a Delphi consensus. *The Lancet Oncology*, 17(6):e231–e239, June 2016. ISSN 14702045. doi: 10.1016/S1470-2045(16)30035-3. URL https://linkinghub.elsevier.com/retrieve/pii/S1470204516300353.

[86] Robert A. Price and Warren W. Johnson. The central nervous system in childhood leukemia: I. The arachnoid. *Cancer*, 31(3):520–533, March 1973. ISSN 0008-543X, 1097-0142. doi: 10.1002/1097-0142(197303)31:3<520::AID-CNCR2820310306>3.0.CO;2-2. URL https://onlinelibrary.wiley.com/doi/10.1002/1097-0142(197303)31:3<520::AID-CNCR2820310306>3.0.CO;2-2.

[87] Felix Seyfried, Felix Uli Stirnweiß, Alexandra Niedermayer, Stefanie Enzenmüller, Rebecca Louise Hörl, Vera Münch, Stefan Köhrer, Klaus-Michael Debatin, and Lüder Hinrich Meyer. Synergistic activity of combined inhibition of anti-apoptotic molecules in B-cell precursor ALL. *Leukemia*, 36(4):901–912, April 2022. ISSN 0887-6924, 1476-5551. doi: 10.1038/s41375-021-01502-z. URL https://www.nature.com/articles/s41375-021-01502-z.

[88] Veit Bücklein, Michaela Scheurer, Bettina Brauchle, Roman Kischel, Michael Von Bergwelt, Karsten Spiekermann, and Marion Subklewe. Predictors of Efficacy for Blinatumomab in BCP-ALL Patients: Non-Responders Show Impaired CD19-BiTE®-Mediated Cytotoxicity in Vitro. *Blood*, 134(Supplement_1):2632–2632, November 2019. ISSN 0006-4971, 1528-0020. doi: 10.1182/blood-2019-129057. URL https://ashpublications.org/blood/article/134/Supplement_1/2632/423113/Predictors-of-Efficacy-for-Blinatumomab-in-BCPALL.

[89] Anna Birgersdotter, Rickard Sandberg, and Ingemar Ernberg. Gene expression perturbation in vitro–a growing case for three-dimensional (3D) culture systems. *Seminars in Cancer Biology*, 15(5):405–412, October 2005. ISSN 1044-579X. doi: 10.1016/j.semcancer.2005.06.009.

[90] Edna Cukierman, Roumen Pankov, and Kenneth M. Yamada. Cell interactions with three-dimensional matrices. *Current Opinion in Cell Biology*, 14(5):633–639, October 2002. ISSN 0955-0674. doi: 10.1016/s0955-0674(02)00364-2.

[91] Linda G. Griffith and Melody A. Swartz. Capturing complex 3D tissue physiology in vitro. *Nature Reviews Molecular Cell Biology*, 7(3):211–224, March 2006. ISSN 1471-0072, 1471-0080. doi: 10.1038/nrm1858. URL `https://www.nature.com/articles/nrm1858`.

[92] Celeste M. Nelson and Mina J. Bissell. Of extracellular matrix, scaffolds, and signaling: tissue architecture regulates development, homeostasis, and cancer. *Annual Review of Cell and Developmental Biology*, 22:287–309, 2006. ISSN 1081-0706. doi: 10.1146/annurev.cellbio.22.010305.104315.

[93] Kenneth M. Yamada and Edna Cukierman. Modeling Tissue Morphogenesis and Cancer in 3D. *Cell*, 130(4):601–610, August 2007. ISSN 00928674. doi: 10.1016/j.cell.2007.08.006. URL `https://linkinghub.elsevier.com/retrieve/pii/S0092867407010288`.

[94] Elad Jacoby, Christopher D. Chien, and Terry J. Fry. Murine Models of Acute Leukemia: Important Tools in Current Pediatric Leukemia Research. *Frontiers in Oncology*, 4, 2014. ISSN 2234-943X. URL `https://www.frontiersin.org/article/10.3389/fonc.2014.00095`.

[95] Yinxi Zhou, Jinghua Xia, Shuonan Xu, Tao She, Yanning Zhang, Ying Sun, Miaomiao Wen, Tao Jiang, Yanlu Xiong, and Jie Lei. Experimental mouse models for translational human cancer research. *Frontiers in Immunology*, 14:1095388, March 2023. ISSN 1664-3224. doi: 10.3389/fimmu.2023.1095388. URL `https://www.frontiersin.org/articles/10.3389/fimmu.2023.1095388/full`.

[96] João Rodrigues, Marcel A. Heinrich, Liliana Moreira Teixeira, and Jai Prakash. 3D In Vitro Model (R)evolution: Unveiling Tumor–Stroma Interactions. *Trends in Cancer*, 7(3):249–264, March 2021. ISSN 24058033. doi: 10.1016/j.trecan.2020.

10.009. URL https://linkinghub.elsevier.com/retrieve/pii/S2405803320302831.

[97] Krishnapriya Syama, Eman M. Hassan, and Shan Zou. Advances in culture methods for acute myeloid leukemia research. *Oncoscience*, 8:82–90, August 2021. ISSN 2331-4737. doi: 10.18632/oncoscience.540. URL https://www.oncoscience.us/lookup/doi/10.18632/oncoscience.540.

[98] Jan H. Lui, David V. Hansen, and Arnold R. Kriegstein. Development and Evolution of the Human Neocortex. *Cell*, 146(1):18–36, July 2011. ISSN 0092-8674, 1097-4172. doi: 10.1016/j.cell.2011.06.030. URL https://www.cell.com/cell/abstract/S0092-8674(11)00705-7. Publisher: Elsevier.

[99] Mototsugu Eiraku, Kiichi Watanabe, Mami Matsuo-Takasaki, Masako Kawada, Shigenobu Yonemura, Michiru Matsumura, Takafumi Wataya, Ayaka Nishiyama, Keiko Muguruma, and Yoshiki Sasai. Self-organized formation of polarized cortical tissues from ESCs and its active manipulation by extrinsic signals. *Cell Stem Cell*, 3(5):519–532, November 2008. ISSN 1875-9777. doi: 10.1016/j.stem.2008.09.002.

[100] Yoshiki Sasai. Next-Generation Regenerative Medicine: Organogenesis from Stem Cells in 3D Culture. *Cell Stem Cell*, 12(5):520–530, May 2013. ISSN 19345909. doi: 10.1016/j.stem.2013.04.009. URL https://linkinghub.elsevier.com/retrieve/pii/S1934590913001458.

[101] Jessica Mariani and Flora M. Vaccarino. Breakthrough Moments: Yoshiki Sasai's Discoveries in the Third Dimension. *Cell Stem Cell*, 24(6):837–838, June 2019. ISSN 19345909. doi: 10.1016/j.stem.2019.05.007. URL https://linkinghub.elsevier.com/retrieve/pii/S1934590919302115.

[102] Madeline A. Lancaster, Magdalena Renner, Carol-Anne Martin, Daniel Wenzel, Louise S. Bicknell, Matthew E. Hurles, Tessa Homfray, Josef M. Penninger, Andrew P. Jackson, and Juergen A. Knoblich. Cerebral organoids model human brain development and microcephaly. *Nature*, 501(7467):373–379, September 2013. ISSN 1476-4687. doi: 10.1038/nature12517. URL https://www.nature.com/articles/nature12517. Number: 7467 Publisher: Nature Publishing Group.

[103] Hans Clevers. Modeling Development and Disease with Organoids. *Cell*, 165(7):

1586–1597, June 2016. ISSN 00928674. doi: 10.1016/j.cell.2016.05.082. URL https://linkinghub.elsevier.com/retrieve/pii/S0092867416307292.

[104] Gustavo Tiscornia, Erica Lorenzo Vivas, and Juan Carlos Izpisúa Belmonte. Diseases in a dish: modeling human genetic disorders using induced pluripotent cells. *Nature Medicine*, 17(12):1570–1576, December 2011. ISSN 1078-8956, 1546-170X. doi: 10.1038/nm.2504. URL https://www.nature.com/articles/nm.2504.

[105] Elizabeth Di Lullo and Arnold R. Kriegstein. The use of brain organoids to investigate neural development and disease. *Nature Reviews Neuroscience*, 18(10): 573–584, October 2017. ISSN 1471-003X, 1471-0048. doi: 10.1038/nrn.2017.107. URL https://www.nature.com/articles/nrn.2017.107.

[106] Sally K. Mak, Y. Anne Huang, Shifteh Iranmanesh, Malini Vangipuram, Ramya Sundararajan, Loan Nguyen, J. William Langston, and Birgitt Schüle. Small molecules greatly improve conversion of human-induced pluripotent stem cells to the neuronal lineage. *Stem Cells International*, 2012:140427, 2012. ISSN 1687-9678. doi: 10.1155/2012/140427.

[107] Asuka Morizane, Daisuke Doi, Tetsuhiro Kikuchi, Kaneyasu Nishimura, and Jun Takahashi. Small-molecule inhibitors of bone morphogenic protein and activin/nodal signals promote highly efficient neural induction from human pluripotent stem cells. *Journal of Neuroscience Research*, 89(2):117–126, 2011. ISSN 1097-4547. doi: 10.1002/jnr.22547. URL https://onlinelibrary.wiley.com/doi/abs/10.1002/jnr.22547. _eprint: https://onlinelibrary.wiley.com/doi/pdf/10.1002/jnr.22547.

[108] Yichen Shi, Peter Kirwan, and Frederick J. Livesey. Directed differentiation of human pluripotent stem cells to cerebral cortex neurons and neural networks. *Nature Protocols*, 7(10):1836–1846, October 2012. ISSN 1750-2799. doi: 10.1038/nprot.2012.116. URL https://www.nature.com/articles/nprot.2012.116. Number: 10 Publisher: Nature Publishing Group.

[109] Jiaxi Zhou, Pei Su, Dong Li, Stephanie Tsang, Enkui Duan, and Fei Wang. High-efficiency induction of neural conversion in human ESCs and human induced pluripotent stem cells with a single chemical inhibitor of transforming growth

factor beta superfamily receptors. *Stem Cells (Dayton, Ohio)*, 28(10):1741–1750, October 2010. ISSN 1549-4918. doi: 10.1002/stem.504.

[110] R. Bjerkvig, A. Tønnesen, O. D. Laerum, and E. O. Backlund. Multicellular tumor spheroids from human gliomas maintained in organ culture. *Journal of Neurosurgery*, 72(3):463–475, March 1990. ISSN 0022-3085. doi: 10.3171/jns.1990.72.3.0463.

[111] E. O. Backlund and R. Bjerkvig. Stereotactic biopsies as a model for studying the interaction between gliomas and normal brain tissue in vitro. *Journal of Neurosurgical Sciences*, 33(1):31–33, 1989. ISSN 0390-5616.

[112] P. C. De Witt Hamer, A. a. G. Van Tilborg, P. P. Eijk, P. Sminia, D. Troost, C. J. F. Van Noorden, B. Ylstra, and S. Leenstra. The genomic profile of human malignant glioma is altered early in primary cell culture and preserved in spheroids. *Oncogene*, 27(14):2091–2096, March 2008. ISSN 1476-5594. doi: 10.1038/sj.onc.1210850.

[113] Eliane Klein. Glioblastoma Organoids: Pre-Clinical Applications and Challenges in the Context of Immunotherapy. *Frontiers in Oncology*, 10:18, 2020.

[114] Roberta Azzarelli. Organoid Models of Glioblastoma to Study Brain Tumor Stem Cells. *Frontiers in Cell and Developmental Biology*, 8:220, April 2020. ISSN 2296-634X. doi: 10.3389/fcell.2020.00220. URL https://www.frontiersin.org/article/10.3389/fcell.2020.00220/full.

[115] Gladiola Goranci-Buzhala, Aruljothi Mariappan, Elke Gabriel, Anand Ramani, Lucia Ricci-Vitiani, Mariachiara Buccarelli, Quintino Giorgio D'Alessandris, Roberto Pallini, and Jay Gopalakrishnan. Rapid and Efficient Invasion Assay of Glioblastoma in Human Brain Organoids. *Cell Reports*, 31(10):107738, June 2020. ISSN 22111247. doi: 10.1016/j.celrep.2020.107738. URL https://linkinghub.elsevier.com/retrieve/pii/S221112472030718X.

[116] Elke Gabriel and Jay Gopalakrishnan. Generation of iPSC-derived Human Brain Organoids to Model Early Neurodevelopmental Disorders. *JoVE (Journal of Visualized Experiments)*, (122):e55372, April 2017. ISSN 1940-087X. doi: 10.3791/55372. URL https://www.jove.com/de/v/55372/generation-ipsc-derived-human-brain-organoids-to-model-early.

[117] Christopher N. Mayhew and Richa Singhania. A review of protocols for brain organoids and applications for disease modeling. *STAR Protocols*, 4(1):101860, March 2023. ISSN 26661667. doi: 10.1016/j.xpro.2022.101860. URL https://linkinghub.elsevier.com/retrieve/pii/S2666166722007407.

[118] Jason J. Han. FDA Modernization Act 2.0 allows for alternatives to animal testing. *Artificial Organs*, page aor.14503, February 2023. ISSN 0160-564X, 1525-1594. doi: 10.1111/aor.14503. URL https://onlinelibrary.wiley.com/doi/10.1111/aor.14503.

[119] Abdullah O. Khan, Antonio Rodriguez-Romera, Jasmeet S. Reyat, Aude-Anais Olijnik, Michela Colombo, Guanlin Wang, Wei Xiong Wen, Nikolaos Sousos, Lauren C. Murphy, Beata Grygielska, Gina Perrella, Christopher B. Mahony, Rebecca E. Ling, Natalina E. Elliott, Christina Simoglou Karali, Andrew P. Stone, Samuel Kemble, Emily A. Cutler, Adele K. Fielding, Adam P. Croft, David Bassett, Gowsihan Poologasundarampillai, Anindita Roy, Sarah Gooding, Julie Rayes, Kellie R. Machlus, and Bethan Psaila. Human Bone Marrow Organoids for Disease Modeling, Discovery, and Validation of Therapeutic Targets in Hematologic Malignancies. *Cancer Discovery*, 13(2):364–385, February 2023. ISSN 2159-8274, 2159-8290. doi: 10.1158/2159-8290.CD-22-0199. URL https://aacrjournals.org/cancerdiscovery/article/13/2/364/716300/Human-Bone-Marrow-Organoids-for-Disease-Modeling.

[120] Judith Pape, Mark Emberton, and Umber Cheema. 3D Cancer Models: The Need for a Complex Stroma, Compartmentalization and Stiffness. *Frontiers in Bioengineering and Biotechnology*, 9:660502, April 2021. ISSN 2296-4185. doi: 10.3389/fbioe.2021.660502. URL https://www.frontiersin.org/articles/10.3389/fbioe.2021.660502/full.

[121] Alexandre Albanese, Justin M. Swaney, Dae Hee Yun, Nicholas B. Evans, Jenna M. Antonucci, Silvia Velasco, Chang Ho Sohn, Paola Arlotta, Lee Gehrke, and Kwanghun Chung. Multiscale 3D phenotyping of human cerebral organoids. *Scientific Reports*, 10(1):21487, December 2020. ISSN 2045-2322. doi: 10.1038/s41598-020-78130-7. URL https://www.nature.com/articles/s41598-020-78130-7. Number: 1 Publisher: Nature Publishing Group.

[122] PubChem. Plerixafor. URL https://pubchem.ncbi.nlm.nih.gov/compound/

65015.

[123] Momoko Watanabe, Jessie E. Buth, Neda Vishlaghi, Luis De La Torre-Ubieta, Jiannis Taxidis, Baljit S. Khakh, Giovanni Coppola, Caroline A. Pearson, Ken Yamauchi, Danyang Gong, Xinghong Dai, Robert Damoiseaux, Roghiyh Aliyari, Simone Liebscher, Katja Schenke-Layland, Christine Caneda, Eric J. Huang, Ye Zhang, Genhong Cheng, Daniel H. Geschwind, Peyman Golshani, Ren Sun, and Bennett G. Novitch. Self-Organized Cerebral Organoids with Human-Specific Features Predict Effective Drugs to Combat Zika Virus Infection. *Cell Reports*, 21 (2):517–532, October 2017. ISSN 22111247. doi: 10.1016/j.celrep.2017.09.047. URL https://linkinghub.elsevier.com/retrieve/pii/S2211124717313372.

[124] Xiao-Qi Wang, Xiu-Mei Duan, Li-Hua Liu, Yan-Qiu Fang, and Yan Tan. Carboxyfluorescein diacetate succinimidyl ester fluorescent dye for cell labeling. *Acta Biochimica Et Biophysica Sinica*, 37(6):379–385, June 2005. ISSN 1672-9145. doi: 10.1111/j.1745-7270.2005.00051.x.

[125] S.M. Stief, A.-L. Hanneforth, S. Weser, R. Mattes, M. Carlet, W.-H. Liu, M.D. Bartoschek, H.D. Moreno, M. Oettle, and J. Kempf. Loss of KDM6A confers drug resistance in acute myeloid leukemia. *Leukemia*, pages 1–13.

[126] R. Pelossof, L. Fairchild, C.-H. Huang, C. Widmer, V.T. Sreedharan, N. Sinha, D.-Y. Lai, Y. Guan, P.K. Premsrirut, and D.F. Tschaharganeh. Prediction of potent shRNAs with a sequential classification algorithm. *Nature biotechnology*, 35:350–353, 2017.

[127] Daisuke Kamide, Taku Yamashita, Koji Araki, Masayuki Tomifuji, Yuya Tanaka, Shingo Tanaka, Shunichi Shiozawa, and Akihiro Shiotani. Selective activator protein-1 inhibitor T-5224 prevents lymph node metastasis in an oral cancer model. *Cancer Science*, 107(5):666–673, May 2016. ISSN 1349-7006. doi: 10.111 1/cas.12914.

[128] Dandan Song, Yan Lian, and Lin Zhang. The potential of activator protein 1 (AP-1) in cancer targeted therapy. *Frontiers in Immunology*, 14, July 2023. ISSN 1664-3224. doi: 10.3389/fimmu.2023.1224892. URL https://www.frontiersin.org/journals/immunology/articles/10.3389/fimmu.2023.1224892/full. Publisher: Frontiers.

[129] Wouter Masselink, Daniel Reumann, Prayag Murawala, Pawel Pasierbek, Yuka Taniguchi, François Bonnay, Katharina Meixner, Jürgen A. Knoblich, and Elly M. Tanaka. Broad applicability of a streamlined ethyl cinnamate-based clearing procedure. *Development (Cambridge, England)*, 146(3):dev166884, February 2019. ISSN 1477-9129. doi: 10.1242/dev.166884.

[130] Dmitry Ershov, Minh-Son Phan, Joanna W. Pylvänäinen, Stéphane U. Rigaud, Laure Le Blanc, Arthur Charles-Orszag, James R. W. Conway, Romain F. Laine, Nathan H. Roy, Daria Bonazzi, Guillaume Duménil, Guillaume Jacquemet, and Jean-Yves Tinevez. TrackMate 7: integrating state-of-the-art segmentation algorithms into tracking pipelines. *Nature Methods*, 19(7):829–832, July 2022. ISSN 1548-7091, 1548-7105. doi: 10.1038/s41592-022-01507-1. URL `https://www.nature.com/articles/s41592-022-01507-1`.

[131] Jean-Yves Tinevez, Nick Perry, Johannes Schindelin, Genevieve M. Hoopes, Gregory D. Reynolds, Emmanuel Laplantine, Sebastian Y. Bednarek, Spencer L. Shorte, and Kevin W. Eliceiri. TrackMate: An open and extensible platform for single-particle tracking. *Methods*, 115:80–90, February 2017. ISSN 10462023. doi: 10.1016/j.ymeth.2016.09.016. URL `https://linkinghub.elsevier.com/retrieve/pii/S1046202316303346`.

[132] Luke L. B. Davis. ProPlot, October 2021. URL `https://zenodo.org/record/5602155`. Language: eng.

[133] Qian-Yi Zhou, Jaesik Park, and Vladlen Koltun. Open3D: A Modern Library for 3D Data Processing, January 2018. URL `http://arxiv.org/abs/1801.09847`. arXiv:1801.09847 [cs].

[134] John D. Hunter. Matplotlib: A 2D Graphics Environment. *Computing in Science & Engineering*, 9(3):90–95, 2007. ISSN 1521-9615. doi: 10.1109/MCSE.2007.55. URL `http://ieeexplore.ieee.org/document/4160265/`.

[135] Charles R. Harris, K. Jarrod Millman, Stéfan J. Van Der Walt, Ralf Gommers, Pauli Virtanen, David Cournapeau, Eric Wieser, Julian Taylor, Sebastian Berg, Nathaniel J. Smith, Robert Kern, Matti Picus, Stephan Hoyer, Marten H. Van Kerkwijk, Matthew Brett, Allan Haldane, Jaime Fernández Del Río, Mark Wiebe, Pearu Peterson, Pierre Gérard-Marchant, Kevin Sheppard,

Tyler Reddy, Warren Weckesser, Hameer Abbasi, Christoph Gohlke, and Travis E. Oliphant. Array programming with NumPy. *Nature*, 585(7825):357–362, September 2020. ISSN 0028-0836, 1476-4687. doi: 10.1038/s41586-020-2649-2. URL https://www.nature.com/articles/s41586-020-2649-2.

[136] Wes McKinney. Data Structures for Statistical Computing in Python. pages 56–61, Austin, Texas, 2010. doi: 10.25080/Majora-92bf1922-00a. URL https://conference.scipy.org/proceedings/scipy2010/mckinney.html.

[137] Michael Kazhdan, Matthew Bolitho, and Hugues Hoppe. Poisson Surface Reconstruction.

[138] Weijia Wang, Xuequan Lu, Di Shao, Xiao Liu, Richard Dazeley, Antonio Robles-Kelly, and Wei Pan. Weighted Point Cloud Normal Estimation, May 2023. URL http://arxiv.org/abs/2305.04007. arXiv:2305.04007 [cs].

[139] Michael Waskom. seaborn: statistical data visualization. *Journal of Open Source Software*, 6(60):3021, April 2021. ISSN 2475-9066. doi: 10.21105/joss.03021. URL https://joss.theoj.org/papers/10.21105/joss.03021.

[140] Nicolas Gaspard, Tristan Bouschet, Raphael Hourez, Jordane Dimidschstein, Gilles Naeije, Jelle van den Ameele, Ira Espuny-Camacho, Adèle Herpoel, Lara Passante, Serge N. Schiffmann, Afsaneh Gaillard, and Pierre Vanderhaeghen. An intrinsic mechanism of corticogenesis from embryonic stem cells. *Nature*, 455 (7211):351–357, September 2008. ISSN 1476-4687. doi: 10.1038/nature07287. URL https://www.nature.com/articles/nature07287. Number: 7211 Publisher: Nature Publishing Group.

[141] Stefano L. Giandomenico, Magdalena Sutcliffe, and Madeline A. Lancaster. Generation and long-term culture of advanced cerebral organoids for studying later stages of neural development. *Nature Protocols*, 16(2):579–602, February 2021. ISSN 1750-2799. doi: 10.1038/s41596-020-00433-w.

[142] Juliana Minardi Nascimento, Verônica M. Saia-Cereda, Rafaela C. Sartore, Rodrigo Madeiro da Costa, Clarissa S. Schitine, Hercules Rezende Freitas, Michael Murgu, Ricardo A. de Melo Reis, Stevens K. Rehen, and Daniel Martins-de Souza. Human Cerebral Organoids and Fetal Brain Tissue Share Proteomic Similarities. *Frontiers in Cell and Developmental Biology*, 7:303, 2019. ISSN 2296-634X. doi:

10.3389/fcell.2019.00303. URL https://www.frontiersin.org/article/10.3389/fcell.2019.00303.

[143] Adam A. Sivitilli, Jessica T. Gosio, Bibaswan Ghoshal, Alesya Evstratova, Daniel Trcka, Parisa Ghiasi, J. Javier Hernandez, Jean Martin Beaulieu, Jeffrey L. Wrana, and Liliana Attisano. Robust production of uniform human cerebral organoids from pluripotent stem cells. *Life Science Alliance*, 3(5), May 2020. ISSN 2575-1077. doi: 10.26508/lsa.202000707. URL https://www.life-science-alliance.org/content/3/5/e202000707. Publisher: Life Science Alliance Section: Methods.

[144] Morgane Belle, David Godefroy, Chloé Dominici, Céline Heitz-Marchaland, Pavol Zelina, Farida Hellal, Frank Bradke, and Alain Chédotal. A Simple Method for 3D Analysis of Immunolabeled Axonal Tracts in a Transparent Nervous System. *Cell Reports*, 9(4):1191–1201, November 2014. ISSN 2211-1247. doi: 10.1016/j.celrep.2014.10.037. URL https://www.cell.com/cell-reports/abstract/S2211-1247(14)00906-1. Publisher: Elsevier.

[145] Morgane Belle, David Godefroy, Gérard Couly, Samuel A. Malone, Francis Collier, Paolo Giacobini, and Alain Chédotal. Tridimensional Visualization and Analysis of Early Human Development. *Cell*, 169(1):161–173.e12, March 2017. ISSN 0092-8674, 1097-4172. doi: 10.1016/j.cell.2017.03.008. URL https://www.cell.com/cell/abstract/S0092-8674(17)30287-8. Publisher: Elsevier.

[146] Michael N Economo, Nathan G Clack, Luke D Lavis, Charles R Gerfen, Karel Svoboda, Eugene W Myers, and Jayaram Chandrashekar. A platform for brain-wide imaging and reconstruction of individual neurons. *eLife*, 5:e10566, January 2016. ISSN 2050-084X. doi: 10.7554/eLife.10566. URL https://doi.org/10.7554/eLife.10566. Publisher: eLife Sciences Publications, Ltd.

[147] M.A. Lancaster and J.A. Knoblich. Organogenesisin a dish: Modeling development and disease using organoid technologies. *Science*, 345(6194), 2014. ISSN 0036-8075. doi: 10.1126/science.1247125.

[148] Andrew E. Whiteley, Trevor T. Price, Gaia Cantelli, and Dorothy A. Sipkins. Leukaemia: a model metastatic disease. *Nature Reviews Cancer*, 21(7):461–475,

July 2021. ISSN 1474-175X, 1474-1768. doi: 10.1038/s41568-021-00355-z. URL https://www.nature.com/articles/s41568-021-00355-z.

[149] Johanna F. Dekkers, Maria Alieva, Astrid Cleven, Farid Keramati, Amber K. L. Wezenaar, Esmée J. Van Vliet, Jens Puschhof, Peter Brazda, Inez Johanna, Angelo D. Meringa, Heggert G. Rebel, Maj-Britt Buchholz, Mario Barrera Román, Amber L. Zeeman, Sam De Blank, Domenico Fasci, Maarten H. Geurts, Annelisa M. Cornel, Else Driehuis, Rosemary Millen, Trudy Straetemans, Mara J. T. Nicolasen, Tineke Aarts-Riemens, Hendrikus C. R. Ariese, Hannah R. Johnson, Ravian L. Van Ineveld, Froso Karaiskaki, Oded Kopper, Yotam E. Bar-Ephraim, Kai Kretzschmar, Alexander M. M. Eggermont, Stefan Nierkens, Ellen J. Wehrens, Henk G. Stunnenberg, Hans Clevers, Jürgen Kuball, Zsolt Sebestyen, and Anne C. Rios. Uncovering the mode of action of engineered T cells in patient cancer organoids. *Nature Biotechnology*, 41(1):60–69, January 2023. ISSN 1087-0156, 1546-1696. doi: 10.1038/s41587-022-01397-w. URL https://www.nature.com/articles/s41587-022-01397-w.

[150] Shannon Otsuka and Gwyn Bebb. The CXCR4/SDF-1 Chemokine Receptor Axis: A New Target Therapeutic for Non-small Cell Lung Cancer. *Journal of Thoracic Oncology*, 3(12):1379–1383, December 2008. ISSN 15560864. doi: 10.1097/JTO.0b013e31818dda9d. URL https://linkinghub.elsevier.com/retrieve/pii/S1556086415324680.

[151] Brian A. Zabel, Yu Wang, Susanna Lewén, Robert D. Berahovich, Mark E. T. Penfold, Penglie Zhang, Jay Powers, Bretton C. Summers, Zhenhua Miao, Bin Zhao, Ali Jalili, Anna Janowska-Wieczorek, Juan C. Jaen, and Thomas J. Schall. Elucidation of CXCR7-mediated signaling events and inhibition of CXCR4-mediated tumor cell transendothelial migration by CXCR7 ligands. *Journal of Immunology (Baltimore, Md.: 1950)*, 183(5):3204–3211, September 2009. ISSN 1550-6606. doi: 10.4049/jimmunol.0900269.

[152] Jenna L Galloway and Leonard I Zon. 3 Ontogeny of hematopoiesis: Examining the emergence of hematopoietic cells in the vertebrate embryo. In *Current Topics in Developmental Biology*, volume 53, pages 139–158. Elsevier, 2003. ISBN 978-0-12-153153-9. doi: 10.1016/S0070-2153(03)53004-6. URL https://linkinghub.elsevier.com/retrieve/pii/S0070215303530046.

[153] A. Cousins, O. Olivares, E. Markert, A. Manoharan, X. Bubnova, S. Bresolin, M. Degn, Z. Li, D. Silvestri, G. McGregor, S. Tumanov, D. Sumpton, J. J. Kamphorst, A. M. Michie, P. Herzyk, M. G. Valsecchi, A. E. Yeoh, K. Schmiegelow, G. te Kronnie, E. Gottlieb, and C. Halsey. Central nervous system involvement in childhood acute lymphoblastic leukemia is linked to upregulation of cholesterol biosynthetic pathways. *Leukemia*, 36(12):2903–2907, December 2022. ISSN 0887-6924, 1476-5551. doi: 10.1038/s41375-022-01722-x. URL `https://www.nature.com/articles/s41375-022-01722-x`.

[154] Yukihiko Aikawa, Kimiko Morimoto, Tetsuya Yamamoto, Hisaaki Chaki, Akira Hashiramoto, Hirokazu Narita, Shuichi Hirono, and Shunichi Shiozawa. Treatment of arthritis with a selective inhibitor of c-Fos/activator protein-1. *Nature Biotechnology*, 26(7):817–823, July 2008. ISSN 1546-1696. doi: 10.1038/nbt1412.

[155] Daniel E. Johnson, Barbara Burtness, C. René Leemans, Vivian Wai Yan Lui, Julie E. Bauman, and Jennifer R. Grandis. Head and neck squamous cell carcinoma. *Nature Reviews Disease Primers*, 6(1):1–22, November 2020. ISSN 2056-676X. doi: 10.1038/s41572-020-00224-3. URL `https://www.nature.com/articles/s41572-020-00224-3`. Publisher: Nature Publishing Group.

[156] Hua Kang, Gareth Watkins, Christian Parr, Anthony Douglas-Jones, Robert E Mansel, and Wen G Jiang. Stromal cell derived factor-1: its influence on invasiveness and migration of breast cancer cells in vitro, and its association with prognosis and survival in human breast cancer. *Breast Cancer Research*, 7(4): R402, August 2005. ISSN 1465-542X. doi: 10.1186/bcr1022. URL `http://breast-cancer-research.biomedcentral.com/articles/10.1186/bcr1022`.

[157] Marcus A. Healey, Daniel J. Allendorf, Uma Borate, and Ankit Madan. CNS Involvement in a Patient with Chronic Myeloid Leukemia. *Case Reports in Hematology*, 2021:8891376, March 2021. ISSN 2090-6560. doi: 10.1155/2021/8891376. URL `https://www.ncbi.nlm.nih.gov/pmc/articles/PMC7972862/`.

[158] Heike Pfeifer, Barbara Wassmann, Wolf-Karsten Hofmann, Martina Komor, Urban Scheuring, Patrick Brück, Anja Binckebanck, Eberhard Schleyer, Nicola Gökbuget, Thomas Wolff, Michael Lübbert, Lothar Leimer, Harald Gschaidmeier, Dieter Hoelzer, and Oliver G. Ottmann. Risk and prognosis of central nervous system leukemia in patients with Philadelphia chromosome-positive acute leukemias

treated with imatinib mesylate. *Clinical Cancer Research: An Official Journal of the American Association for Cancer Research*, 9(13):4674–4681, October 2003. ISSN 1078-0432.

[159] Juliana Gomez and Victor Duenas. Isolated Central Nervous System Relapse in Chronic Myeloid Leukemia. *Case Reports in Medicine*, 2015:232915, 2015. ISSN 1687-9627. doi: 10.1155/2015/232915. URL https://www.ncbi.nlm.nih.gov/pmc/articles/PMC4386294/.

[160] Rajiv W. Jain and V. Wee Yong. B cells in central nervous system disease: diversity, locations and pathophysiology. *Nature Reviews Immunology*, 22(8): 513–524, August 2022. ISSN 1474-1741. doi: 10.1038/s41577-021-00652-6. URL https://www.nature.com/articles/s41577-021-00652-6. Publisher: Nature Publishing Group.

[161] Shu-Cheng Chen, Michael W. Leach, Yuetian Chen, Xiao-Yan Cai, Lee Sullivan, Maria Wiekowski, B. J. Dovey-Hartman, Albert Zlotnik, and Sergio A. Lira. Central Nervous System Inflammation and Neurological Disease in Transgenic Mice Expressing the CC Chemokine CCL21 in Oligodendrocytes. *The Journal of Immunology*, 168(3):1009–1017, February 2002. ISSN 0022-1767. doi: 10.4049/jimmunol.168.3.1009. URL https://doi.org/10.4049/jimmunol.168.3.1009.

[162] Lea Spory, Johannes Zimmermann, Michaela Vossen-Gajcy, Thomas Beder, Lorenz Bastian, Ameera Alsadeq, Dorothee Winterberg, Fotini Vogiatzi, Tim Wirbelauer, Hilal Bhat, Arndt Borkhardt, Sanil Bhatia, Martin Schrappe, Gunnar Cario, Denis M. Schewe, and Lennart Lenk. AP-1 Transcription Factor Complex Members FOSB and FOS are Linked With CNS Infiltration and Inferior Prognosis in Childhood T-ALL. *HemaSphere*, 7(9):e945, September 2023. ISSN 2572-9241. doi: 10.1097/HS9.0000000000000945. URL https://www.ncbi.nlm.nih.gov/pmc/articles/PMC10476750/.

[163] Keith R. Laderoute, Joy M. Calaoagan, Cindy Gustafson-Brown, A. Merrill Knapp, Guo-Chun Li, Holly L. Mendonca, Heather E. Ryan, Zhaohui Wang, and Randall S. Johnson. The response of c-jun/AP-1 to chronic hypoxia is hypoxia-inducible factor 1 alpha dependent. *Molecular and Cellular Biology*, 22(8):2515–2523, April 2002. ISSN 0270-7306. doi: 10.1128/MCB.22.8.2515-2523.2002.

[164] M. Kesarwani, Z. Kincaid, A. Gomaa, E. Huber, S. Rohrabaugh, Z. Siddiqui, M.F. Bouso, T. Latif, M. Xu, and K. Komurov. Targeting c-FOS and DUSP1 abrogates intrinsic resistance to tyrosine-kinase inhibitor therapy in BCR-ABL-induced leukemia. *Nature medicine*, 23:472–482, 2017.

[165] C. Zhou, E. Martinez, D. Marcantonio, N. Solanki-Patel, T. Aghayev, S. Peri, F. Ferraro, T. Skorski, C. Scholl, and S. Fröhling. JUN is a key transcriptional regulator of the unfolded protein response in acute myeloid leukemia. *leu*, 31: 1196–1205, 2017.

[166] Sarah Krause, Christian Pfeiffer, Susanne Strube, Ameera Alsadeq, Henning Fedders, Christian Vokuhl, Sonja Loges, Jonas Waizenegger, Isabel Ben-Batalla, Gunnar Cario, Anja Möricke, Martin Stanulla, Martin Schrappe, and Denis M. Schewe. Mer tyrosine kinase promotes the survival of t(1;19)-positive acute lymphoblastic leukemia (ALL) in the central nervous system (CNS). *Blood*, 125 (5):820–830, January 2015. ISSN 1528-0020. doi: 10.1182/blood-2014-06-583062.

[167] L. Frishman-Levy and S. Izraeli. Advances in understanding the pathogenesis of CNS acute lymphoblastic leukaemia and potential for therapy. *British journal of haematology*, 176:157–167, 2017.

[168] J. Hess, P. Angel, and M. Schorpp-Kistner. AP-1 subunits: quarrel and harmony among siblings. *Journal of cell science*, 117:5965–5973, 2004.

[169] Rainer Zenz, Robert Eferl, Clemens Scheinecker, Kurt Redlich, Josef Smolen, Helia B Schonthaler, Lukas Kenner, Erwin Tschachler, and Erwin F Wagner. Activator protein 1 (Fos/Jun) functions in inflammatory bone and skin disease. *Arthritis Research & Therapy*, 10(1):201, 2007. ISSN 1478-6354. doi: 10.1186/ar 2338. URL `http://arthritis-research.biomedcentral.com/articles/10.1186/ar2338`.

[170] Michael Karin, Zheng-gang Liu, and Ebrahim Zandi. AP-1 function and regulation. *Current Opinion in Cell Biology*, 9(2):240–246, April 1997. ISSN 0955-0674. doi: 10.1016/S0955-0674(97)80068-3. URL `https://www.sciencedirect.com/science/article/pii/S0955067497800683`.

[171] Mo Li and Juan C. Izpisua Belmonte. Organoids — Preclinical Models of Human Disease. *New England Journal of Medicine*, 380(6):569–579, February 2019. ISSN

0028-4793. doi: 10.1056/NEJMra1806175. URL https://www.nejm.org/doi/10.1056/NEJMra1806175. Publisher: Massachusetts Medical Society.

[172] Donald E. Ingber. Human organs-on-chips for disease modelling, drug development and personalized medicine. *Nature Reviews Genetics*, 23(8):467–491, August 2022. ISSN 1471-0064. doi: 10.1038/s41576-022-00466-9. URL https://www.nature.com/articles/s41576-022-00466-9. Number: 8 Publisher: Nature Publishing Group.

[173] Elmira Jalilian and Su Ryon Shin. Novel model of cortical–meningeal organoid co-culture system improves human cortical brain organoid cytoarchitecture. *Scientific Reports*, 13(1):7809, May 2023. ISSN 2045-2322. doi: 10.1038/s41598-023-35077-9. URL https://www.nature.com/articles/s41598-023-35077-9.

[174] Lisette M. Acevedo, Jeffrey N. Lindquist, Breda M. Walsh, Peik Sia, Flavio Cimadamore, Connie Chen, Martin Denzel, Cameron D. Pernia, Barbara Ranscht, Alexey Terskikh, Evan Y. Snyder, and David A. Cheresh. hESC Differentiation toward an Autonomic Neuronal Cell Fate Depends on Distinct Cues from the Co-Patterning Vasculature. *Stem Cell Reports*, 4(6):1075–1088, June 2015. ISSN 22136711. doi: 10.1016/j.stemcr.2015.04.013. URL https://linkinghub.elsevier.com/retrieve/pii/S2213671115001253.

[175] Liqing Song, Xuegang Yuan, Zachary Jones, Kyle Griffin, Yi Zhou, Teng Ma, and Yan Li. Assembly of Human Stem Cell-Derived Cortical Spheroids and Vascular Spheroids to Model 3-D Brain-like Tissues. *Scientific Reports*, 9(1): 5977, April 2019. ISSN 2045-2322. doi: 10.1038/s41598-019-42439-9. URL https://www.nature.com/articles/s41598-019-42439-9. Number: 1 Publisher: Nature Publishing Group.

[176] Qirui Wu, Jinfeng Liu, Xiaohong Wang, Lingyan Feng, Jinbo Wu, Xiaoli Zhu, Weijia Wen, and Xiuqing Gong. Organ-on-a-chip: recent breakthroughs and future prospects. *BioMedical Engineering OnLine*, 19(1):9, February 2020. ISSN 1475-925X. doi: 10.1186/s12938-020-0752-0. URL https://doi.org/10.1186/s12938-020-0752-0.

[177] Laura Pellegrini, Claudia Bonfio, Jessica Chadwick, Farida Begum, Mark Skehel, and Madeline A. Lancaster. Human CNS barrier-forming organoids

with cerebrospinal fluid production. *Science*, 369(6500):eaaz5626, July 2020. ISSN 0036-8075, 1095-9203. doi: 10.1126/science.aaz5626. URL https://www.science.org/doi/10.1126/science.aaz5626.

[178] Taisuke Kadoshima, Hideya Sakaguchi, Tokushige Nakano, Mika Soen, Satoshi Ando, Mototsugu Eiraku, and Yoshiki Sasai. Self-organization of axial polarity, inside-out layer pattern, and species-specific progenitor dynamics in human ES cell–derived neocortex. *Proceedings of the National Academy of Sciences*, 110(50): 20284–20289, December 2013. ISSN 0027-8424, 1091-6490. doi: 10.1073/pnas.1315710110. URL https://pnas.org/doi/full/10.1073/pnas.1315710110.

[179] Anca M. Paşca, Steven A. Sloan, Laura E. Clarke, Yuan Tian, Christopher D. Makinson, Nina Huber, Chul Hoon Kim, Jin-Young Park, Nancy A. O'Rourke, Khoa D. Nguyen, Stephen J. Smith, John R. Huguenard, Daniel H. Geschwind, Ben A. Barres, and Sergiu P. Paşca. Functional cortical neurons and astrocytes from human pluripotent stem cells in 3D culture. *Nature Methods*, 12(7):671–678, July 2015. ISSN 1548-7105. doi: 10.1038/nmeth.3415. URL https://www.nature.com/articles/nmeth.3415. Number: 7 Publisher: Nature Publishing Group.

[180] Camille Cassel de Camps, Saba Aslani, Nicholas Stylianesis, Harris Nami, Nguyen-Vi Mohamed, Thomas M. Durcan, and Christopher Moraes. Hydrogel Mechanics Influence the Growth and Development of Embedded Brain Organoids. *ACS Applied Bio Materials*, 5(1):214–224, January 2022. doi: 10.1021/acsabm.1c01047. URL https://doi.org/10.1021/acsabm.1c01047. Publisher: American Chemical Society.

[181] Mark T. Kozlowski, Christiana J. Crook, and Hsun Teresa Ku. Towards organoid culture without Matrigel. *Communications Biology*, 4(1):1–15, December 2021. ISSN 2399-3642. doi: 10.1038/s42003-021-02910-8. URL https://www.nature.com/articles/s42003-021-02910-8. Number: 1 Publisher: Nature Publishing Group.

[182] Cheng Chen, Venkatakrishnan Rengarajan, Andrew Kjar, and Yu Huang. A matrigel-free method to generate matured human cerebral organoids using 3D-Printed microwell arrays. *Bioactive Materials*, 6(4):1130–1139, April 2021. ISSN

2452199X. doi: 10.1016/j.bioactmat.2020.10.003. URL https://linkinghub.elsevier.com/retrieve/pii/S2452199X20302541.

[183] Madeline A. Lancaster, Nina S. Corsini, Simone Wolfinger, E. Hilary Gustafson, Alex W. Phillips, Thomas R. Burkard, Tomoki Otani, Frederick J. Livesey, and Juergen A. Knoblich. Guided self-organization and cortical plate formation in human brain organoids. *Nature Biotechnology*, 35(7):659–666, July 2017. ISSN 1546-1696. doi: 10.1038/nbt.3906. URL https://www.nature.com/articles/nbt.3906. Number: 7 Publisher: Nature Publishing Group.

[184] Zilong Zhou, Lele Cong, and Xianling Cong. Patient-Derived Organoids in Precision Medicine: Drug Screening, Organoid-on-a-Chip and Living Organoid Biobank. *Frontiers in Oncology*, 11:762184, December 2021. ISSN 2234-943X. doi: 10.3389/fonc.2021.762184. URL https://www.frontiersin.org/articles/10.3389/fonc.2021.762184/full.

[185] Yaqi Li, Peiyuan Tang, Sanjun Cai, Junjie Peng, and Guoqiang Hua. Organoid based personalized medicine: from bench to bedside. *Cell Regeneration*, 9(1):21, December 2020. ISSN 2045-9769. doi: 10.1186/s13619-020-00059-z. URL https://cellregeneration.springeropen.com/articles/10.1186/s13619-020-00059-z.